AD-A160 579 EFFECTS OF INFLOW CONDITIONS ON DISCRETE FREQUENCY NOISE GENERATED BY SMA..(U) PENNSYLVANIA STATE UNIV UNIVERSITY PARK APPLIED RESEARCH LAB.. 1/2

UNCLASSIFIED K B WASHBURN ET AL. SEP 85 F/G 13/1 NL

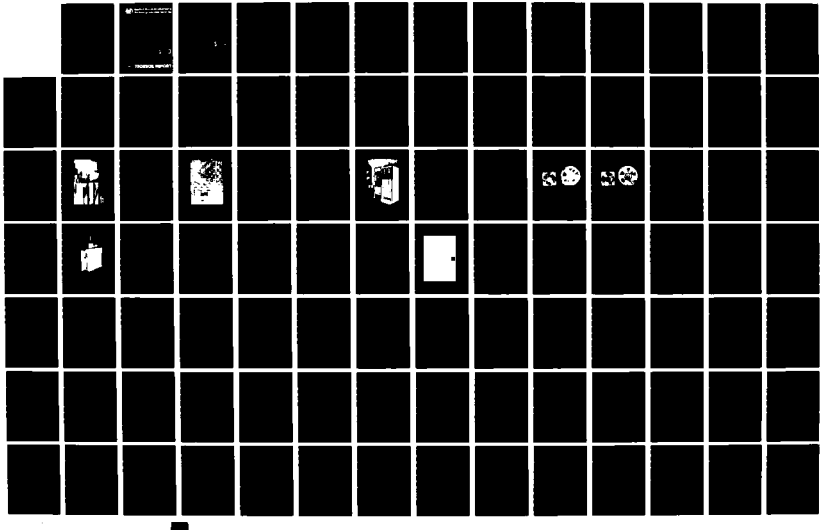

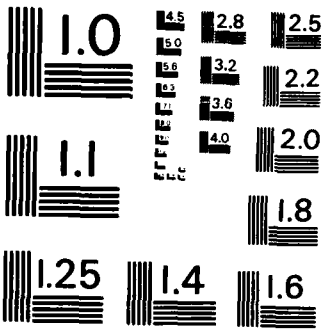

Applied Research Laboratory
The Pennsylvania State University

EFFECTS OF INFLOW CONDITIONS ON DISCRETE FREQUENCY NOISE GENERATED BY SMALL, AXIAL FLOW FANS

by

Karl B. Washburn & Gerald C. Lauchle

ARL PSU **TECHNICAL REPORT**

85 10 25 007

The Pennsylvania State University
Intercollege Research Programs and Facilities
APPLIED RESEARCH LABORATORY
P. O. Box 30
State College, PA 16804

EFFECTS OF INFLOW CONDITIONS ON DISCRETE FREQUENCY NOISE GENERATED BY SMALL, AXIAL FLOW FANS

by

Karl B. Washburn & Gerald C. Lauchle

Technical Report TR 85-001
September 1985

Supported by: IBM Corporation

L. R. Hettche, Director
Applied Research Laboratory

Unclassified

SECURITY CLASSIFICATION OF THIS PAGE (When Data Entered)

REPORT DOCUMENTATION PAGE		READ INSTRUCTIONS BEFORE COMPLETING FORM
1. REPORT NUMBER TR 85-001	2. GOVT ACCESSION NO. AD-A166 174	3. RECIPIENT'S CATALOG NUMBER
4. TITLE (and Subtitle) EFFECTS OF INFLOW CONDITIONS ON DISCRETE FREQUENCY NOISE GENERATED BY SMALL, AXIAL FLOW FANS		5. TYPE OF REPORT & PERIOD COVERED 6. PERFORMING ORG. REPORT NUMBER
7. AUTHOR(s) Karl B. Washburn & Gerald C. Lauchle		8. CONTRACT OR GRANT NUMBER(s)
9. PERFORMING ORGANIZATION NAME AND ADDRESS Applied Research Laboratory P.O. Box 30 State College, PA 16804		10. PROGRAM ELEMENT, PROJECT, TASK AREA & WORK UNIT NUMBERS
11. CONTROLLING OFFICE NAME AND ADDRESS IBM Corporation P.O. Box 390 Poughkeepsie, NY 12601		12. REPORT DATE September 1985 13. NUMBER OF PAGES 148
14. MONITORING AGENCY NAME & ADDRESS(if different from Controlling Office)		15. SECURITY CLASS. (of this report) Unclassified 15a. DECLASSIFICATION DOWNGRADING SCHEDULE

16. DISTRIBUTION STATEMENT (of this Report)

17. DISTRIBUTION STATEMENT (of the abstract entered in Block 20, if different from Report)

Approved for public release; distribution unlimited

18. SUPPLEMENTARY NOTES

19. KEY WORDS (Continue on reverse side if necessary and identify by block number)

Axial flow fans, discrete frequency radiation, subsonic flow

20. ABSTRACT (Continue on reverse side if necessary and identify by block number)

Discrete frequency acoustic radiation is generated by subsonic axial flow fans through both steady and unsteady blade loading. Steady loading is a function of pumping requirement, and unsteady loading is generated by spatially periodic inflow distortions. The latter effect is the dominant generation mechanism when small fans are used to cool electronic equipment. Fans mounted to exhaust out of a device ingest distortions

DD FORM 1 JAN 73 1473 EDITION OF 1 NOV 65 IS OBSOLETE

Unclassified

SECURITY CLASSIFICATION OF THIS PAGE (When Data Entered)

Block 20. (cont'd)

created by all objects within the unit. This work represents an empirical survey of noise generated by small axial flow cooling fans in the presence of upstream obstructions and various inlet configurations. The obstructions include a cylinder, a thin rectangle, a thick rectangle, and an electronic card gate model. Each of these represents obstructions found in a typical installation. Simple and modified inlet baffles, finger guards, and honeycomb flow straighteners are investigated. Sound pressure data is gathered by a single microphone, and narrowband frequency analysis is performed to resolve discrete tones. Signal harmonics which are phase-related to the blade passage frequency (BPF) are enhanced with synchronous time averaging which effectively reduces independently generated random noise by up to 40 dB. Application of this technique to directivity and flow coefficient data confirms that steady loading is the dominant source of the BPF x 1 tone, while unsteady loading dominates in generating BPF harmonics. Synchronous averaging is also applied to the obstruction and inlet surveys to isolate phase-locked radiation from time random noise in the same frequency bands. Design recommendations are offered to minimize discrete tone generation. These include aerodynamic shaping of unavoidable obstructions, a minimum axial distance of 0.3 fan radii for obstructions in the inlet, the avoidance of blockage in the lateral inflow, and the use of an inlet baffle to smooth inlet distortions. Account is taken of the spatial restrictions of typical installations.

ABSTRACT

Discrete frequency acoustic radiation is generated by subsonic axial flow fans through both steady and unsteady blade loading. Steady loading is a function of pumping requirement, and unsteady loading is generated by spatially periodic inflow distortions. The latter effect is the dominant generation mechanism when small fans are used to cool electronic equipment. Fans mounted to exhaust out of a device ingest distortions created by all objects within the unit. This work represents an empirical survey of noise generated by small axial flow cooling fans in the presence of upstream obstructions and various inlet configurations. The obstructions include a cylinder, a thin rectangle, a thick rectangle, and an electronic card gate model. Each of these represents obstructions found in a typical installation. Simple and modified inlet baffles, finger guards, and honeycomb flow straighteners are investigated. Sound pressure data is gathered by a single microphone, and narrowband frequency analysis is performed to resolve discrete tones. Signal harmonics which are phase-related to the blade passage frequency (BPF) are enhanced with synchronous time averaging which effectively reduces independently generated random noise by up to 40 dB. Application of this technique to directivity and flow coefficient data confirms that steady loading is the dominant source of the BPF x 1 tone, while unsteady loading dominates in generating BPF harmonics. Synchronous averaging is also applied to the obstruction and inlet surveys to isolate phase-locked radiation from time random noise in the same frequency bands. Design recommendations are offered

to minimize discrete tone generation. These include aerodynamic shaping of unavoidable obstructions, a minimum axial distance of 0.3 fan radii for obstructions in the inlet, the avoidance of blockage in the lateral inflow, and the use of an inlet baffle to smooth inlet distortions. Account is taken of the spatial restrictions of typical installations.

TABLE OF CONTENTS

TABLE OF CONTENTS [continuation]

LIST OF TABLES

LIST OF FIGURES

LIST OF FIGURES [continuation]

LIST OF FIGURES [continuation]

LIST OF FIGURES [continuation]

ACKNOWLEDGEMENTS

This work was performed at the Applied Research Laboratory of The Pennsylvania State University with support provided by the International Business Machines Corporation Acoustics Laboratory, Poughkeepsie, New York. The author gratefully acknowledges the support and guidance of his advisor, Dr. Gerald C. Lauchle, whose expertise and suggestions greatly contributed to this work. The author also wishes to thank Dr. Donald E. Thompson and Dr. Robert E. Henderson for participating on the thesis committee and for their suggestions. The assistance of the staff members of the Garfield Thomas Water Tunnel, particularly James H. Prout, is greatly appreciated. The author wishes to thank J. Eric Hallander for the use of his computer plotting software and for his helpful recommendations.

1. INTRODUCTION

1.1. Motivation for Surveys

As the technology of electronic systems progresses, individual components tend to provide more functions in less space. If the power consumed per component increases or even stays the same as previous components, heat dissipation requirements per unit area must increase to prevent component failure. In smaller installations typical of business machines, office and personal computers, and computer peripheral equipment, heat is commonly removed through forced air cooling provided by small, axial flow fans.

These fans do work by applying thrust to a body of fluid. By their very nature, they apply force to the fluid in a manner that varies dynamically. Thus, they are potential acoustic sources. Likewise, when flow nonuniformities occur, noise results (Gray, 1983). The frequency spectrum of noise generated by fans contains two major components: broadband noise and discrete frequency noise (Sharland, 1964).

The fans investigated here are often installed in otherwise quiet office environments. As such, they are principle sources of noise in these environments. The noise would not be as objectionable if it was only broadband in nature. However, since the noise contains discrete tones, an observer is likely to judge that it is "noisier" (though not necessarily "louder"), as reported by Kryter and Pearsons (1965). In a quiet environment, this can lead to increased annoyance, irritability and speech interference.

There is a large body of literature concerning the generation of acoustic radiation by axial flow devices (Morfey, 1973). The first quantitative model was the propeller theory of Gutin (1948), but Prandtl (1921) had earlier surmised that asymmetry and unsteadiness in the inlet flow are responsible for tonal radiation. Since then, a great deal of evidence shows that periodic blade forces are the chief contributor to discrete tones (Wright, 1971) and that the generation of tones is largely dependent on the fan flow environment (Gray, 1983). It is recognized that intake flow must be as smooth as possible to reduce periodic forces and the noise they generate (Sharland, 1964).

There are several elements of any fan design that can be altered. These include the rotor and blades, the hub shape, the shape and position of struts to support the hub, and the blade tip clearance in shrouded devices. The designer can also modify the shroud and the local inlet and outflow environments (Mellin, 1975). The former elements, which deal with the fans themselves, were investigated in detail by Fitzgerald (1982). However, there exists a need to understand the effect that the local fan flow environment has on the generation of discrete frequency noise. This work represents a parametric investigation of several inlet configurations related to a typical fan installation and their effects on discrete tone generation.

1.2. The Nature of Low Tip-Speed, Axial Flow Fan Noise

1.2.1. Aerodynamic Sources of Sound

One of the first theories put forth to quantitatively explain the aerodynamic sources of sound was that of Lighthill (1952). While the details of his theory have been modified several times to account for

observations, the fundamental principles remain intact. In order for flow to produce sound, fluid kinetic energy must be converted into acoustic energy. Three basic actions are involved. The first is forced mass fluctuation, in which new mass is introduced or extracted from a volume. This action, likened to puffs of air, is a monopole source of acoustic radiation. The second is forced momentum fluctuation. Sound is generated by a fluctuating external force field. The source strength per unit volume is equal to the flux of force on the volume. A boundary must be present on which the forces can act, and the acoustic radiation is that of a dipole source. The third action arises from a fluctuating stress field, producing equal and opposite forces on both sides of a fluid element. In this forced rate-of-momentum-flux fluctuation, both the volume and centroid of the fluid element remain fixed. It resembles a quadrupole acoustic source and is considered the truly aerodynamic contribution to flow-generated sound since no mass sources or boundaries are needed.

The most important facet of these three sources is their relative efficiency in producing acoustic radiation. Like their classical acoustic analogies, and for subsonic velocities, they are ranked as monopole, dipole, and quadrupole in order of decreasing efficiency. The relative sound power from each source is dependent upon velocity, most often reported as rotor blade tip Mach number for axial flow fans (Mugridge and Morfey, 1972). Since a fan does not introduce new mass to the system, it cannot be considered a monopole source of sound. This leaves dipoles and quadrupoles. Dimensional analysis shows that broadband noise power generated by dipoles varies as velocity to the sixth power, and for quadrupoles as velocity to the eighth power

(Sharland, 1964). Since the tip speeds of the fans used to cool electronic equipment are only a few percent of the sonic velocity, it is likely that quadrupole sources contribute little to the radiated noise.

This leaves dipole sources, or fluctuating forces, as the principal contributor to noise from such fans. This is further supported in terms of the blades acting as boundaries against which fluctuating forces are applied. It is expected that sound output depends upon airflow separation and turbulence over the blades, the pumping performance of the rotor, and the lift generated by the blades (Mellin, 1975).

1.2.2. The Effect of Pumping Requirement on Noise

The objective of a fan is to transport a fluid by doing work on the fluid. Any attempts at altering its noise characteristics must be related to its aerodynamic performance (Gray, 1983). For the low pressure, low speed fans studied in this survey, there is no need to be concerned about compressibility, flow Reynolds number, or Mach number. Full-scale fans are used under their designed conditions. The pumping requirement of any system is then simply defined by the required airflow and pressure rise. Noise can be related to the pumping requirement through its dependence on the flow coefficient, ϕ. This coefficient is a measure of the fan operating characteristics, in that it is the ratio of axial flow velocity-to-blade tip velocity. It may be computed from:

$$\phi = C_1 \, Q/U_T \, D_T^2 = C_2 \, Q/N \, D_T^3 \quad , \tag{1.1}$$

where Q is the airflow rate in m^3/min (ft^3/min), U_T is the blade tip speed in m/sec (ft/sec), D_T is the blade tip diameter in m (ft), and N is the rotor speed in rpm. The two constants are C_1 = 166.67 (2.4) and $C_2 = 3.1831 \times 10^5$ (550) (Mellin, 1975).

In order to perform the same pumping task with the same fan design, but at a flow coefficient other than the original design, the fan must be scaled geometrically. Any fan thus scaled becomes a member of the same "fan family." The advantage of determining noise as a function of flow coefficient is that there exists a value of ϕ for any fan family that will produce minimum noise. An optimum fan can be designed by scaling the diameter and tip speed within the family that satisfies the given pumping requirement (Mellin, 1975).

A tradeoff exists in terms of the two types of noise associated with axial flow fans. Broadband noise tends to dominate the acoustic spectrum for low flow coefficients. In this region, a given fan is heavily loaded and is either approaching or is in stall. Discrete frequency noise tends to dominate at the higher flow coefficients, where the fan is lightly loaded and the volume flow rate is high. The designer must account for this tradeoff in light of final acoustic expectations and required fan performance.

1.2.3. Mechanisms of Noise Generation

Two major classes of noise sources can be identified and linked to the two types of fan-generated noise. Inflow turbulence interacts with the blades to generate broadband noise; repetitious blade interactions generate discrete frequency noise, mostly at the Blade Passage Frequency (BPF) and its harmonics (Mather et al., 1971).

Longhouse (1976) refers to these as nonrotational and rotational noise, respectively. Rotational noise is caused by periodic blade interaction with inflow distortion, as well as the rotating pressure pattern due to steady loading associated with the Gutin propeller mechanism (Mugridge and Morfey, 1972). The non-rotational noise is broadband, associated with time-random fluctuating forces.

The major broadband noise sources include (in order of increasing power level) the surface pressure field of the blade turbulent boundary layer, vortex shedding from the blade trailing edge, and blade interaction with inflow turbulence (Sharland, 1964). Blade tip vortex interaction and nonlinear turbulence interactions may contribute, but to a smaller degree. Wright (1969) suggests that vortex shedding noise may be important at low lift conditions in high-solidity rotors. Robbins and Lakshminarayana (1974) show that noise generated by inflow turbulence increases with both the turbulence intensity and its integral length scale.

As mentioned before, the discrete frequency noise has two primary sources: the propeller mechanism and interaction with periodically fluctuating aerodynamic force regions. Soon after the Gutin theory was proposed, it was realized that the theory underestimated levels for harmonics of the BPF. Part of the explanation for this lies in the nature of the calculation involved. The analysis of rotating pressure patterns requires the use of Bessel functions. These functions tend to attenuate harmonics of the principal rotation frequency. This attenuation could be avoided by seeking non-rotating, periodic sources (Ffowes-Williams, and Hawkings, 1969). Such sources are created by the periodically varying velocity field encountered by the blade as it

traverses the rotor disk (Sharland, 1964). As a blade passes through velocity disturbances, it experiences fluctuating angles of attack, causing unsteady lift forces. With the blade as a boundary, these unsteady lifts radiate noise as acoustic dipoles. If the disturbances are periodic, the radiation will be discrete (Hanson, 1974). A schematic representation of the fluctuating velocity vectors, adapted from Sharland (1964), is shown in Figure 1.1.

The next section details the sources of these fluctuating velocities.

1.2.4. Sources of Unsteady Blade Loading

The fluctuating velocities that cause unsteady blade loading result from disturbances in the fan inlet flow. These disturbances are of two types: ambient air turbulence and obstacle-generated flow distortions (Bekofske et al., 1977). The latter include:

- interaction between blade and potential flow fields induced by obstructions;
- interaction of the blade with vortices and wakes shed by upstream obstructions;
- other inlet distortions, including circumferential asymmetry, cross flow, and streamwise vortices from nearby solid surfaces (Mugridge and Morfey, 1972).

While interaction mechanisms dominate at normal operating conditions (Sharland, 1964), the effects of ambient turbulence on discrete tone generation are not negligible. Even in an ideal flow situation (i.e., no obstructions), Metzger and Hanson (1972) found harmonics much higher than predicted by propeller theory and presumed

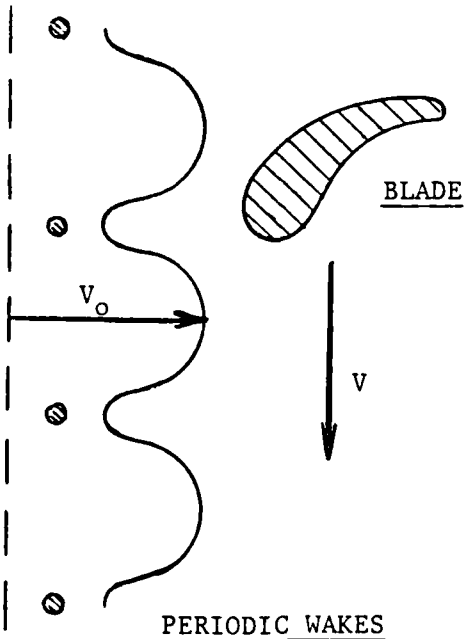

(a)

V = ROTOR VELOCITY

V_o = FREE STREAM VELOCITY

(b)

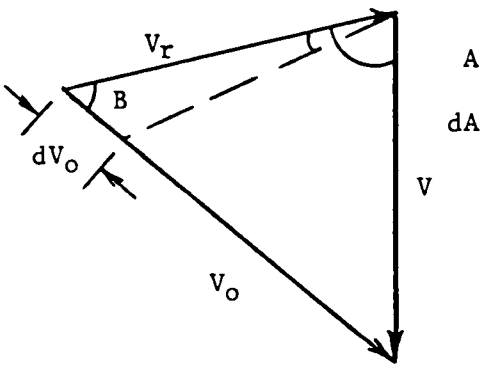

A = RELATIVE ANGLE OF AIR INTO ROTOR

$V_r = V_o - V$

$$dV_r \sim \frac{dV_o}{V_r} \sin(B)$$

Figure 1.1 . Schematic Representation of Fluctuating Velocities.

(a) Blade Intersecting Velocity Deficits Induced by Periodic Obstructions in Free Stream of Velocity V_o.
(b) Resultant Velocity Relative to Rotor and its Fluctuation Due to Changes in V_o.

some other source of inflow distortion. Hanson (1974) was able to isolate those sources. The static fan acts as a sink, and flow from the region contracts at the inlet. Random, isotropic eddies present in the flow become elongated and anisotropic as they pass through the contraction. If an eddy lasts a time τ and moves at a velocity U through the fan, it has an effective length of $L = U\tau$ at the rotor disk. The number of blades which pass through the eddy is then

$$N_b = \tau \times BPF = (L/U) \times BPF. \qquad (1.2)$$

Due to the anisotropy of the eddy, the blade loading is highly coherent and radiates efficiently. As N_b increases, the acoustic source becomes more efficient as a discrete radiator. In the limit as τ approaches infinity, the source is non-varying (as it would be for an obstruction wake) and becomes most efficient (Bekofske et al., 1977). In certain high-flow cases, the turbulent eddies have approximately the same magnitude as typical obstruction wakes, and the pressure time histories and frequency spectra are remarkably similar in terms of discrete tone location and amplitude (Hanson, 1974). However, for the small fans used in the present work, the most important discrete tone sources are obstruction wakes, and the most important parameter of noise dependence is rotor-obstruction separation distance (Sharland, 1964). A simplified schematic of the wake generated by a cylinder in smooth flow is shown in Figure 1.2. The structure of the wake depends on the shape of the obstruction, the local flow Reynolds number, and the downstream distance from the obstruction trailing edge. The time history of the blade lift depends on the cross-sectional structure of the wake at the plane where the rotor and wake intersect.

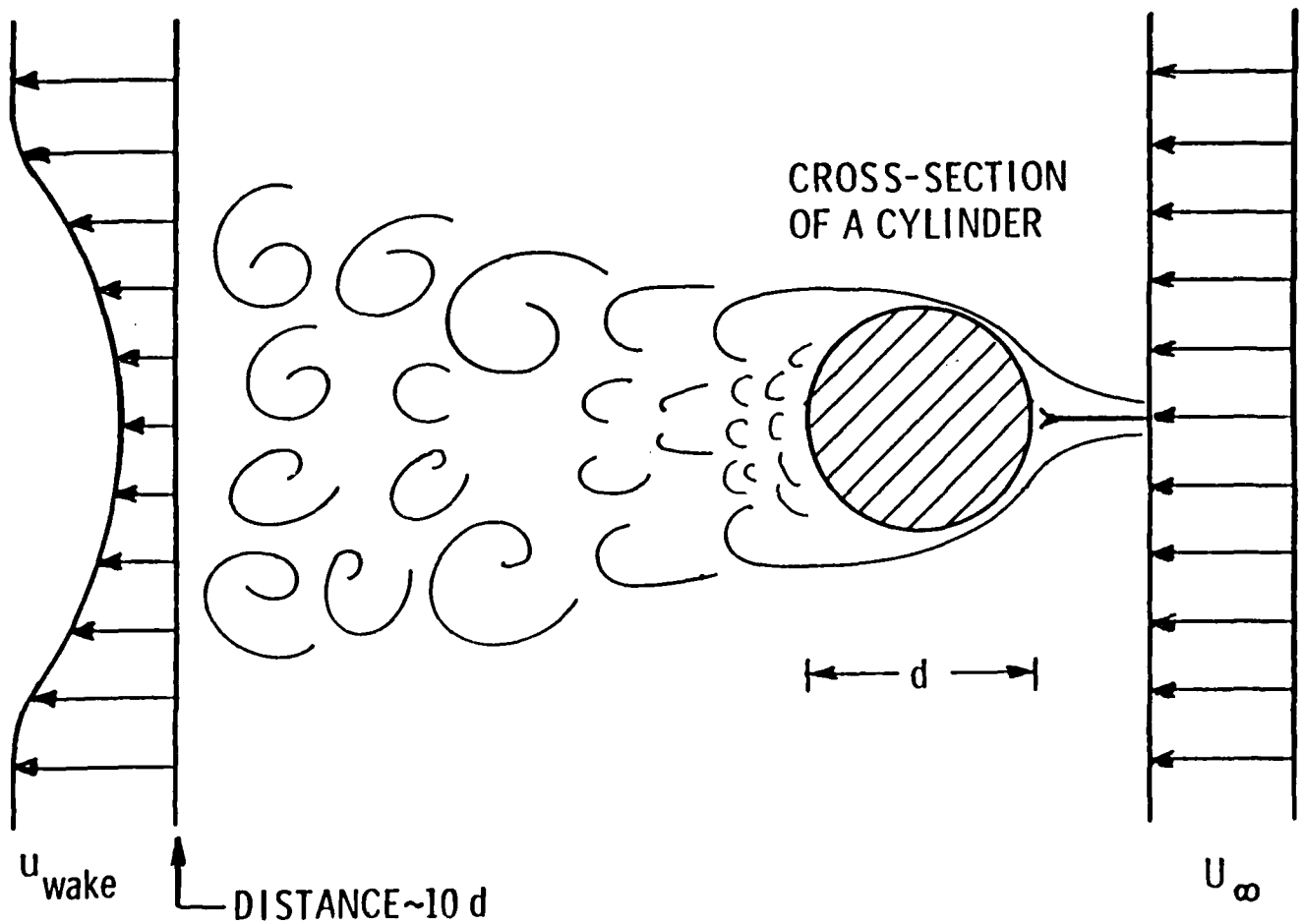

Figure 1.2 . Schematic Representation of the Wake and Velocity Deficit Induced by a Cylindrical Obstruction in the Freestream.

The fluctuating lift on the blade can be Fourier analyzed into a set of blade loading harmonics (Wright, 1969). The tonal radiation at any blade passage harmonic is dependent on the radiation efficiency of the corresponding mode (Chandrasekhara, 1970). For a ducted rotor, it is then necessary to determine those modes which are cut-on and will propagate (Magliozzi and Metzger, 1974; Tyler and Sofrin, 1962). The fans used in cooling business equipment are not usually ducted; they are considered to be diaphragm mounted, and ducted-mode cut-off properties need not be considered. The harmonic content of the blade loading determines the distribution of energy in the radiation spectrum. Impulsive loading, rich in harmonics, is a strong tone generator. Less impulsive loading yields only lower frequency discrete tones (Wright, 1971). The magnitude of the fluctuating force necessary for dominant radiation need only be on the order of one-thousandth of the steady thrust (Wright, 1969). For example, Magliozzi and Metzger (1974) calculate that a 0.5% fluctuation in the third blade loading harmonic increases the sound pressure level of the third blade passage harmonic tone by 66 dB. In essence, a small amount of inflow distortion can be a dominant source of discrete frequency noise.

Some final comments can be made concerning the behavior of discrete tones. The BPF tone level tends to be a function of the rotor steady field at design speed. The harmonics of the BPF have contributions from the Fourier components of the steady loading pressure pattern, but tend to be dominated by rotor-disturbance interaction (Hanson, 1977). The difference manifests itself in the observed directivities for the individual tones. The BPF tone will tend to have uniform directivity. The first few harmonics will show

pronounced lobes due to their unsteady loading source behavior. The higher harmonics show directivities that are a result of the acoustic wavelengths approaching the size of the fan, regardless of the nature of their source (Metzger and Hanson, 1972).

1.3. Survey Requirements

In light of the previous discussion on fan noise generation, several requirements can be established governing the experimental surveys:

- Narrow-band frequency analysis is a necessity in order to resolve tones clearly.
- The test configurations must significantly attenuate test fixture duct modes to prevent cut-off effects which are not present in typical installations.
- Both discrete frequency and broadband noise must be determined as a function of flow coefficient. Additional surveys can be conducted at a flow coefficient which enhances tone generation.
- Directivities of the overall noise and for the discrete tones must be determined to aid in identifying the tone generation mechanisms.
- Noise as a function of rotor-obstruction separation must be determined for obstructions with various known wake characteristics.
- The effects of inflow distortion sources, common to typical installations, should also be determined.
- Various schemes to improve inflow homogeneity and resultant noise reduction can be attempted.

2. EXPERIMENTAL SURVEYS

2.1. Experimental Setup

2.1.1. The ARL/FED Anechoic Chamber

All of the acoustic surveys were conducted in the ARL/FED Anechoic Chamber. The construction and performance of this chamber have been detailed by Marboe and Fitzgerald (1981). The chamber had the advantage of being "air breathing," so that fans exhausted out of the chamber could operate continuously at free delivery. The chamber is classified as anechoic above 230 Hz, moderately anechoic (with spherical spreading of radiation from a point source) above 200 Hz, and semi-anechoic above 50 Hz. The transmission loss of the chamber is greater than 30 dB for frequencies between 100 and 10,000 Hz. For this reason, the data are reported down to 150 Hz.

2.1.2. Fan Mounts and Exhaust Ducting

Each fan was mounted on a wooden ring whose inside diameter was slightly greater than that of the fan shroud at its exit. The fans were then sealed with wax to prevent leakage around the edges. The ring was bolted onto a flange installed on the exhaust duct. The duct was that used by Fitzgerald (1982). The duct was lined with absorbent foam to attenuate modes along its length. Outside the chamber, the duct was seated in a frame which also supported the throttle, as shown in Figure 2.1.1. The throttle was anechoically terminated to alleviate buildup of standing modes within the duct.

The static pressure rise in the duct was measured using a simple fluid manometer. The duct tap was flush-mounted to the inner wall of

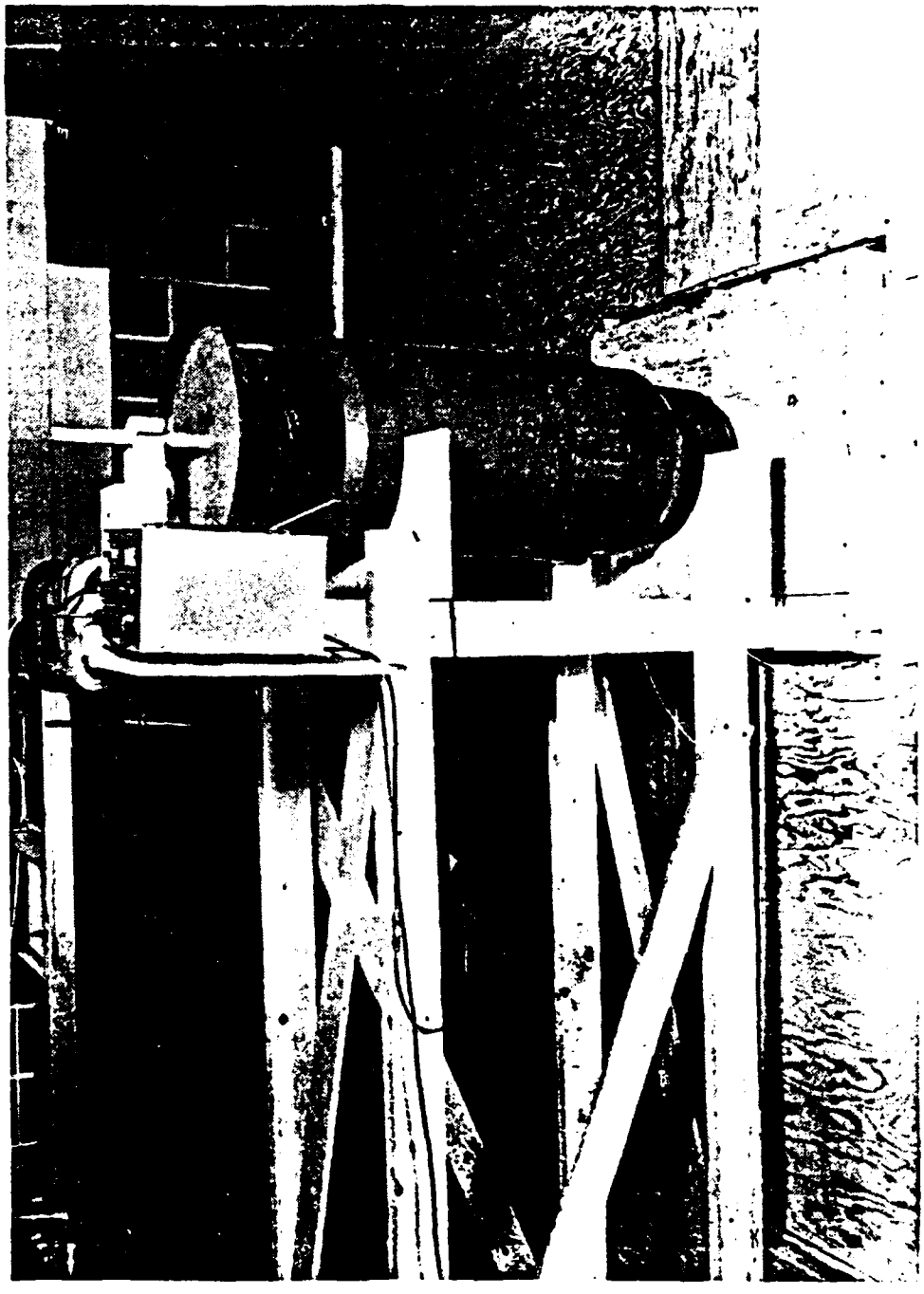

Figure 2.1.1 . Photograph of Fan Exhaust Duct, Throttle, and Duct Support Frame Exterior to Chamber.

the duct, and a tap inside the anechoic chamber was connected to the other end of the manometer.

2.1.3. The Microphone, Its Mount, and the Obstruction Traversing Device

A Bruel and Kjaer 1.27 cm (0.5 in.) microphone #4133 was used throughout the experiment. Mounted on a Bruel and Kjaer #2609 preamp, the assembly was clamped onto the upright of a traversing boom. The boom length was set such that when rotated, the microphone diaphragm was always 1 m (39.4 in.) from the center of the face of the fan hub. The boom was rotated by means of a gear-reduced Slo-Syn Indexer motor at a rate of 3° of arc per 500 counts. The motor mount was seated on a small wooden table set among the floor anechoic wedges. The table was draped with acoustic foam to minimize reflections. The mounting system was adjusted so that at 0° of arc, the microphone was placed along the principal axis of the fan/duct system. For the Phase I survey, the various obstructions were mounted on a two-dimensional linear traversing device. The device, consisting of worm-screw-style traversers operated by Slo-Syn Indexer motors, stood on steel legs that fit among the floor anechoic wedges. The traverser was mounted to provide motion vertically and horizontally (parallel to the fan/duct principal axis). A series of aluminum bars and clamps served to hold the obstructions in place.

The microphone, its mount and boom, the linear traverser, a cylindrical obstruction, and a mounted fan can all be seen in Figure 2.1.2.

2.1.4. The Electronic Instrumentation

Figure 2.1.3 is a schematic diagram of the electronic

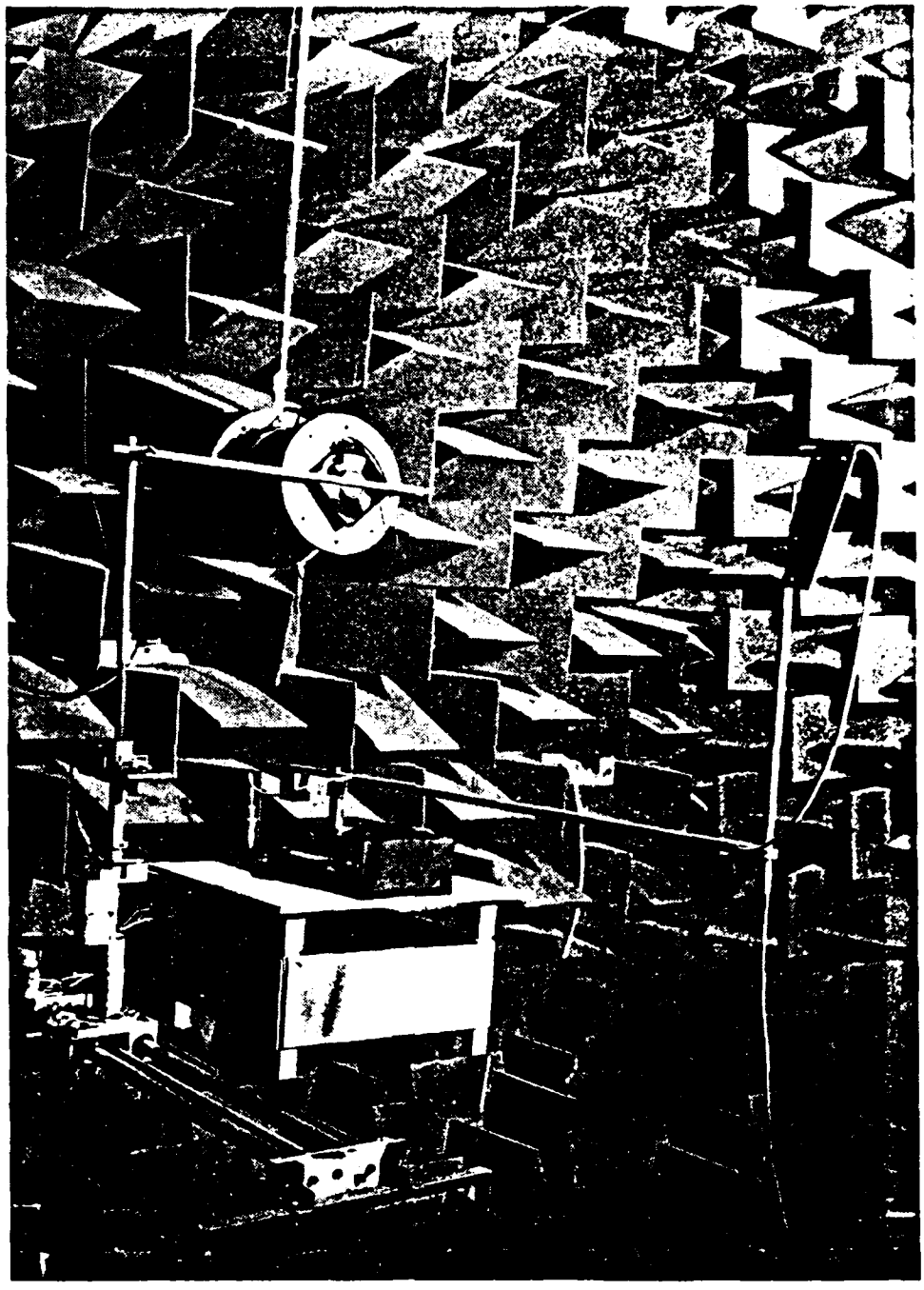

Figure 2.1.2 . Photograph of the Experimental Setup Inside the Anechoic Chamber. Included are a Mounted Muffin XL, the Cylindrical Obstruction on the Two-Dimensional Traverser, and the Microphone on its Mount, Boom, Traverser and Stand.

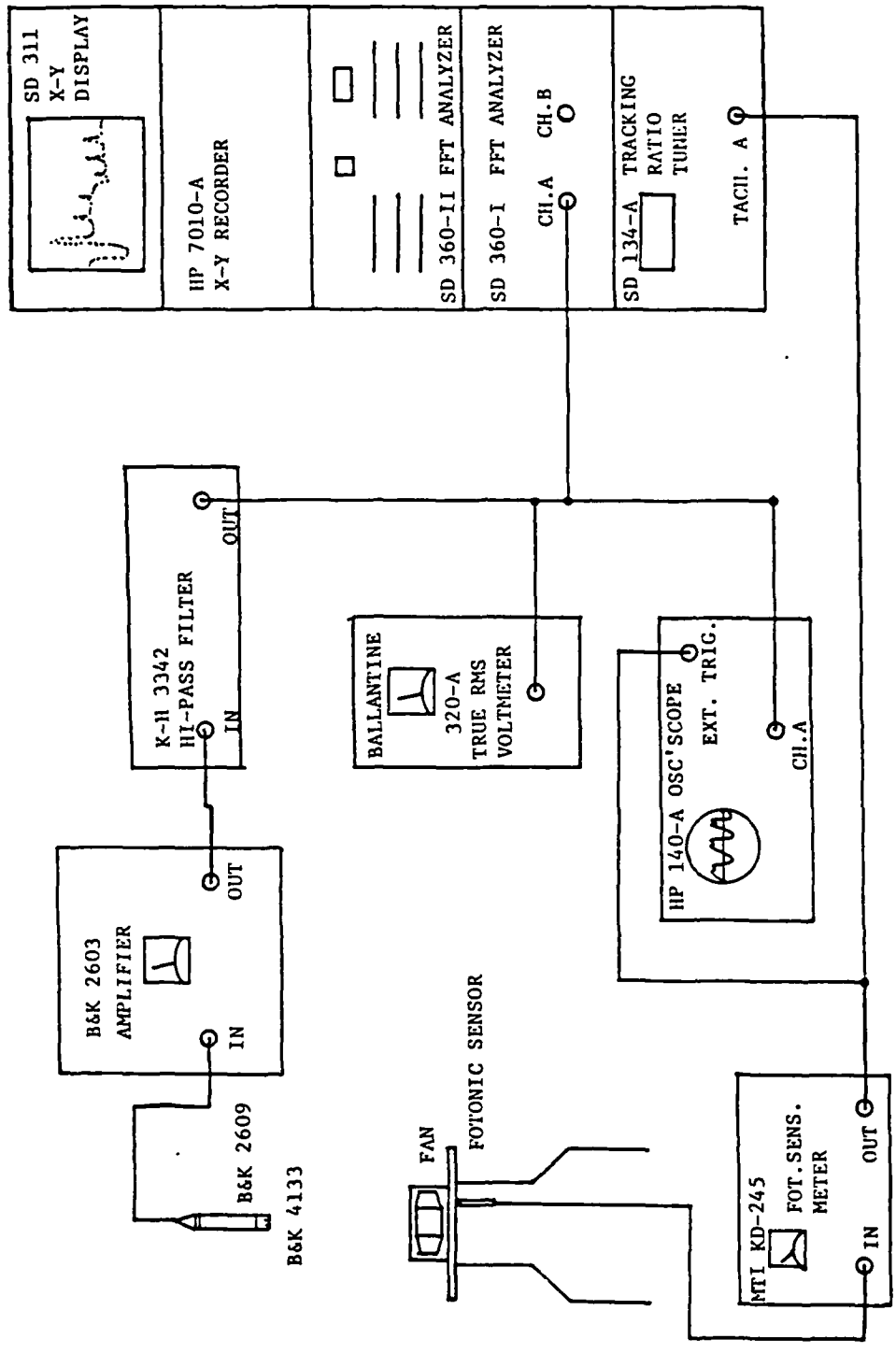

Figure 2.1.3 . Schematic Diagram of the Spectral Analysis Electronics.

instrumentation used in the spectral analyses, and Figure 2.1.4 is a photograph of these instruments. The preamplified microphone signal was passed to a Bruel and Kjaer #2603 amplifier which was set to pass frequencies from 20 Hz to 40,000 Hz. An output signal was taken from the "Recorder" port and filtered by a Krohn-Hite #3342 High-Pass Active Filter. The cut-off frequency was set at 50 Hz to reduce extraneous background noise present in the facility. During Phase II it was set at 130 Hz to reduce the effect of turbulent bursts generated near stall by the larger of the two fans tested. Since electrical noise harmonics at 60 Hz and 120 Hz were reduced as well, the 130 Hz cut-off was used for the remainder of the survey.

The filter output was branched to three instruments. An HP #140-A Oscilloscope was used as a monitor of the microphone signal. A Ballantine #320-A True RMS Voltmeter was used to determine the Overall Sound Pressure Level (OASPL). With a time constant of 3 seconds, the total acoustic pressure represented in the filtered band was free from short-term fluctuations in level. Finally, the filtered signal was the input to one channel of a Spectral Dynamics 360 Fast Fourier Transform (FFT) Spectral Analyzer (SD 360).

A tachometer pulse at the blade passage rate was made available by an MTI #KD245 Fotonic Sensor. Light from its fiber-optic probe was reflected by tiny pieces of aluminum tape fixed to the trailing edge of each fan blade near the hub. The sensor driver translated the return light pulse into a voltage pulse of about 2 volts peak height. This pulse signal was used as an external trigger for the oscilloscope and as the tachometer signal for the spectral analyzer.

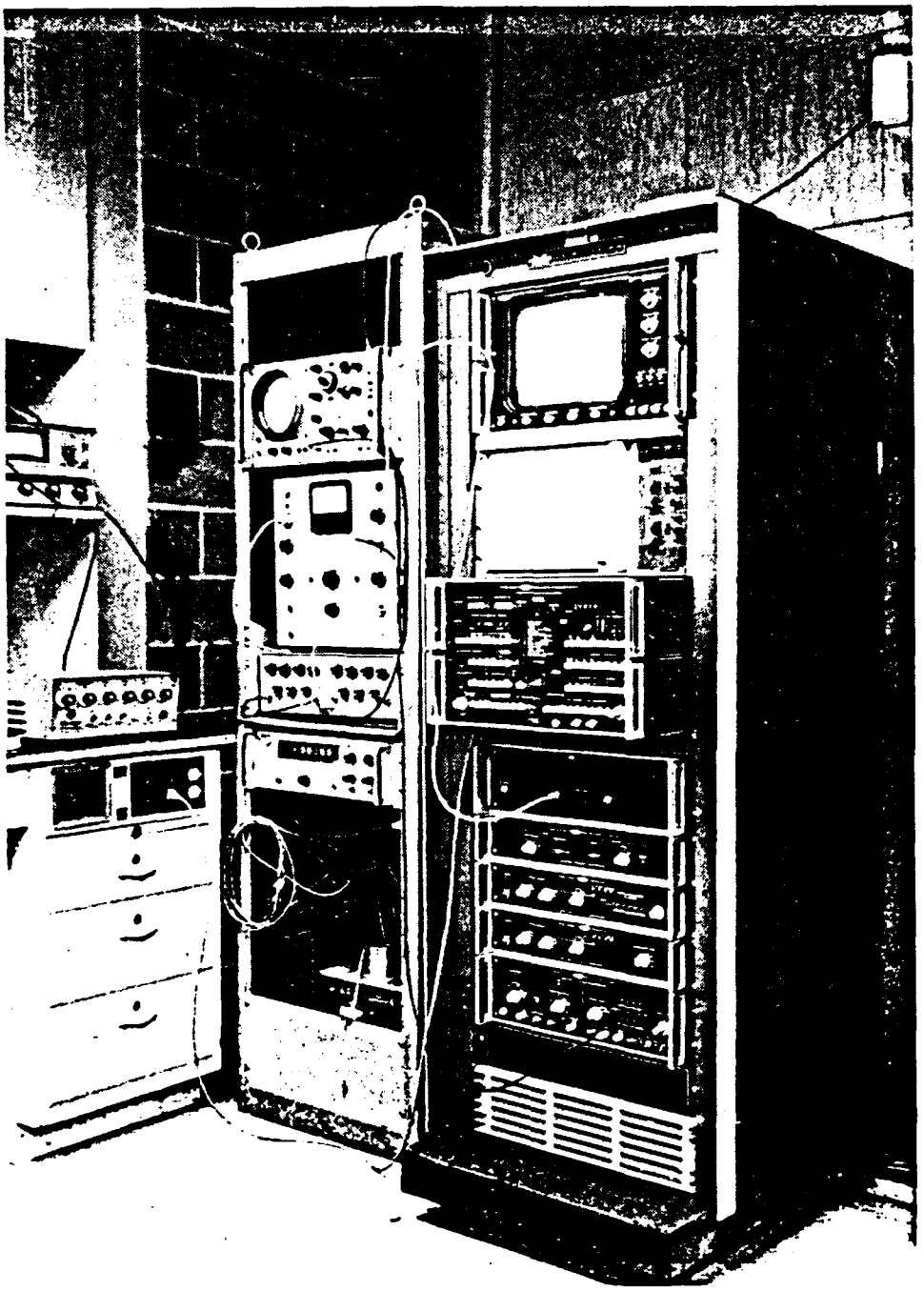

Figure 2.1.4 . Photograph of the Electronic Instruments. Far Left: Slo-Syn Indexer. Center: Oscilloscope, Amplifier, Filter, Up-Down Counter, 220 V Transformer (Partially Hidden). Right: SD 360 Spectral Analysis System.

Synchronous Signal Averaging (as explained in Section 3.1.1) was achieved through use of a Spectral Dynamics #134-A Tracking Ratio Tuner (TRT). The Fotonic Sensor pulse train was the input to "Tach A." The Blade Passage Frequency (BPF) was available from the front panel LED read-out. (Internal multiplication by 100 yielded steady accuracy to 0.1 Hz.) A conditioned tachometer pulse train (TTL compatible) was taken from output J7 of the TRT and sent to input J14 ("Sync In") of the SD 360. When the analyzer was run in functions #13 or #12, its memory update rate was locked to the incoming tachometer rate and to the fan BPF.

Control of the two-dimensional linear traverser and the rotating microphone boom was achieved using a Slo-Syn Preset Indexer. The position of each traverser was displayed as a number of counts by a Hewlett-Packard #5280-A Reversible Counter. Each Slo-Syn motor was operated individually by transferring the drive cable.

The temperature inside the chamber was monitored using a thermistor mounted on the boom near the microphone. The thermistor was part of a STO-LAB #911 Electronic Thermometer, whose output (in degrees Celsius) was displayed on a digital DC voltmeter.

2.1.5. System Calibration

For each experimental run, the entire system was calibrated to a known acoustic standard. The microphone was removed from the chamber and mounted vertically in a stand. A Bruel and Kjaer #4220 Piston phone was placed on the microphone. It produced a signal whose level in the controlled volume is 124 dB relative to 2×10^{-5} N/m^2 (20 μPa). The gain of the 2603 amplifier was adjusted so that the Ballantine

Voltmeter read a total of 124 dB (including a constant additive factor).

After using the internal calibrator of the SD360 Analyzer to adjust the output gains to the display screen and plotter, the signal from the 2603 was applied, and the input attenuation was adjusted to get a full-scale output from the primary frequency of the Piston phone. This input attenuation, called A_1, was noted. The microphone was returned to the the chamber, and a 60 dB gain (G) was added at the amplifier for the levels of fan noise encountered.

During a run, the input attenuation of the SD 360 was adjusted to allow full dynamic range without distortion. This value was noted as A_2. At that point, the level for each bin of the digital analyzer could be read as an equivalent Sound Pressure Level (SPL) for each frequency band through the use of the relation:

$$SPL\ (f) = (124 - G) + (A_2 - A_1) + L(f), \qquad (2.1)$$

where L is the value in dB read from the analyzer. All spectral levels were subsequently reported in dB re 20 μPa at 1 m (39.4 in.) per unit bandwidth.

2.2. Description of the Fans

Two fans were chosen for this study: the Muffin XL (MX 2A1) and the Patriot (PA 77 B3), both manufactured by Rotron, Inc. of Woodstock, NY. These were two of the four fans whose acoustic properties were studied in detail by Fitzgerald (1982) and are described in his Appendix A. A front elevation photograph of the fans appears in Figure 2.2.1a, while Figure 2.2.1b shows a rear view including the mounting tubes for the Fotonic Sensor probe.

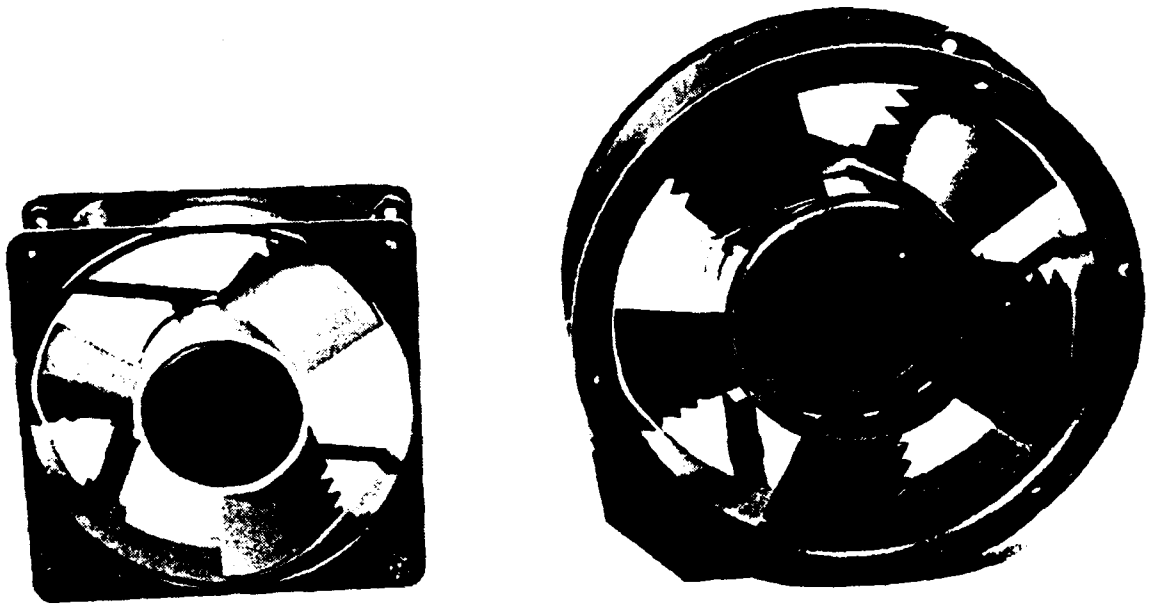

Figure 2.2.1 . Photographs of the Muffin XL Fan and the Patriot Fan.

(a) Front View (Patriot on Right).

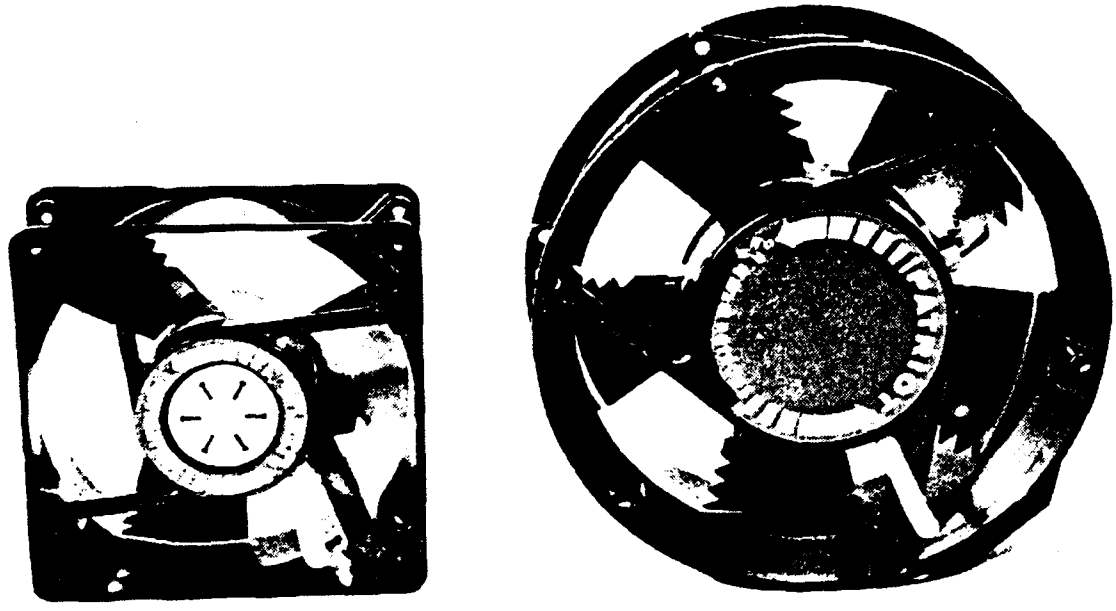

Figure 2.2.1. Continued.

(b) Rear View. Note Fotonic Sensor Guides Attached to Hubs.

These fans were chosen for several reasons. First, they are in common use in many cooling applications. Second, they represent a wide range of pumping duties. Third, they differ from one another in significant ways.

The Muffin XL is a 3-bladed fan with an operating speed of 3120 rpm. At free delivery, it nominally provides a flow rate of 54.3 Liters/sec (115 CFM). It features four struts mounted tangentially downstream of the fan, and a square housing with a cylindrical shroud. The tip diameter is 11.1 cm (4.37 in.) and the tip Mach number is nominally 0.054.

The Patriot is the larger of the two fans. While the rotor speed of 3420 rpm is only slightly higher, the 5-bladed design delivers a nominal 113.3 Liters/sec (240 CFM). With a tip diameter of 14.3 cm (5.63 in), the Patriot has a tip Mach number of 0.075. It features three tangentially mounted downstream struts, and both its housing and shroud are cylindrical.

A significant feature of both fans is the presence of trailing edge serrations on the rotors. The original intent of these serrations was to diminish the effects of vortex shedding noise. This noise is prominent at high flow rates where loading is light, and is predominantly broadband. Longhouse (1977) observes that the noise can be reduced if the laminar boundary layer is tripped prior to leaving the trailing edge of the blade. He further states that trailing edge serrations are not a viable means of reducing rotational noise since they exist in the separation bubble of the trailing edge, and that they reduce aerodynamic performance. Fitzgerald (1982) confirms this and shows that leading edge serrations are a better solution. The models

of the Patriot received from the manufacturer for this survey do have small indentations formed in the blade leading edges which were not present on the models used by Fitzgerald. They do not appear to significantly alter noise generation. Since the goal of this survey is to examine the effect of inlet conditions on fan noise generation, no alterations were made to the fans or blades themselves.

2.3. Survey Phases

2.3.1. Phase I: Inflow Obstructions

2.3.1.1. Types of Obstructions

In the first phase of the experimental surveys, some measure of the acoustical effect of upstream obstructions was desired. In a typical installation, the fans are mounted to move air from the interior of the device being cooled to the exterior environment, as shown in Figure 2.3.1. Cooling engineers have found that this configuration provides more desirable flow and better cooling throughout the device. Unfortunately, it is not desirable acoustically, since the fan inlets are obstructed to different degrees by various structures inside the device. The wakes shed by these structures, when ingested into the fan, are the major sources of discrete frequency acoustic radiation, as discussed in Chapter 1.

Four different types of obstructions were used in the surveys. The choice of their shapes was based on observations of obstructions found in typical installations. The first three are shown schematically in Figure 2.3.2a. The first was a cylindrical, aluminum rod, 1.27 cm (0.5 in.) in diameter. The rod was long enough to extend well past the inlet of the fan on either side. While it

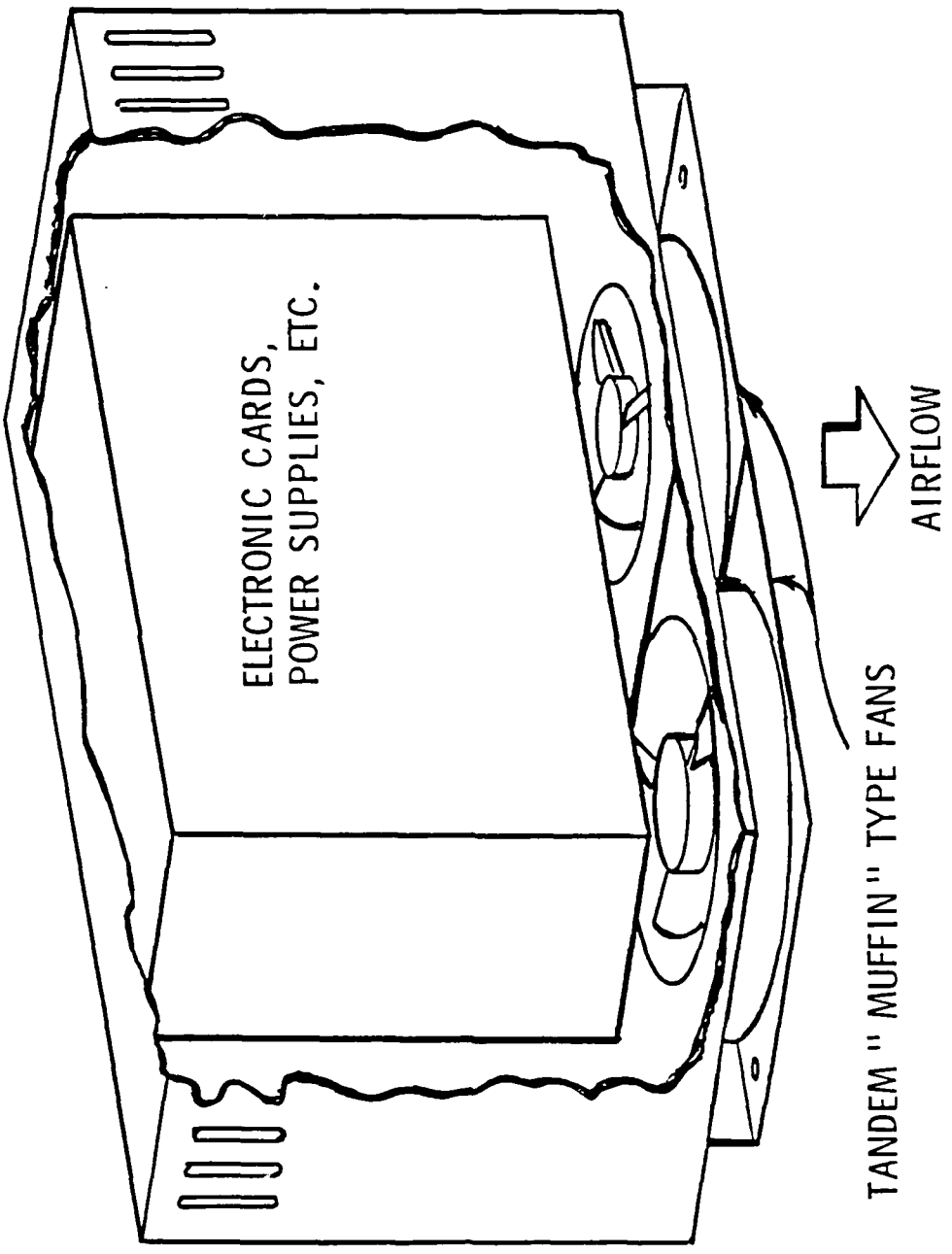

Figure 2.3.1 . Schematic Diagram of a Typical Cooling Fan Installation in Computer Equipment.

CYLINDRICAL ROD

"THIN" RECTANGLE

"THICK" RECTANGLE

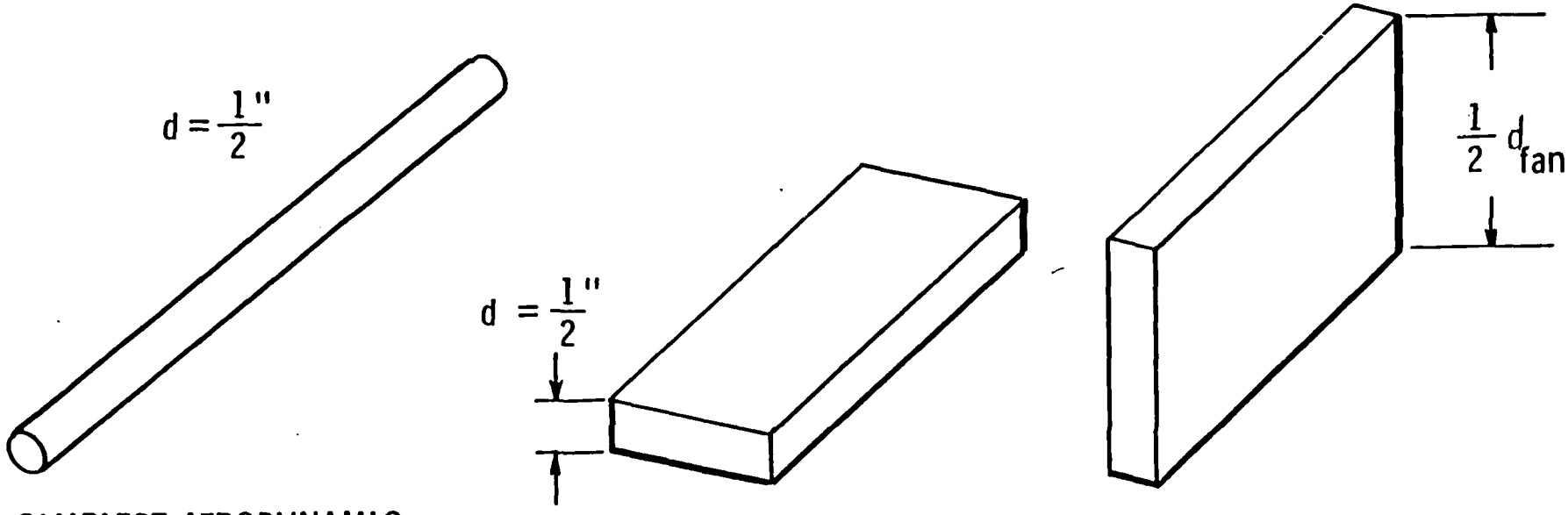

SIMPLEST AERODYNAMIC SHAPE

CABLES, STRUTS, SUPPORTS, ETC.

SIMPLEST NON-AERODYNAMIC SHAPE

STRUCTURAL MEMBERS FOR CARD RACKS, ETC.

LARGE OBSTRUCTIONS, POWER SUPPLIES, ETC.

Figure 2.3.2 . Obstruction Models.

(a) Schematic Diagram of Simple Obstructions (Airflow from Right to Left).

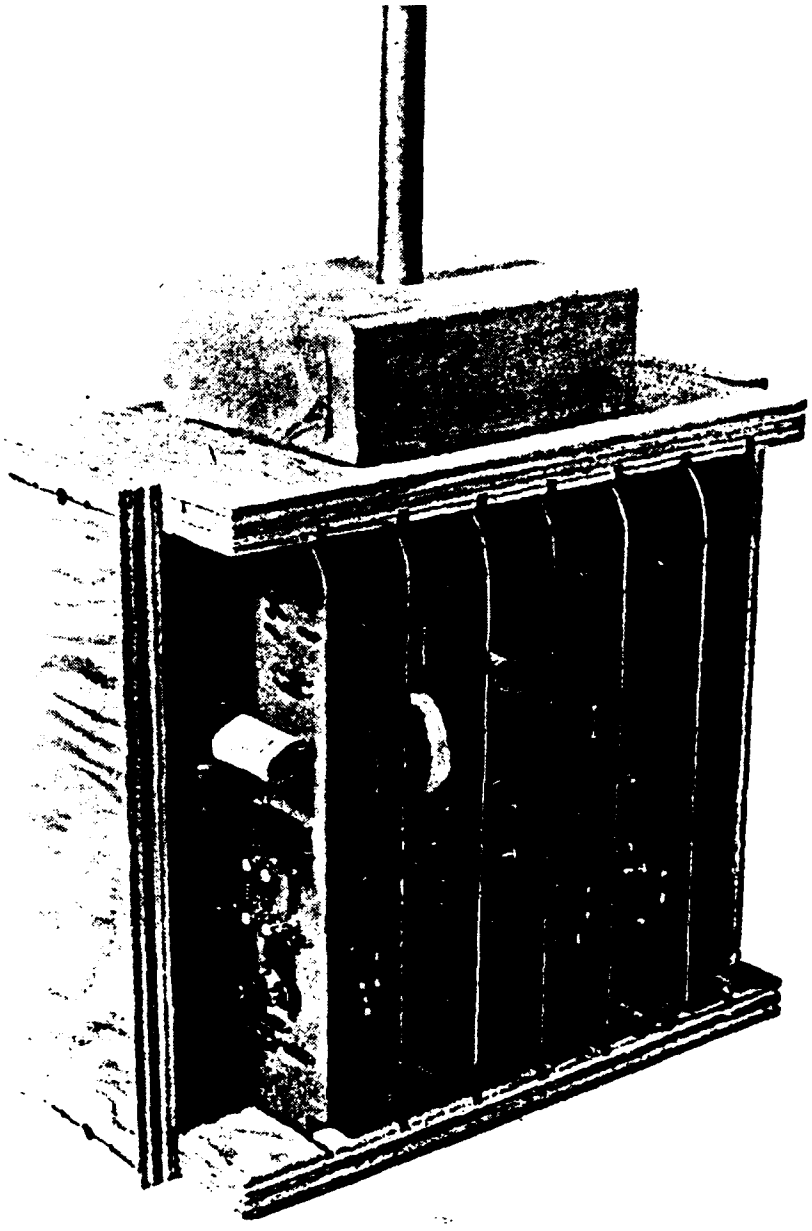

Figure 2.3.2 . Continued.

(b) Photograph of Card Gate Model (Airflow Parallel to Card Widths).

adequately modeled cables and struts seen in typical installations, it was chosen primarily because its shape is aerodynamically simple. As such, it received the most attention of all the obstructions. The second was a rectangle which presented its smallest side, 1.27 cm (0.5 in.) to the fan inlet and will be referred to as the "thin" rectangle. Like the rod, its length was greater than two fan diameters. In typical devices, internal structural members used to physically support those items which require cooling are found crossing the fan inlet. The thin rectangle was chosen as a simple "non-aerodynamic" shape to model these structures. In one installation, a box containing a large power supply was found blocking approximately one-fourth of the fan inlet. To model these large obstructions, a "thick" rectangle was used. The dimension presented to the fan inlet was approximately equal to one fan radius. The fourth upstream obstruction, shown in Figure 2.3.2b, was a crude model of a typical rack of electronic cards. The intent was to create a large, spatially periodic structure with complex internal flow paths. Because the primary purpose of using these fans is to cool electronic components, it is necessary to obtain a measure of their influence on fan noise generation. The outside walls were made of 1.3 cm (1/2 in.) plywood with outer dimensions 19.4 cm (7 5/8 in.) by 22.9 cm (9 in.). The cards were .16 cm (1/16 in.) thick and were separated by 2.54 cm (1 in.).

2.3.1.2. Obstruction Locations

Each obstruction was mounted in turn and moved by the two-dimensional linear traverser described in Section 2.1.3. A coordinate system was established as in Figure 2.3.3. The (x,y)-plane was parallel to the fan inlet face, with the x-direction horizontal and

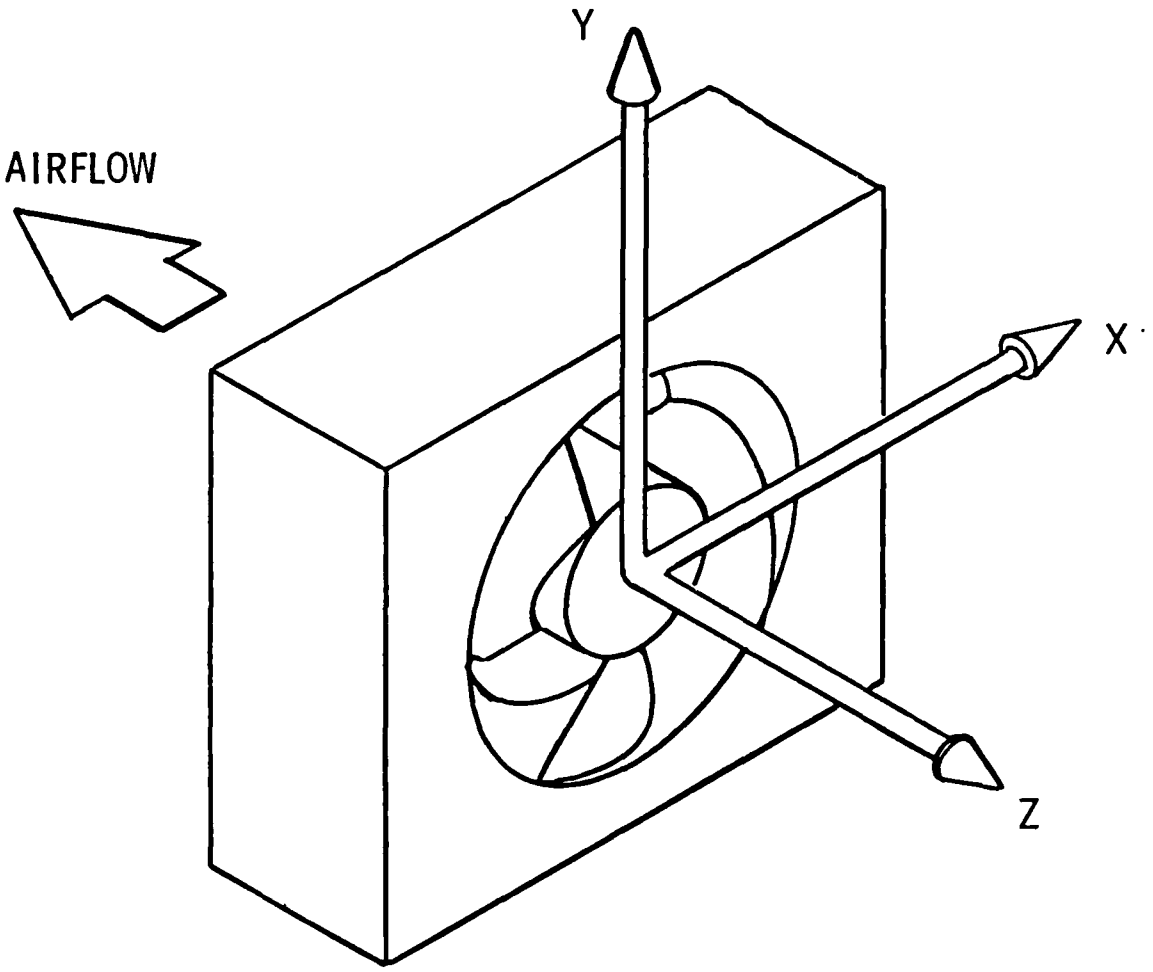

Figure 2.3.3 . Schematic Diagram of Fan Coordinate System Definition. Obstructions were Symmetrical in (x) and Were Moved Axially (z) and Radially (y).

the y-direction vertical. The z-direction described the fan/duct system principle axis, pointing upstream of the fan. The position of (0,0,0) was taken to be the center of the hub, and as close as the obstruction's trailing edge could be placed to the hub face (about 0.15 cm (.063 in.)).

The obstructions were designed to be symmetric in x, i.e., about the (y,z)-plane. In this way, the effect of obstruction location on fan noise was essentially reduced to a two-dimensional problem. The surveys were conducted likewise: an obstruction could be moved in the z-direction, defining its axial location, or it could be moved in the y-direction, defining its radial location. In "z-scans," the obstruction was positioned at (y,0) and moved away from the fan parallel to the principle axis. In "y-scans," the obstruction was moved across the fan inlet from (0,0), so that the center of the obstruction traversed the fan radius. Rectangular arrays of regular (y,z)-positions were usually created through successive z-scans.

The position of an obstruction relative to its starting location was very accurately known, since the traversers had resolutions of 10,000 counts per inch vertically and 20,000 counts per inch horizontally. However, this did not aid the establishment of the (0,0,0)-position, or origin, for each survey. Typically, a trial-and-error process was utilized once the obstruction was mounted. Its radial position relative to the fan would be measured above and below, and it would then be moved by the traverser until the measurements agreed to within 0.04 cm (0.016 in.). Another difficulty arose with the vertical traverser. The worm-screw was loose inside the drive, and as the bearings rotated to lift or lower the screw, the

applied torque would turn the screw slightly on its axis. The angle through which it turned was very small (on the order of 1 degree), but at the center of the obstruction this was translated into approximately 0.3 cm (0.11 in.). Even this small change critically affected the tonal noise in the region very near the fan inlet. The only viable solution was to approach successive points from the same direction as that which was used to set the origin, so that the screw was always rotated to the same limit.

2.3.2. Phase II: Inlet Configurations

The purpose of these surveys was to examine the effect of modifying the fan inlet environment relative to the free-field inflow in which they operated in Phase I. Specifically, three major modifications were used. These included large baffles, commercially available finger guards, and honeycomb flow-straighteners.

2.3.2.1. Inlet Baffles

While investigating noise sources in a statically mounted NASA QF-1B fan, Hanson (1977) showed that streamlines entering the fan near the blade tips could be traced behind the fan inlet. Thus, objects to the rear of a fan can act as obstructions. This was observed on the Muffin XL and will be discussed further in Chapter 3. Since fans in an installation are moving air from one "half-space" to another, flow does not enter a mounted fan from behind. To model this and examine its consequences on the data presented for Phase I, each fan was mounted behind a large baffle. The dimensions of the Muffin XL baffle were 55.24 cm x 89.85 cm (21.75 in. x 35.375 in.), or approximately 5 x 8 fan diameters. Those for the Patriot were 79.38 cm x 89.85 cm (31.25

in. x 35.375 in.), or 5.5 x 6.3 fan diameters. They were large enough to preclude significant flow from beyond their edges.

The baffles were hand cut from 1.27 cm (0.5 in.) plywood, and the inlet diameters were cut to be just larger than the edge of each fan's circular shroud. The mounting bolts were countersunk and smoothed with wax, and the exterior edges of the fans were sealed with wax where they met the baffle.

2.3.2.2. Finger Guards

For safety reasons, finger guards are mounted over fan inlets. Because they are in the immediate proximity of the fan inlet, they were studied as separate inlet configurations. Figure 2.3.4 shows two typical guards used commercially for the Muffin XL (guards for the Patriot were not available). Both are constructed of heavy guage wire spot-welded to create a frame. One guard consists of a simple, square frame that bolts onto the fan inlet, while the other consists of circular pieces on a frame that is raised about 1.3 cm (0.5 in.) above the bolted feet. Tests were made with each guard bolted to the fan alone, as well as bolted onto the inlet baffle in front of the fan.

2.3.2.3. Honeycomb Flow Straighteners

Many of the inflow distortion sources and acoustic radiation problems of axial flow cooling fans resemble those encountered in the testing turbofans which are mounted on static tests stands. To control inlet conditions, many researchers use Inlet Flow Control Devices (IFCD's). Magliozzi and Metzger (1974) recommend the use of upstream flow straighteners made of honeycomb and wire mesh as long as the wake size is small relative to blade chord and span. Lumley and McMahon

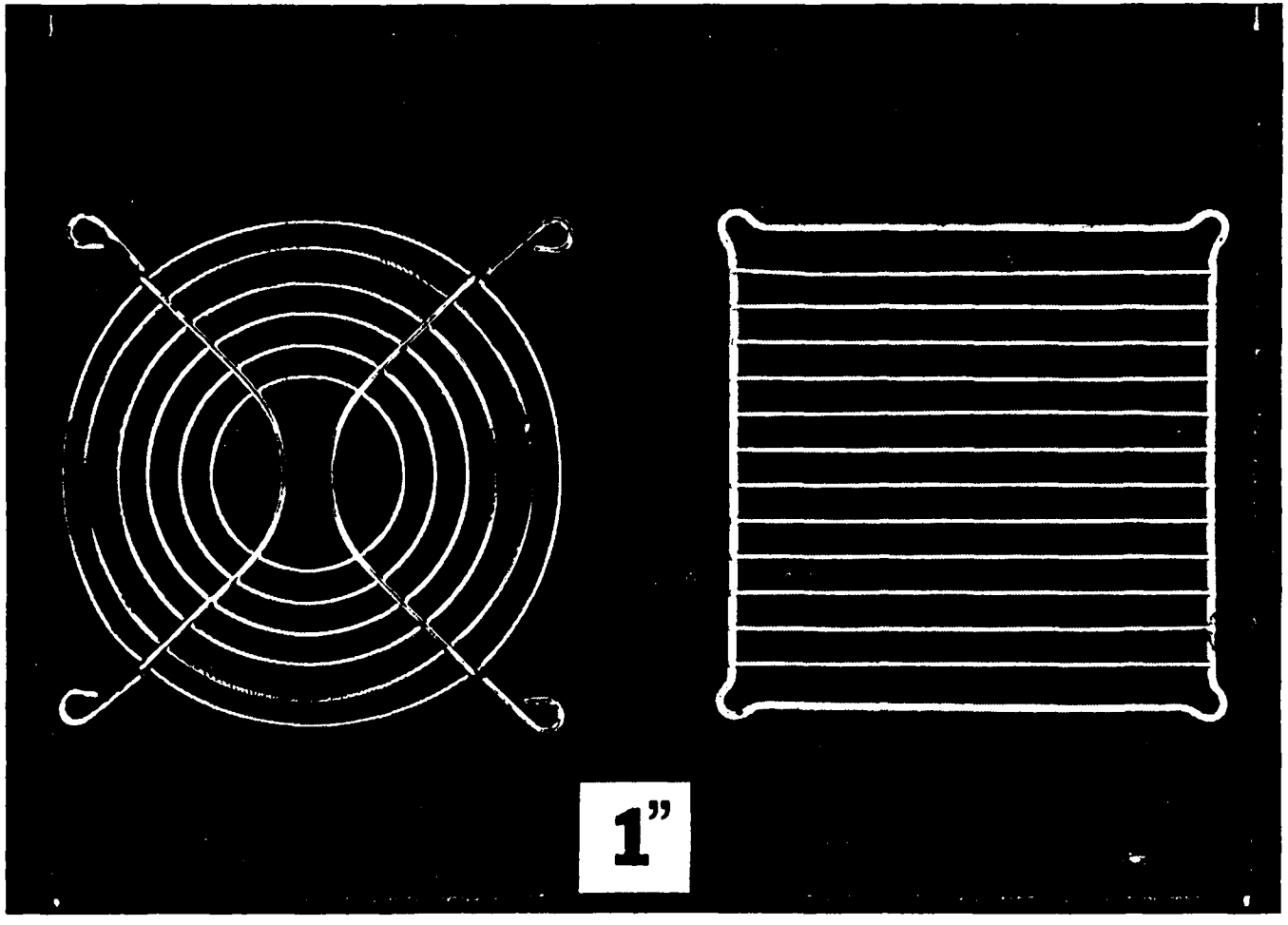

Figure 2.3.4 . Photograph of Muffin XL Finger Guards. Reference is 2.54 cm (1 in.). (Note that Circular Guard has Raised Profile of 1.3 cm (0.5 in.) Not Apparent in Photograph.)

(1967) had tested such a device in a water tunnel to reduce turbulence intensity by destroying transverse velocity components. Redesign of a NASA-Lewis IFCD was completed by Ho, Smith, and Kantola (1979) to reduce axial turbulence intensity as well. These turbofan IFCD's were designed to simulate the lower discrete-tone levels found in flight tests (Woodward, Wazyniak, Shaw, and MacKinnon, 1977). They were made of honeycomb and wire mesh and usually had a large, mushroom-like shape.

The results varied quantitatively, but the qualitative behavior was consistent. Shaw, Woodward, Glaser, and Dastoli (1977) managed to reduce the Sound Pressure Level of the BPF by 5 dB: although circumferential turbulence scales were reduced, axial scales increased. This work was done in a wind tunnel. When transferred to an anechoic chamber (Woodward, et al., 1977), the BPF was reduced 10 dB, and the first harmonic, 2 x BPF, was reduced 5dB. Circumferential turbulence was greatly reduced, but only the length scale of axial turbulence was reduced. The most common trend was that found by Ho, et al. (1979). Their IFCD reduced axial and circumferential turbulence intensities to less than 0.5%, and the BPF was reduced to the broadband background level. Even so, no appreciable reduction was made of the harmonics of the BPF. Peracchio (1981) found similar results. By combining an IFCD with a reverse cone inlet and boundary layer suction, Kantola and Warren (1979) were able to reduce the BPF by 16 dB.

Since the BPF tone proved to be the most difficult to control (see Chapter 3), a honeycomb flow straightener was considered for the Phase II surveys. It offered the possibility of reducing inlet distortion, particularly from flow well off the fan axis, as well as a measure of

safety protection. However, the same space constraints that make use of a bellmouth inlet impractical certainly rule out a large IFCD styled after Woodward, et al. (1977). Even so, a simple single layer sheet of honeycomb was investigated as an inlet configuration.

The honeycomb was 1.27 cm (0.5 in.) thick aluminum with hexagonal 0.32 cm (0.125 in.) cells. The structure was #50/52 aluminum with a foil gauge of 0.0038 cm (0.0015 in.), and it was cut into 30.5 cm x 30.5 cm (12 in. x 12 in.) sheets. They were carefully bolted onto the fan inlets to avoid crushing any cells, and the outside edges of the fan shroud were sealed with wax where they met the honeycomb. Tests were made with the honeycomb flush-mounted in this manner and also with the honeycomb separated from the inlet by a 0.32 cm (0.125 in.) gap (again with the edges sealed).

3. RESULTS AND DISCUSSION OF THE SURVEYS

3.1. General Results and Baseline Acoustic Data

For reference to all further stated and plotted Sound Pressure Levels, the average baseline values of the blade passage tones for the two fans are shown in Table 3.1.

3.1.1. Synchronous Signal Averaging

The primary intent of this investigation is to determine the properties of the discrete frequency acoustic radiation generated by axial flow fans. However, several processes simultaneously generate random, broadband acoustic noise. Likewise, nonstationary changes in the tone levels occured over intervals on the orders of one and ten seconds, due to large-scale turbulence in the chamber. This nonstationarity is also reported by Hanson (1974). It is necessary to process the time history data to resolve the discrete frequencies from the contaminating broadband noise. The technique most commonly employed is spectral averaging. The principle of this scheme is to Fourier transform successive time data records and add each new transform to the previous sum. Each additional spectrum is weighted by a factor (1/n) where n is the number of averages taken. This yields an ensemble average of the energy in each frequency bandwidth.

The result of such a process is shown in Figure 3.1.1a. The Sound Pressure Level per unit bandwidth (4 Hz) of the unobstructed Patriot fan is plotted as a function of frequency. The plot is the result of averaging 128 ensembles. The frequency locations of the BPF x 1 through BPF x 11 tones are marked on the plot. Although the averaging process has reduced considerably the percent confidence

TABLE 3.1

SOUND PRESSURE LEVELS (dB re 20 μPa)* FOR THE BASELINE FANS

	MUFFIN XL		PATRIOT	
HARMONIC #	FREQUENCY	SPL	FREQUENCY	SPL
OVERALL	--	52.9	--	58.3
BPF x 1	160.6	44.8	284.3	47.4
BPF x 2	321.2	31.9	568.6	38.4
BPF x 3	481.8	32.1	852.9	34.0
BPF x 4	642.4	42.1	1137.2	25.7
BPF x 5	803.0	25.8	1421.5	23.0
BPF x 6	963.6	31.8	1705.8	28.2
BPF x 7	1124.2	25.3	1990.0	18.8
BPF x 8	1284.8	29.1	2274.4	21.6
BPF x 9	1445.4	21.7	2558.7	18.2
BPF x 10	1606.0	11.4	2843.0	27.4
BPF x 11	--	--	3127.3	19.2

*BANDWIDTHS: OVERALL 20 kHz
MUFFIN XL 4 Hz
PATRIOT 8 Hz

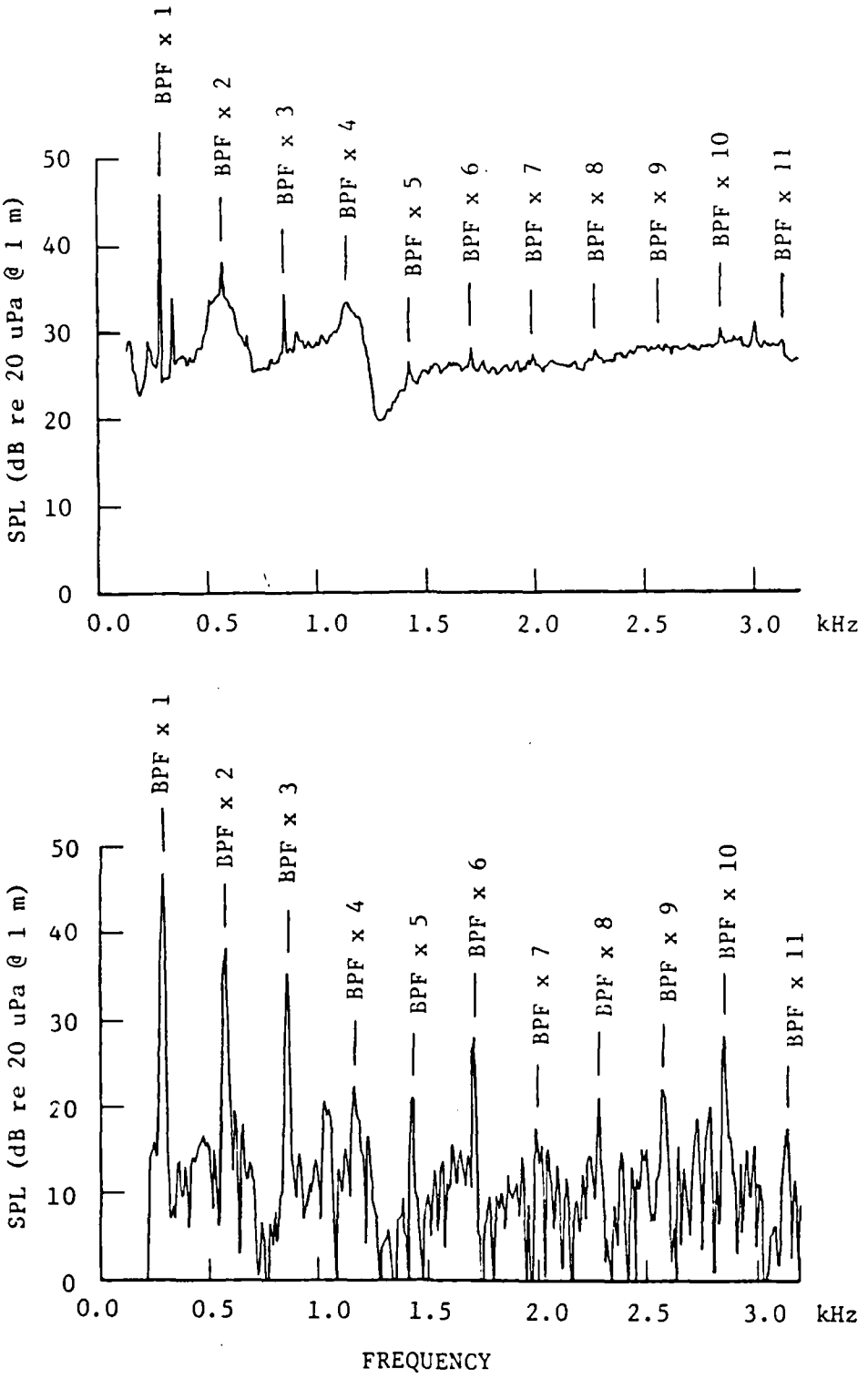

Figure 3.1.1 . Sound Pressure Level (SPL) vs. Frequency for the Unobstructed Patriot Fan.

(a) Unsynchronized Spectrum, 128 Averages (4 Hz Bandwidth).
(b) Synchronized Spectrum, 128 Averages (8 Hz Bandwidth).

interval width for each frequency bin, not all of the marked harmonics can be observed above the broadband background. More averages will not alleviate this problem. It is simply a matter of the random noise contributing more energy per unit bandwidth than the discrete tones at their respective frequencies.

In order to enhance the discrete tones relative to the broadband noise, the process of synchronous signal averaging is utilized. Metzger and Magliozzi (1975) employed this technique to determine the contribution of random noise to the discrete frequency spectrum. To accomplish synchronization, a timing pulse at the blade passage rate is used to synchronize the memory update period of the spectral analyzer. The method of obtaining the timing pulse for these surveys is described in Section (2.1.4.). During each memory period, a record of time history data is taken. Since the period is synchronized to an integer number of blade passages, the next update always begins at a time when the system is physically identical to the previous period. Each successive update is weighted by (1/n), where n is the update number, and it is added to the sum of the previous records. Since the current memory period begins with the same signal phase as its predecessor relative to the rotor blade, any new data which is not phase coherent with the blade rate tends to add to zero over a number of averages. In this way, only that portion of the signal which is phase-locked to the blade will remain following a set of ensemble averages. After a prescribed number of averages (n_d), the time averaged signal is forward transformed once to yield a frequency spectrum. A plot of this transform is shown in Figure 3.1.1b. This spectrum was produced from the Patriot operating identically as it did in Figure 3.1.1a. The

background is reduced approximately 20 dB, and the blade rate tones are clearly visible.

In Figure 3.1.2., an averaged waveform is compared with a single time data record. The turbulence-generated acoustic radiation, which is random in phase as well as magnitude, is largely removed by the 128 averages. In the figure, seven repetitions of the waveform are plotted. Since the fan has only five blades, two of the blade pressure pulses are repeated in this record.

Referring back to Figure 3.1.1b, several features need to be examined. These include the larger apparent bandwidth of the discrete tone peaks, their differences in magnitude relative to the unsynchronized spectrum, and the increased variability in the reduced background. Due to the nature of the spectral analyzer which was used for the surveys, the synchronized spectra used half as many data points as the unsynchronized, thus doubling the bandwidth (8 Hz in the figure). This causes the discrete tones to be wider and alters the levels by a constant factor. Next, because only a single transform is applied to the averaged waveform, the percent confidence interval is relatively wide. This is seen as increased variability of the background levels, but is unimportant as long as the blade passage tones stand out. It also contributes a small amount of variance to the discrete tone levels. These levels also vary from their counterparts in the unsynchronized spectrum because they no longer contain contributions from random-phase noise present in the same bandwidths.

A very important feature of this process is revealed upon close examination of the synchronous signal average plotted in Figure 3.1.2b. Slight variations are apparent in each cycle. These

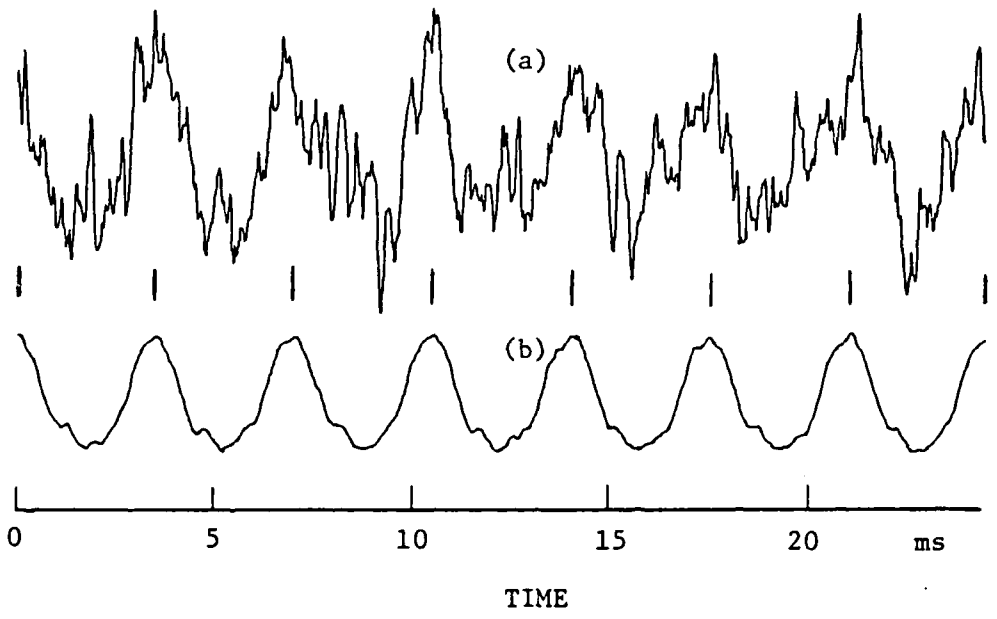

Figure 3.1.2 . Sound Pressure as a Function of Time for the Patriot Fan. (Measured at 1 m, 80 Hz Bandwidth.)

(a) Single Time Record, 512 Points.
(b) Synchronous Signal Averaged Time Waveform, 512 Points.

(Note that the Blade Passage Repetition is Marked Between the Two Waveforms.)

variations have two principal causes. First, the individual blades and their aerodynamic (and acoustic) behavior are not identical, and become less so with increasing frequency. This contributes to the variance in the frequency spectrum. The second cause is an artifact of synchronous averaging. Since the analyzer is synchronized to the blade passage rate, only the BPF x 1 tone undergoes the total number of averages n_d. Each successive harmonic is averaged only (n_d/m) times, where m is the harmonic multiple of the BPF. For example, if the total number of synchronized averages is $n_d = 128$, then the BPF x 8 tone is effectively averaged only $n_d/8 = 16$ times. Since the normalized random error associated with averaging a statistically random process is a function of $1/\sqrt{n_d}$ (Bendat and Piersol, 1980, p. 76), fewer averages inherently yield larger percent confidence intervals. This behavior is plotted in Figure 3.1.3 in terms of total deviation (in dB) as a function of harmonic number caused by random error in averaging for n_d equal to 128 and 256. The higher harmonics are particularly susceptible to this random error, and so they show more variance. This variability in the higher harmonics can only be overcome by increasing the effective number of averages for each harmonic in turn. This is accomplished either by repeating the averaging process once for each desired harmonic and increasing the number of averages accordingly, or synchronizing the analyzer to the higher harmonic rate and averaging n_d times. Both schemes were impractical because of the time involved in gathering the already prodigious amount of data required for each survey.

The residual variance in the averaged waveform also contributes to the broadening of the discrete peaks, since only one transform is

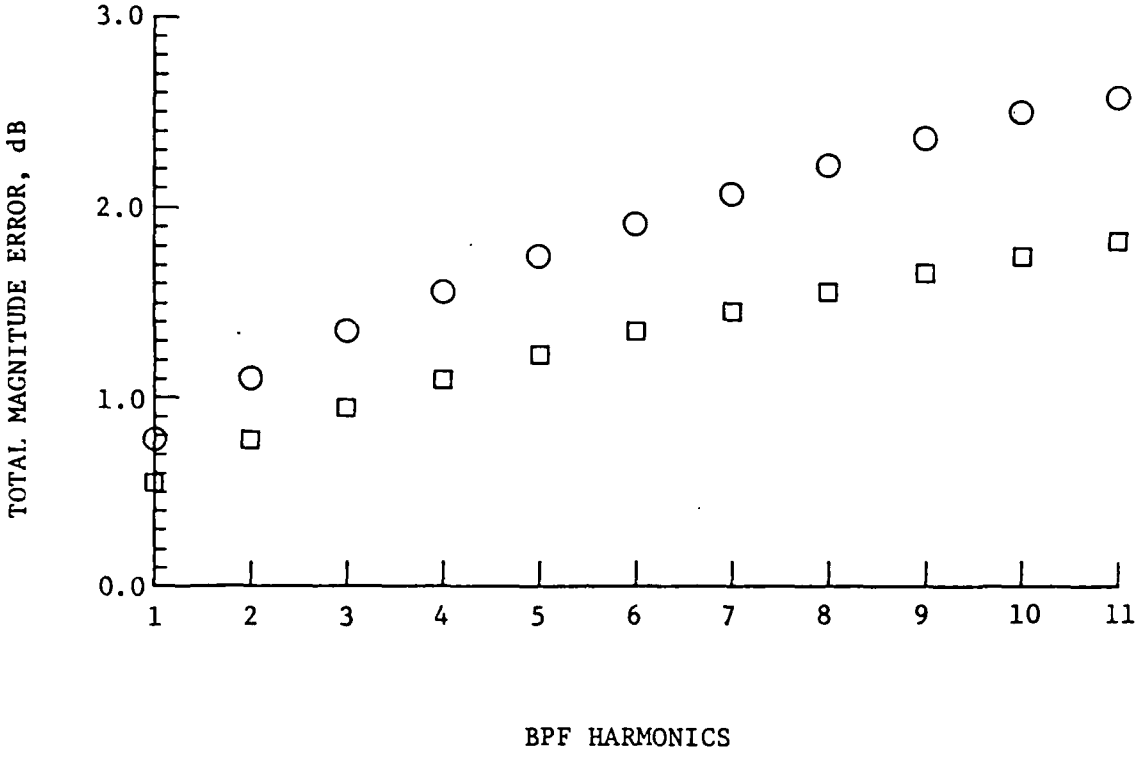

Figure 3.1.3 . Total Magnitude Error in dB vs. Blade Passage Frequency Multiple Number for a Given Total Number of Averages of the BPF ($e_r = 1/\sqrt{n_d}$).

○-- n_d = 128, □-- n_d = 256.

taken. While periodogram-type analyses would reduce the variance in the data, particularly in the background, it does so by smoothing the spectrum. Obviously, this would alter the discrete tones and render the surveys less useful.

3.1.2. Sound Pressure Level vs. Flow Coefficient

The behavior of the Overall Sound Pressure Level (OASPL) as a function of flow coefficient for both fans was like that observed by Mellin (1975). The Muffin XL and Patriot are compared in Figure 3.1.4. The curves are similarly shaped: a high level of turbulent noise associated with stall condition at lower coefficients, a sharp drop in noise in the transition out of stall, and a gradual increase in OASPL as flow velocity increases. The curves do not collapse onto one another on the dimensionless flow coefficient axis because the two fans do not belong to the same fan "family."

Using synchronized spectral analysis, the behavior of the Blade Passage Frequency (BPF) and its first nine harmonics (BPF x 2 - 10) are shown as a function of flow coefficient in Figure 3.1.5 for the Muffin XL and Figure 3.1.6 for the Patriot. As expected, most of the higher harmonics "turn on" as the fans are brought out of stall and flow interactions become less random. It is apparent that the BPF is a major contributor to the OASPL for the highest flow coefficients and tends to control the shape of the OASPL curve in that range. The BPF × 4 tone is also a major contributor for the Muffin XL. It is interesting to note that many of the discrete harmonics increased in level at the lowest flow coefficients. It is likely that in complete stall, the recirculating flow behavior becomes spatially coherent to some degree.

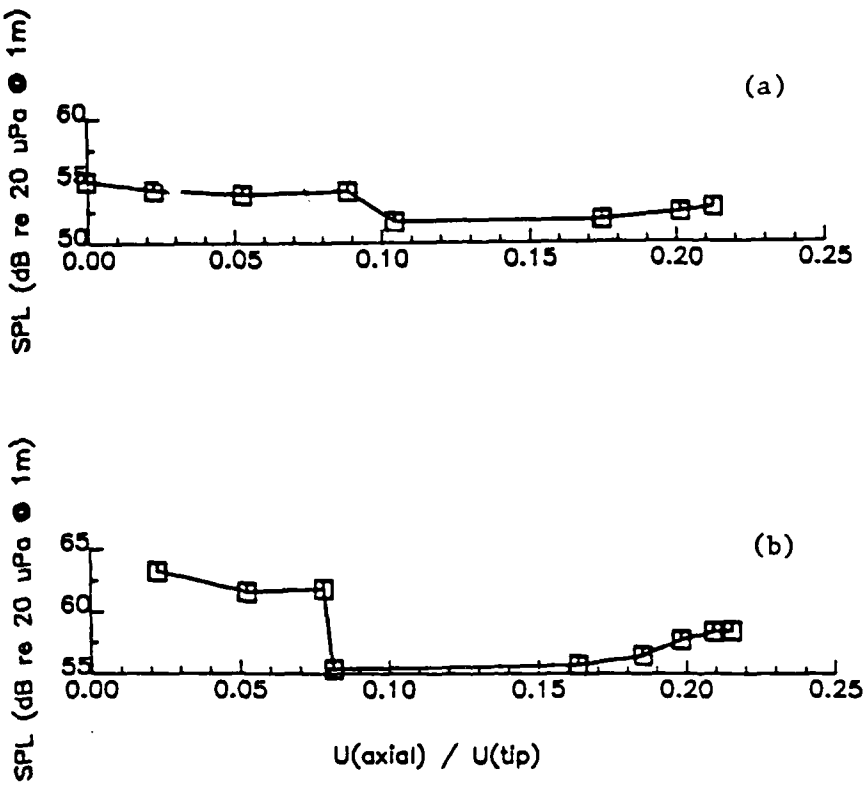

Figure 3.1.4 . Overall Sound Pressure Level (OASPL) vs. Flow Coefficient (Uaxial/Utip).

(a) OASPL for the Muffin XL (20 kHz Bandwidth).
(b) OASPL for the Patriot (20 kHz Bandwidth).

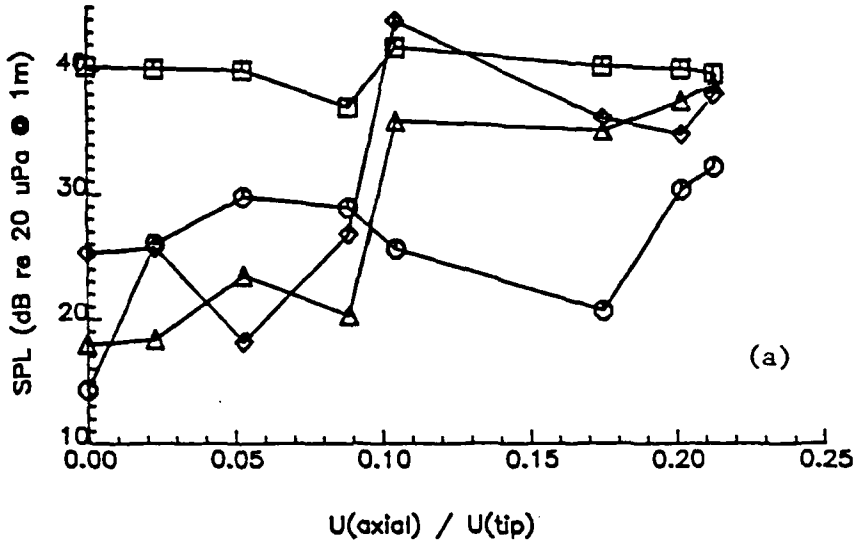

Figure 3.1.5 . SPL of the Blade Passage Tones of the Muffin XL vs. Flow Coefficient (Synchronized Spectra, 4 Hz Bandwidth).

(a) □ -- BPF x 1, ○ -- BPF x 2, Δ -- BPF x 3, ◇ -- BPF x 4.

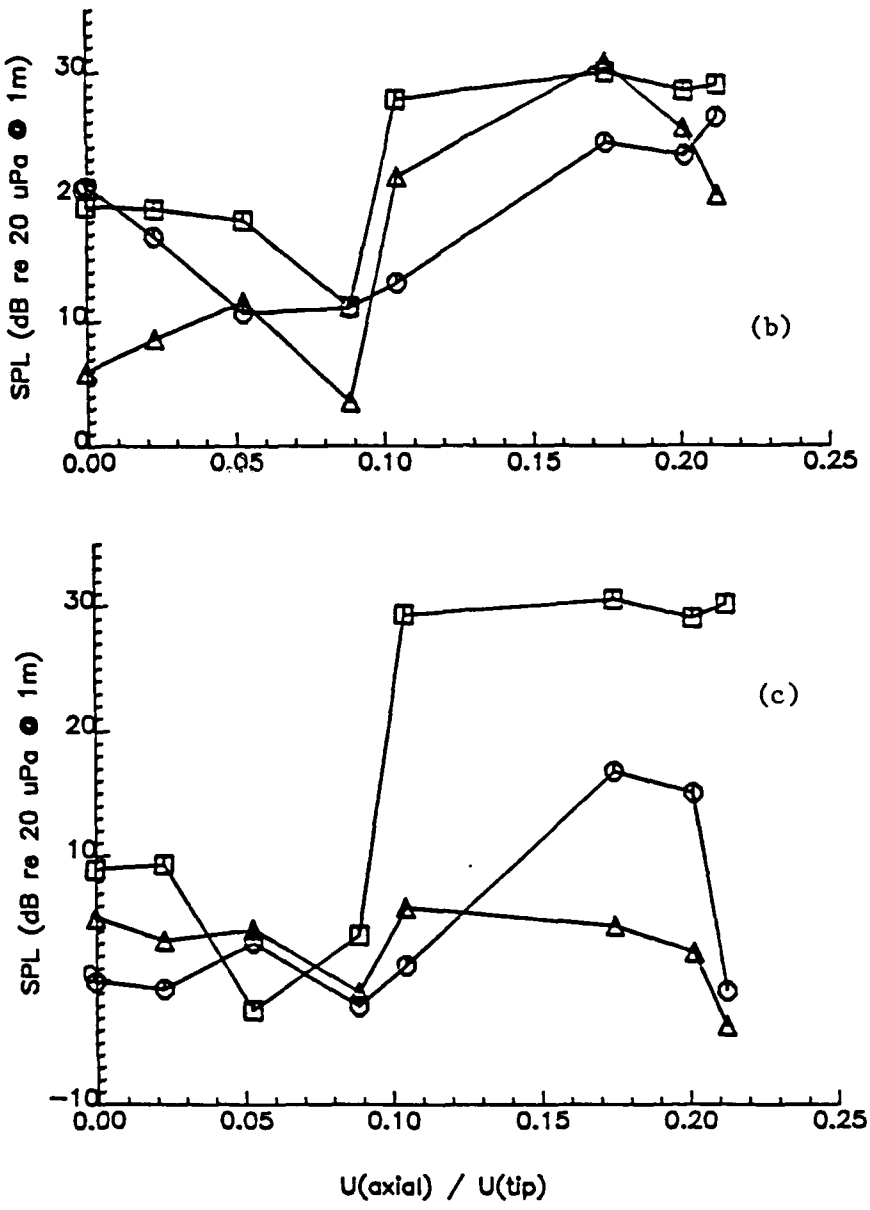

Figure 3.1.5 . Continued.

(b) □ -- BPF x 5, ○ -- BPF x 6, Δ -- BPF x 7.
(c) □ -- BPF x 8, ○ -- BPF x 9, Δ -- BPF x 10.

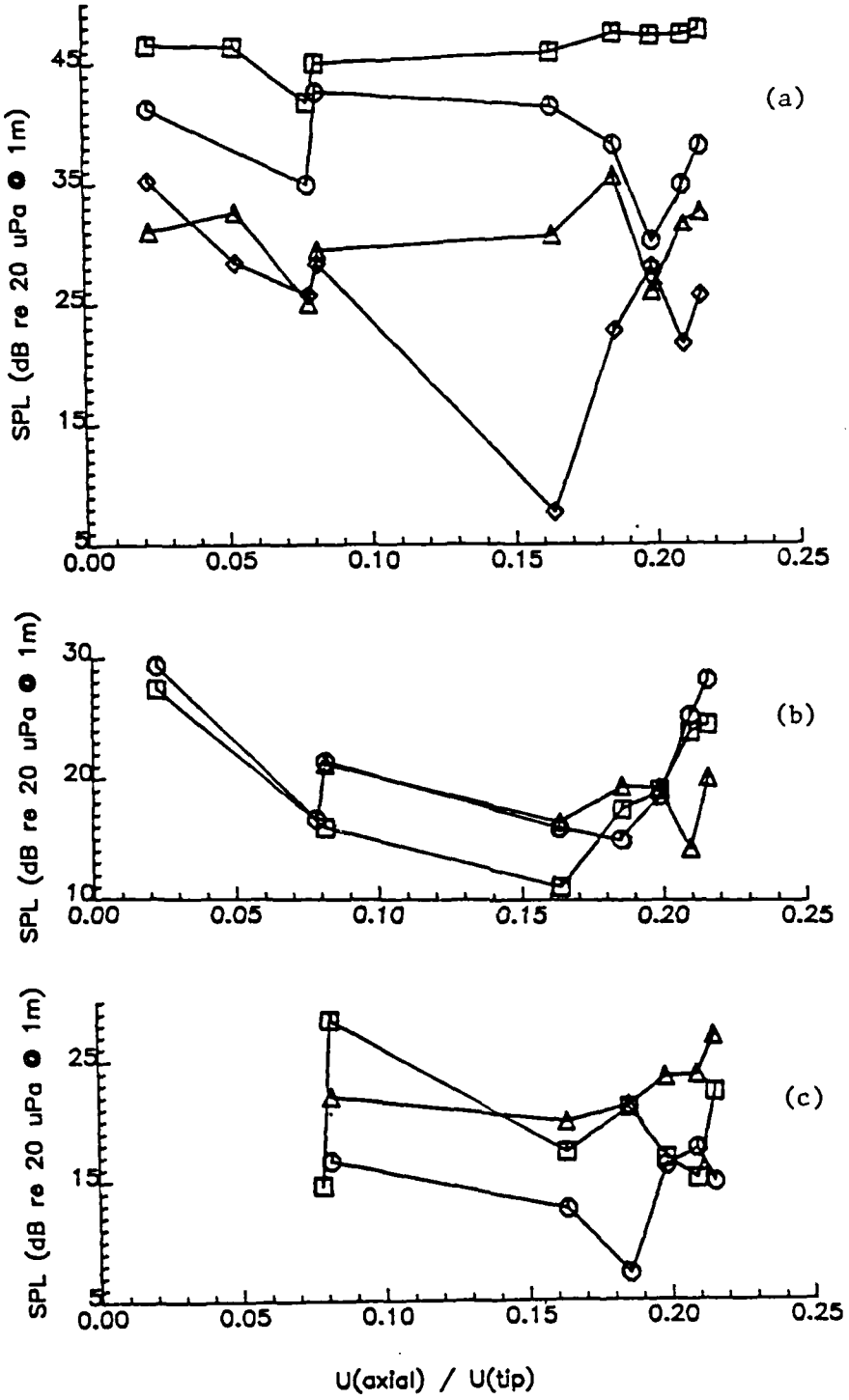

Figure 3.1.6 . SPL of the Blade Passage Tones of the Patriot vs. Flow Coefficient (Synchronized Spectra, 8 Hz Bandwidth).

(a) □-- BPF x 1, ○-- BPF x 2, Δ -- BPF x 3, ◇-- BPF x 4.
(b) □-- BPF x 5, ○-- BPF x 6, Δ -- BPF x 7.
(c) □-- BPF x 8, ○-- BPF x 9, Δ -- BPF x 10.

While a system designer would best choose to operate the fan in the flow coefficient region that produced the lowest discrete-tone levels for a given pumping duty, the remainder of tests in these surveys were conducted at free flow to maximize the discrete-tone levels and minimize turbulent, broad-band noise.

3.1.3. Sound Pressure Level vs. Angle from the Fan Principal Axis (Directivity)

In fan noise analysis, directivity patterns are often used to determine the probable source, in terms of aerodynamic interactions, of the acoustic radiation in the particular frequency range of interest. In examining the Muffin XL and the Patriot, Fitzgerald's (1982) results show relatively uniform directivities for the OASPL and the various blade passage rate harmonics. He concludes that this evidence supports the supposition that all of the radiating modes are due to zero-order pressure distributions, and are not "cut off" in the sense described by Tyler and Sofrin (1962). However, Fitzgerald used only unsynchronized spectral data. As explained in Chapter 1, the discrete-tone peaks in these spectra contain contributions from random signals at the same frequencies. Generation of broadband radiation is largely due to random turbulence whose farfield acoustic radiation properties are randomly oriented in time and space. Thus, ensemble averaging will tend to show uniform directivity for any given frequency to the extent that random noise is a contributor at that frequency, regardless of the properties associated with the generation of the particular discrete tone. This aspect is clearly demonstrated in Figure 3.1.7, which shows the directivity of the OASPL for both fans.

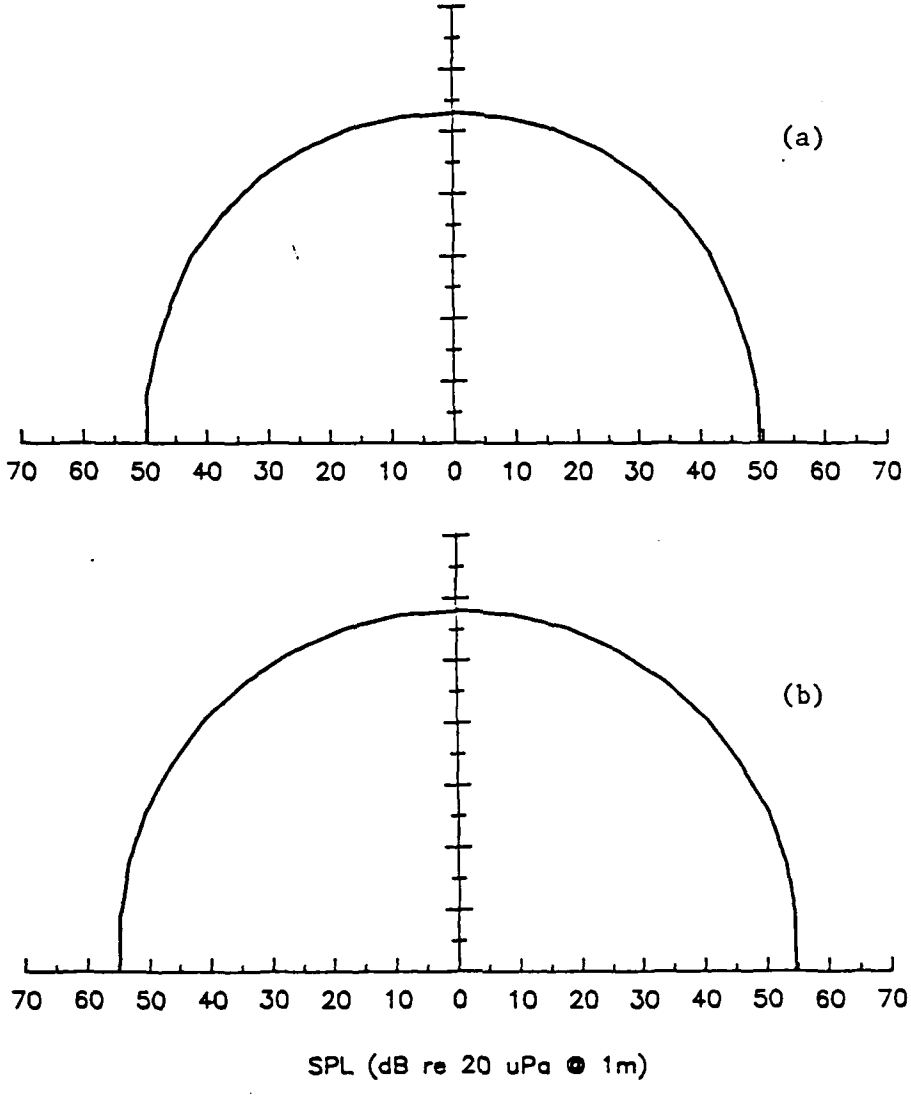

Figure 3.1.7 . OASPL vs. Angle From the Fan Principle Axis (Directivity). (20 kHz Bandwidth.)

(a) Muffin XL.
(b) Patriot.

Within the limitation of the true anechoicity of the chamber, these patterns are uniform.

Figures 3.1.8 and 3.1.9 show directivities for the BPF x 1 through BPF x 10 tones for the Muffin XL and the Patriot, respectively. These data were taken using synchronized spectral analysis. Since the synchronization tends to average out phase-random contributions to multiples of the synchronization rate, only the true discrete-tone contributions remain. The BPF is the only discrete tone that has a uniform directivity: the harmonics of the BPF exhibit lobes. The figure-eight pattern predicted by Tyler and Sofrin (1962) is apparent, with appreciable level along the rotation axis as shown by Wright (1969). The uniform directivity of the BPF indicates that its source differs from that of the higher harmonics. Hanson (1977) observes that the BPF radiation is due to steady, rather than unsteady blade loading. This means that its source is the rotating pressure pattern attached to each blade, as accounted in the original propeller theory of Gutin (1948). The marked nonuniformity of the Patriot blade passage harmonics is in part a consequence of the fan losing its acoustic "compactness". The tone at BPF x 7 has a frequency of about 1995 Hz: the acoustic wavelength at this frequency is just over 17 cm (6.8 in.), quickly approaching the fan diameter of 14.3 cm (5.63 in.). This is the condition at which a source is considered to be non-compact.

A clear demonstration of the difference between the directivities of discrete tones for unsynchronized and synchronized processing is revealed in Figure 3.1.10. The harmonics of the Patriot BPF are shown two at a time. Without synchronization, the directivities appear to be quite uniform. Their shapes are controlled by the random-phase

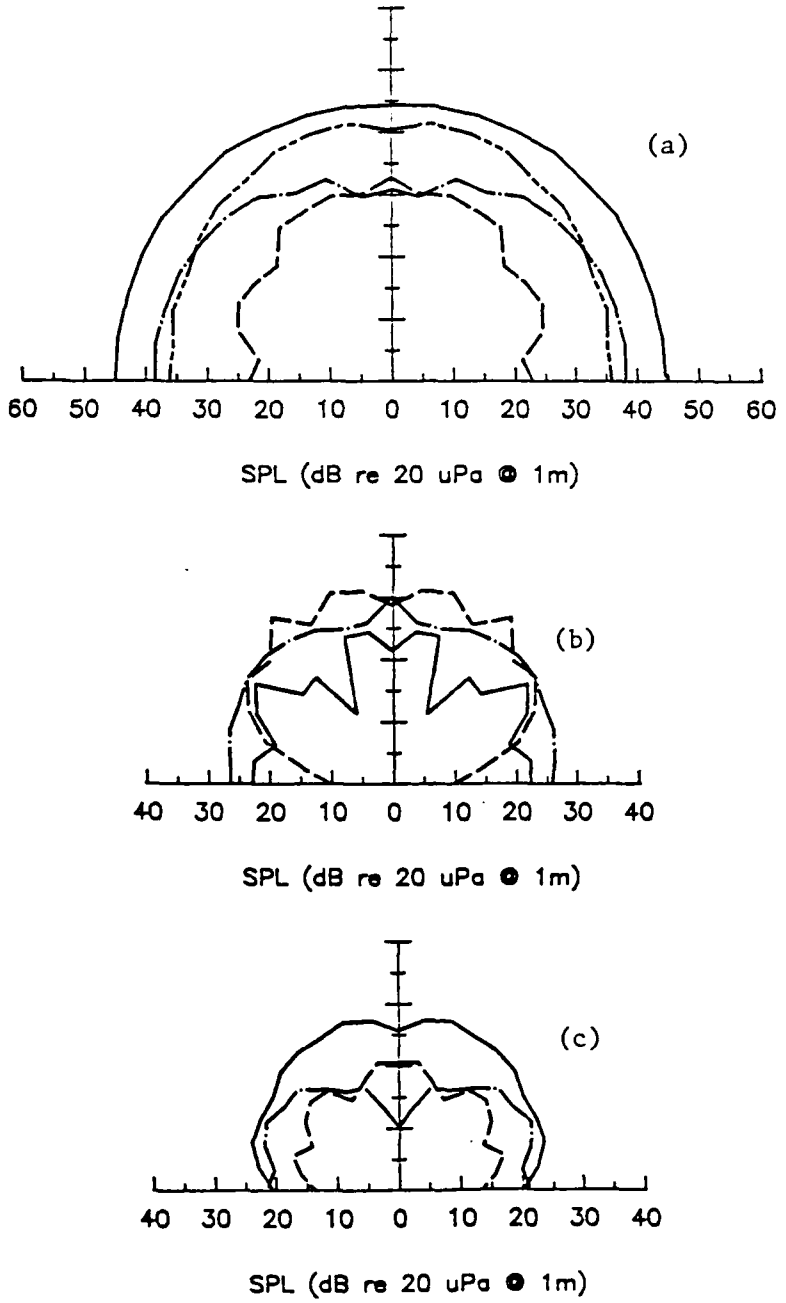

Figure 3.1.8 . SPL of the Blade Passage Tones of the Muffin XL vs. Angle From the Fan Principle Axis (Directivity). (Synchronized Spectra, 4 Hz Bandwidth.)

(a) —— BPF x 1, - - - BPF x 2, — · — BPF x 3, — - - - — BPF x 4.
(b) —— BPF x 5, - - - BPF x 6, — · — BPF x 7.
(c) —— BPF x 8, - - - BPF x 9, — · — BPF x 10.

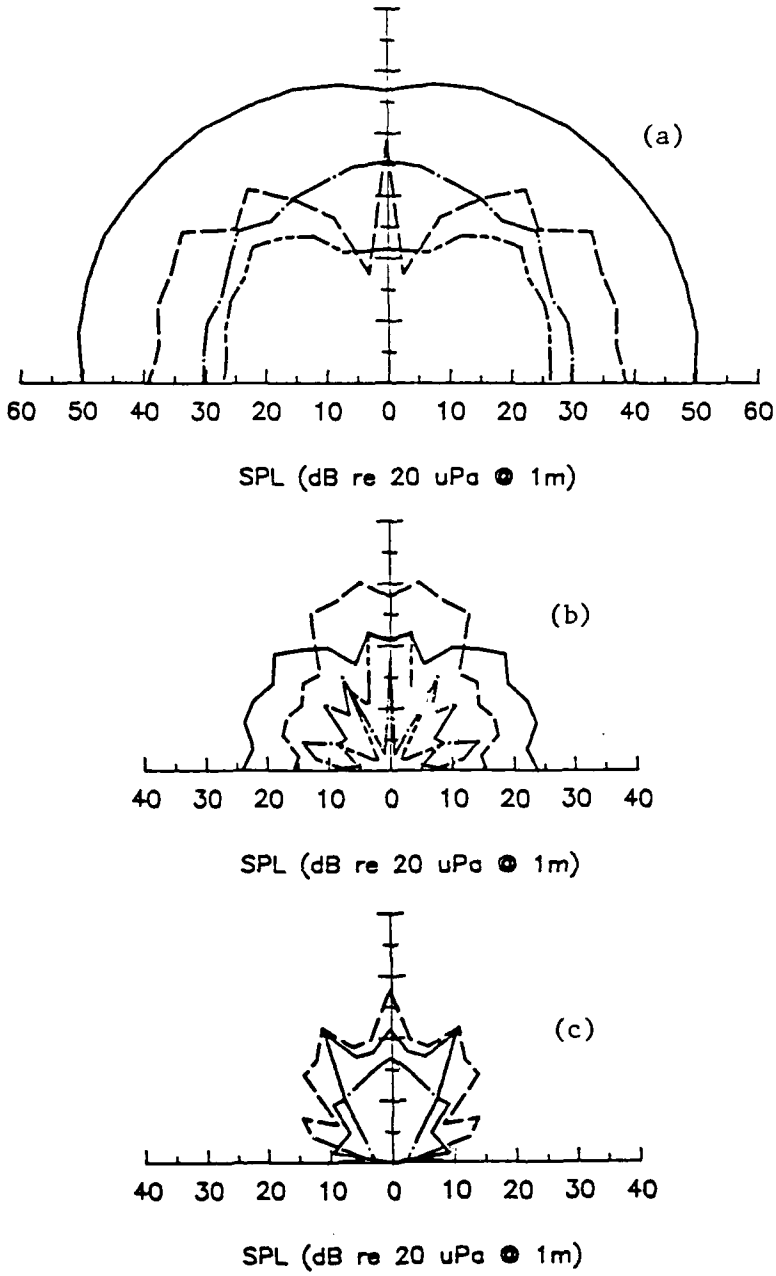

Figure 3.1.9 . SPL of the Blade Passage Tones of the Patriot vs. Angle From the Fan Principle Axis (Directivity). (Synchronized Spectra, 8 Hz Bandwidth.)

(a) ---- BPF x 1, - - - BPF x 2, -- • -- BPF x 3, -- - - -- BPF x 4.
(b) ---- BPF x 5, - - - BPF x 6, -- • -- BPF x 7.
(c) ---- BPF x 8, - - - BPF x 9, -- • -- BPF x 10.

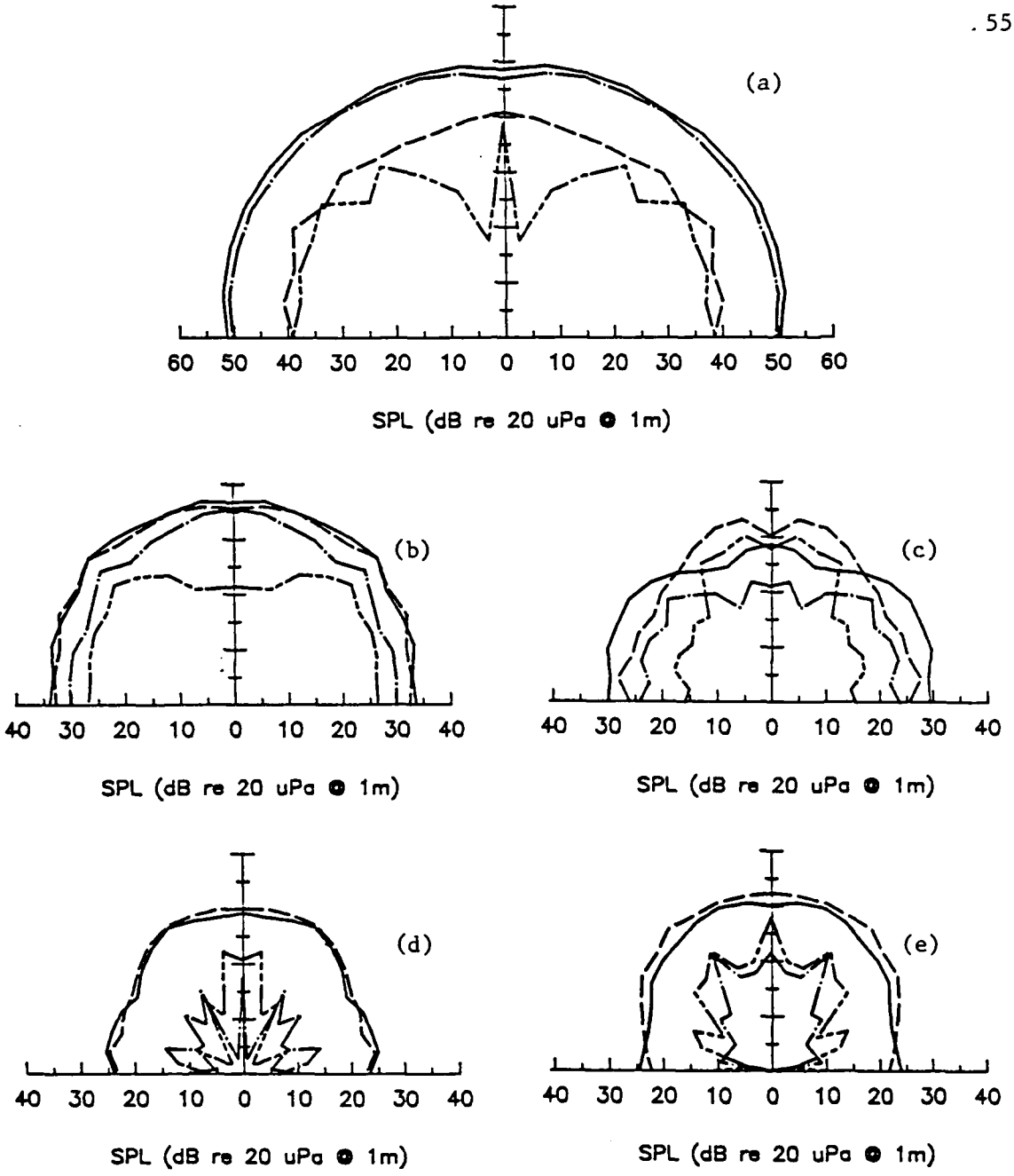

Figure 3.1.10 . SPL of Blade Passage Tones of the Patriot vs. Angle From the Fan Principle Axis, Comparing Unsynchronized Spectra (U) with Synchronized Spectra (S). (U: 4 Hz Bandwidth, S: 8 Hz Bandwidth.)

Line Shape: ——— , — — — , — · — , — - - —

(a) BPF x 1 (U), BPF x 2 (U), BPF x 1 (S), BPF x 2 (S).
(b) BPF x 3 (U), BPF x 4 (U), BPF x 3 (S), BPF x 4 (S).
(c) BPF x 5 (U), BPF x 6 (U), BPF x 5 (S), BPF x 6 (S).
(d) BPF x 7 (U), BPF x 8 (U), BPF x 7 (S), BPF x 8 (S).
(e) BPF x 9 (U), BPF x 10 (U), BPF x 9 (S), BPF x 10 (S).

components in the frequency bins, and they mask the true behavior of the discrete tones.

3.2. Phase I: Inflow Obstructions

The data for obstructions are reported in terms of Sound Pressure Level (SPL) as a function of the obstruction location. The positions refer to those directions shown in Figure 2.3.3, with the origin defined in Section (2.3.1.2.). The z-direction, parallel to the fan rotation axis, will be referred to as "axial" location; the y-direction will be referred to as "radial" location. All distances are expressed in terms of the fan radius.

3.2.1. The Cylindrical Obstruction

3.2.1.1. The Effect of Axial Location

Figure 3.2.1 shows the OASPL of the Muffin XL and the Patriot as a function of the axial, or upstream, location of the cylindrical obstruction. Both curves effectively reach the baseline level within 0.3 fan radii, which is a lenient restriction on the placement of an obstruction of this type. When the cylinder is closer than 0.1 fan radii, the sound level rises markedly. This behavior is identical to that shown by Sharland (1964). Within this distance (up to 0.2 fan radii for the Patriot with its higher flow velocity), the boundary layer of the fan is ingested, the velocity deficit in the wake is large, and the potential flow fields of the rotor and cylinder begin to interact.

The first ten blade passage frequency tones (BPF x 1 through BPF × 10) are shown in Figure 3.2.2 for the Muffin XL and Figure 3.2.3

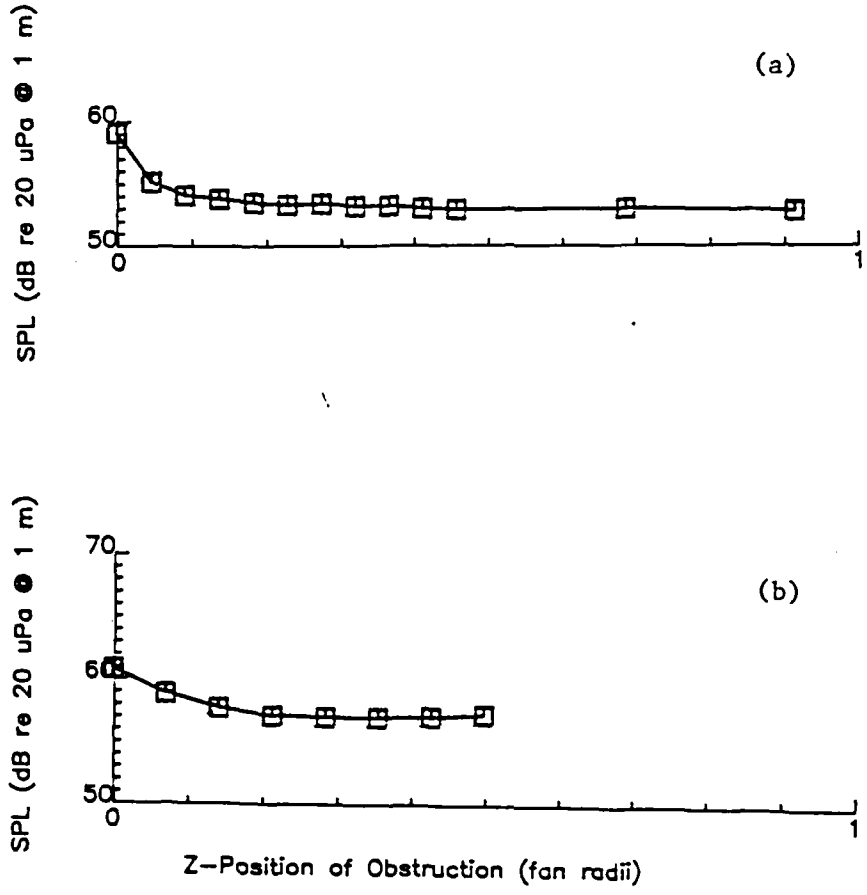

Figure 3.2.1 . OASPL vs. Axial Location of a Cylindrical Obstruction. (y = 0.0 Fan Radii, 20 kHz Bandwidth.)

(a) Muffin XL.
(b) Patriot.

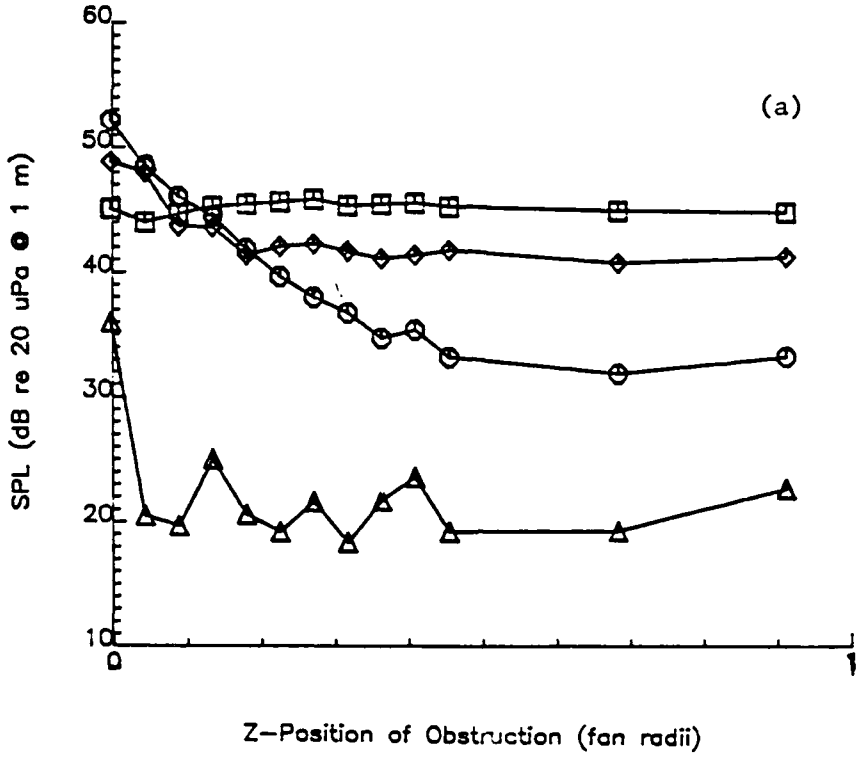

Figure 3.2.2 . SPL of Blade Passage Tones of the Muffin XL vs. Axial Location of a Cylindrical Obstruction. (y = 0.0 Fan Radii, 4 Hz Bandwidth.)

(a) □-- BPF x 1, ○-- BPF x 2, Δ -- BPF x 3, ◇-- BPF x 4.

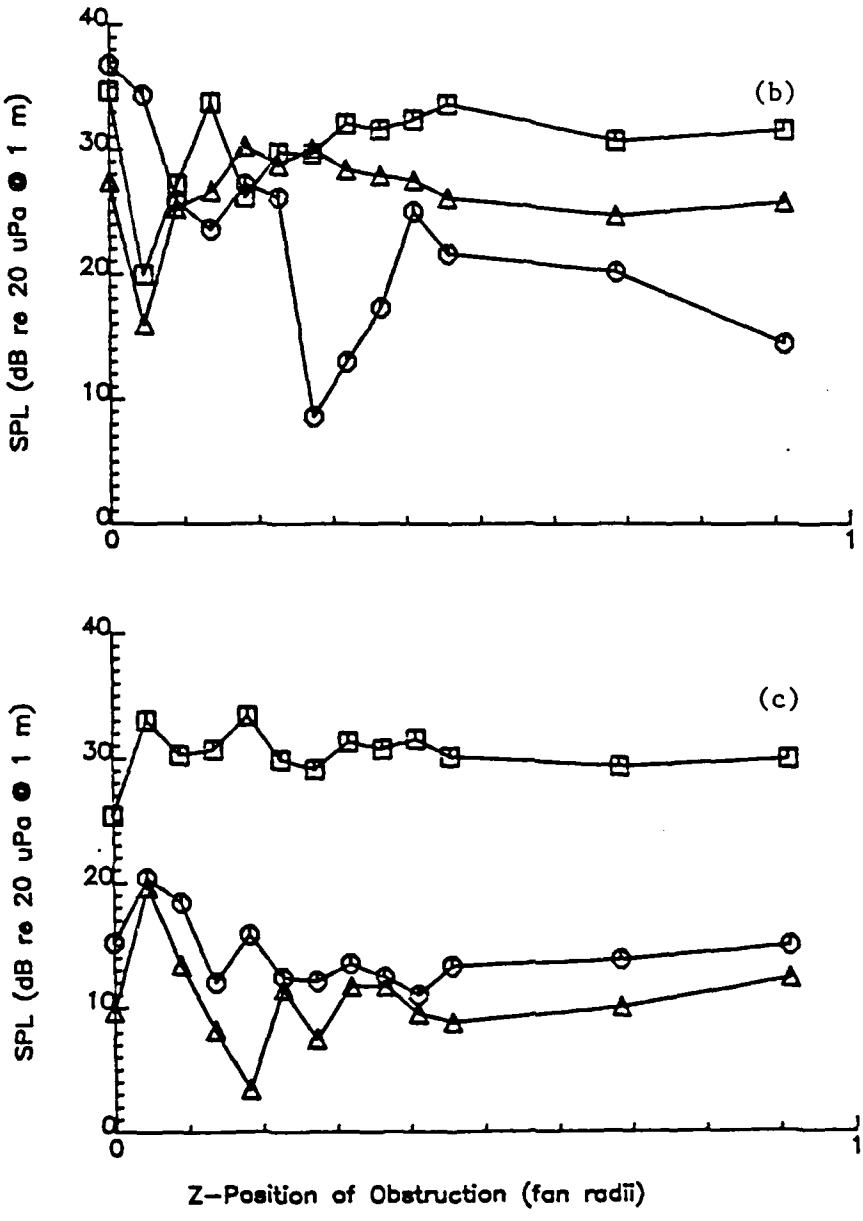

Figure 3.2.2 . Continued.

(b) □-- BPF x 5, ○-- BPF x 6, Δ -- BPF x 7.
(c) □-- BPF x 8, ○-- BPF x 9, Δ -- BPF x 10.

for the Patriot. Several important features are apparent. It seems illogical that the BPF x 1 tone does not increase markedly as the obstruction is brought closer. In fact, it dips slightly for both fans near 0.1 fan radii. However, this can be explained by the steady-loading hypothesis put forward in Section (3.1.3.) to explain the uniform directivity of the BPF x 1 tone. Since generation of the BPF x 1 tone is not strictly related to interaction with the obstruction wake, it tends to be independent of the obstruction position. When the obstruction is brought within 0.1 fan radii of the inlet, the airflow is altered to the extent that the steady blade loading (thrust) is diminished, lowering the SPL of the BPF x 1 accordingly.

For both fans, the BPF x 2 tone is stronger than the BPF x 1 tone at zero separation, and it falls off smoothly with increasing separation. This would be expected for a tone generated by rotor/wake interaction, and this is clearly the source of this tone. The BPF x 3 tone falls off quickly for the Muffin XL, and less so for the Patriot.

The BPF x 4 tone is particularly revealing. It has a level greater than the BPF x 1 tone for the Muffin XL at zero separation, and for both fans the level decreases in a manner similar to the BPF x 2 tone. While the level of the BPF x 4 tone continues to decrease with increasing separation for the Patriot, it reaches a floor near 42 dB for the Muffin for upstream locations greater than 0.2 fan radii. This level is identical to the baseline (unobstructed) value. This result suggests that something inherent to the fan contributes more to the generation of the BPF x 4 tone than does the cylinder wake originating at 0.2 fan radii. A possible explanation is as follows.

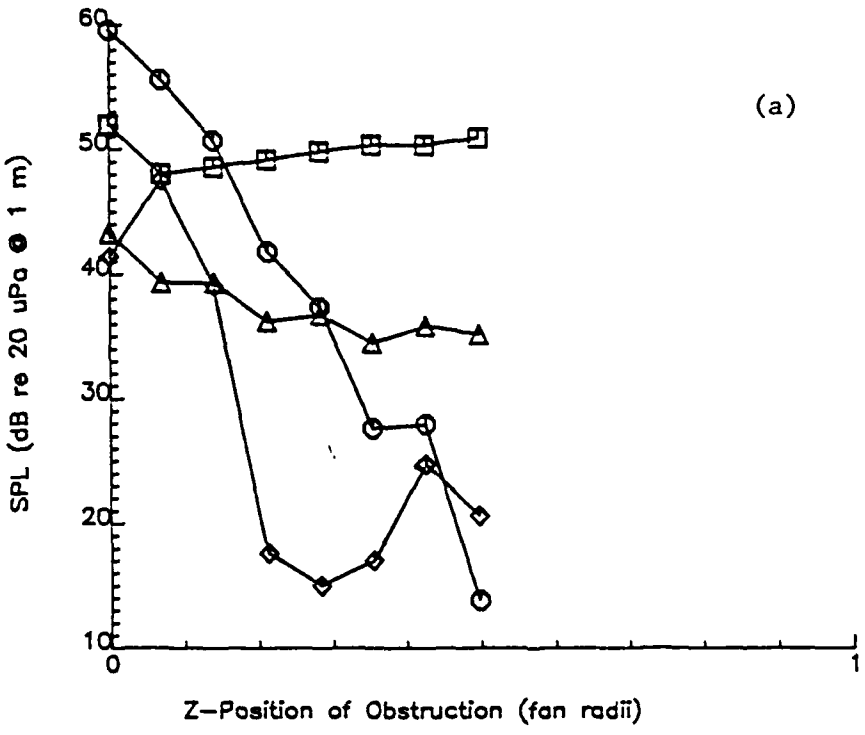

Figure 3.2.3 . SPL of Blade Passage Tones of the Patriot vs. Axial Location of a Cylindrical Obstruction. (y = 0.0 Fan Radii, 8 Hz Bandwidth.)

(a) □ -- BPF x 1, ○ -- BPF x 2, Δ -- BPF x 3, ◇ -- BPF x 4.

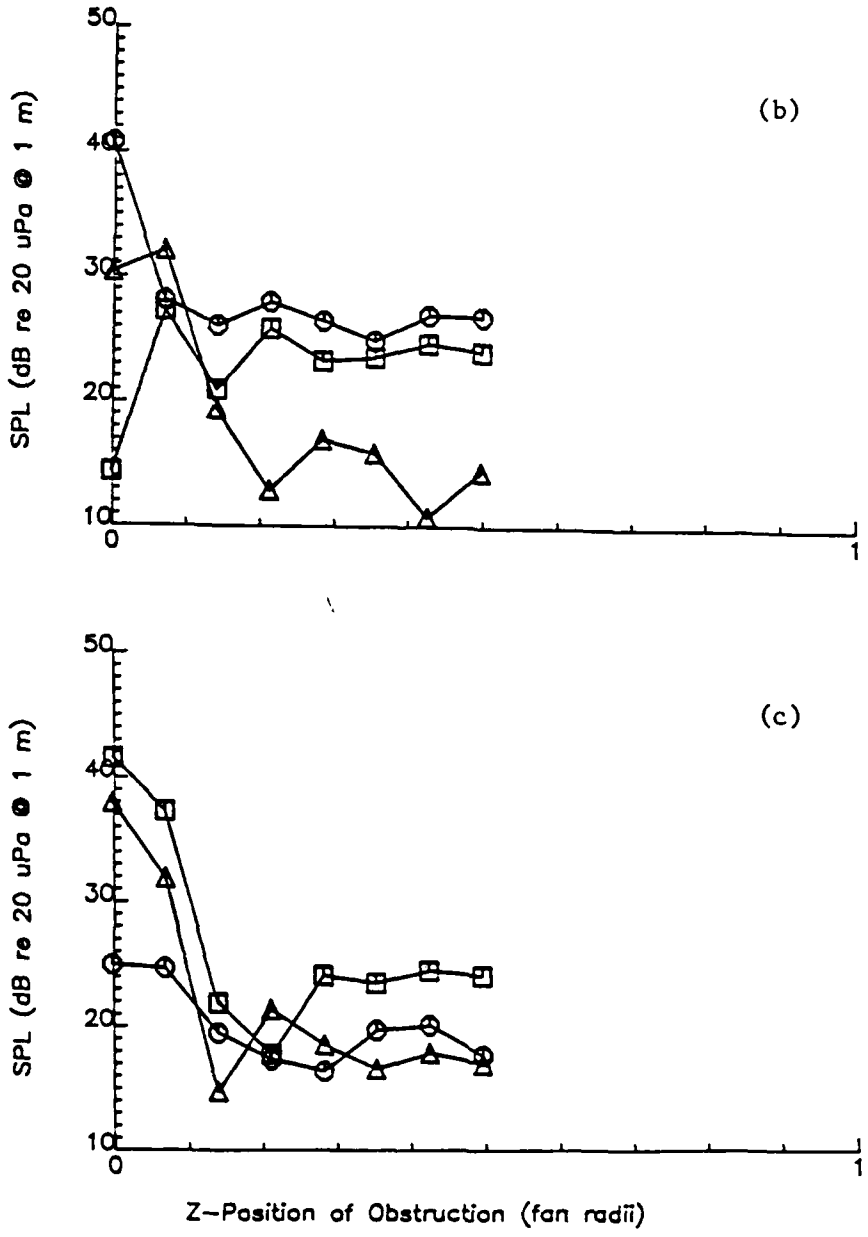

Figure 3.2.3 . Continued.

(b) □ -- BPF x 5, ○ -- BPF x 6, Δ -- BPF x 7.
(c) □ -- BPF x 8, ○ -- BPF x 9, Δ -- BPF x 10.

There are two contributions to a tone at a harmonic of the blade passage frequency. The first is the value of the Fourier component that appears at the harmonic frequency as a result of the shape of the blade passage rate waveform. An example of this is the square wave which is decomposed into an infinite number of frequencies harmonically related to the fundamental repetition rate. The second contribution is any source which independently generates acoustic radiation at a rate which is harmonically related to the blade passage rate. An examination of the synchronized, ensemble-averaged time waveform of the baseline Muffin XL Figure 3.2.4 reveals a pressure excursion which repeats at four times the blade passage rate (indicated by arrows on figures). This indicates that the source is some distortion, other than the cylinder wake, which is present at four equally-spaced locations at the inlet. The four corners of the Muffin XL housing were identified as these sources. Since air was free to flow into the fan from regions behind the housing, the inlet velocity near the housing corners would be different than that midway between (see Section (2.3.2.1)), causing a lift fluctuation at four times the BPF. Thus, even when an obstruction is not present, the BPF x 4 tone is prevalent for the Muffin XL operating with a free inlet.

The trends of the higher harmonics are less well defined. The BPF x 8 tone is quite strong for the Muffin XL due to its relationship as the first harmonic of the BPF x 4 tone. The higher harmonics of the Patriot tend to increase more dramatically with decreasing separation distance than those of the Muffin XL. This is probably due to the higher inlet flow velocity of the Patriot: the profile of the cylinder wake is more pronounced, and the rotor/wake interaction is greater.

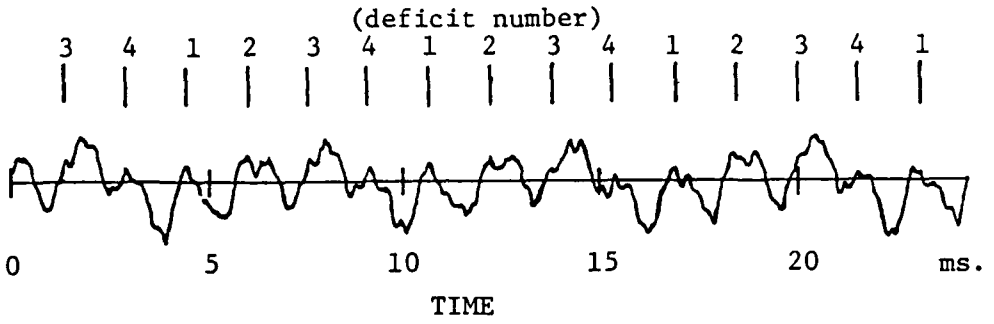

Figure 3.2.4 . Sound Pressure as a Function of Time for the Unobstructed Muffin XL. (128 Synchronized Averages, 80 Hz Bandwidth, 512 Points.) The BPF x 4 Repetition Rate is Marked Above the Waveform, Numbered in Order of the Blades Encountering the Velocity Deficits of the Four Shroud Corners.

The detailed shapes of the curves are a result of changes in the average wake profile as it progresses downstream.

3.2.1.2. The Effect of Radial Location

The keys to interpreting the discrete frequency tones as a function of radial location are the radial span of the hub and the positions and incident angles of the blade leading edges relative to the obstruction wake. The hub of the Muffin XL has a span of 0.46 fan radii, nearly half the total rotor radius. For the Patriot, the hub spans slightly more than half the total rotor radius at 0.57 fan radii. The leading edges of the blades of both fans extend radially from the hub (zero lean). When the obstruction is located at y = 0.0 fan radii, only one blade encounters the wake at a time. For this position, the leading edge is parallel to the obstruction (the condition under which maximum interaction occurs) when it has crossed one half of the wake profile. As the obstruction is displaced slightly along the radial direction, there is a location at which the parallel point is on the edge of the wake profile. Unsteady blade loading reaches its greatest magnitude in this condition. Further radial displacement allows more than one blade to interact with the wake, but the incident angles increase. This lengthens the leading edge of the blade loading pulse, and radiation decreases. As the obstruction reaches the edge of the hub, air that normally flows over the hub and into the blade root is restricted. Unsteady loading increases, as does the noise it generates. Once the obstruction is past the hub, the flow is restored, and the noise decreases again. Noise will then increase slightly as the obstruction moves out along the blade span where the flow velocity

is increasing. This is traded off with a decreasing path length through which a blade travels in the obstruction wake. The result is a tapering of noise to the baseline level.

Figure 3.2.5 shows the OASPL of each fan as a function of the radial location of the cylindrical obstruction. The above explanation is illustrated for both fans. The discrete frequency tones for the Muffin XL are plotted in Figure 3.2.6 and for the Patriot in Figure 3.2.7. The BPF x 2 tones, which are the primary wake interaction tones, demonstrate the previous description clearly, as do the BPF x 4 tones. The BPF x 1 tones are similar for the two fans, but they depend on the degree to which the obstruction alters the steady thrust. Both curves show a minimum near 0.8 fan radii. This is a region of maximum thrust development on the blade span. The wake of the obstruction robs some of that thrust by decreasing the local flow velocity, so that the force which produces the BPF x 1 tone is reduced. Harmonics BPF x 5 through BPF x 10 are shown. The shapes of these curves are more complicated and cannot be explained without a detailed understanding of the wake profile and the spectrum of blade loading harmonics.

3.2.1.3. Non-Symmetric Radial and Axial Locations

Additional SPL data were obtained for both fans with the cylindrical obstruction located at a grid of y-and z-positions. The data for the OASPL and the SPL of tones at BPF x 1 through BPF x 10 are shown in Figure 3.2.8.a - k for the Muffin XL and in Figure 3.2.9.a - k for the Patriot. Originally, it was thought that these data might indicate regions of low noise generation near the fan inlet. Such regions are not clearly shown in the plots. The OASPL plots

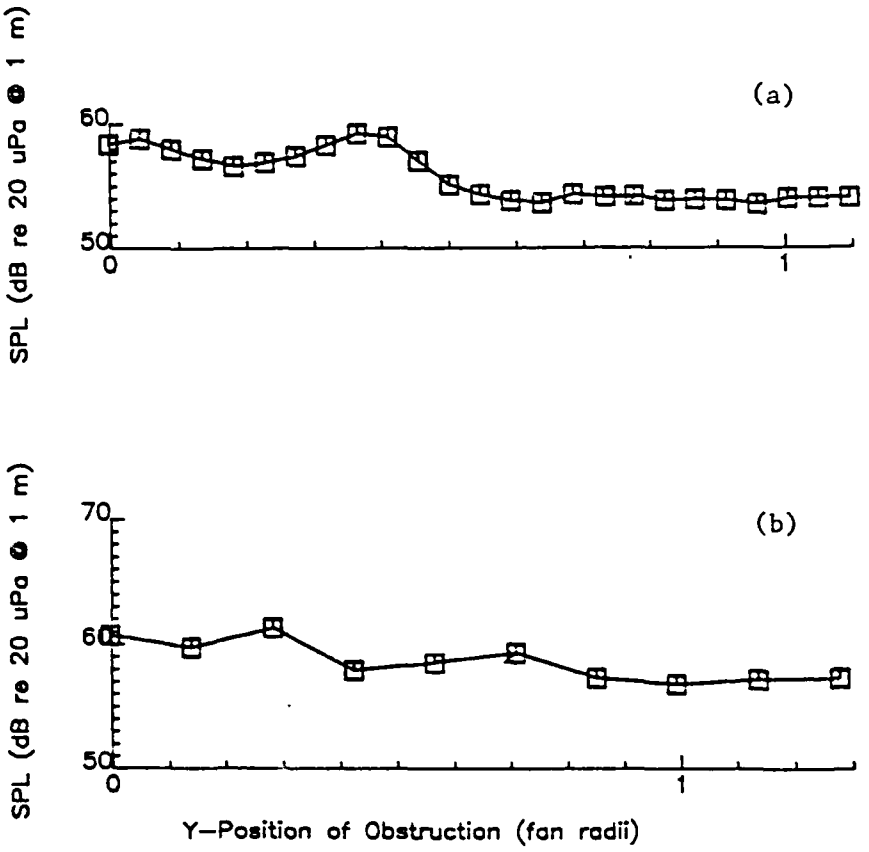

Figure 3.2.5 . OASPL vs. Radial Location of a Cylindrical Obstruction. (z = 0.0 Fan Radii, 20 kHz Bandwidth.)

(a) Muffin XL.
(b) Patriot.

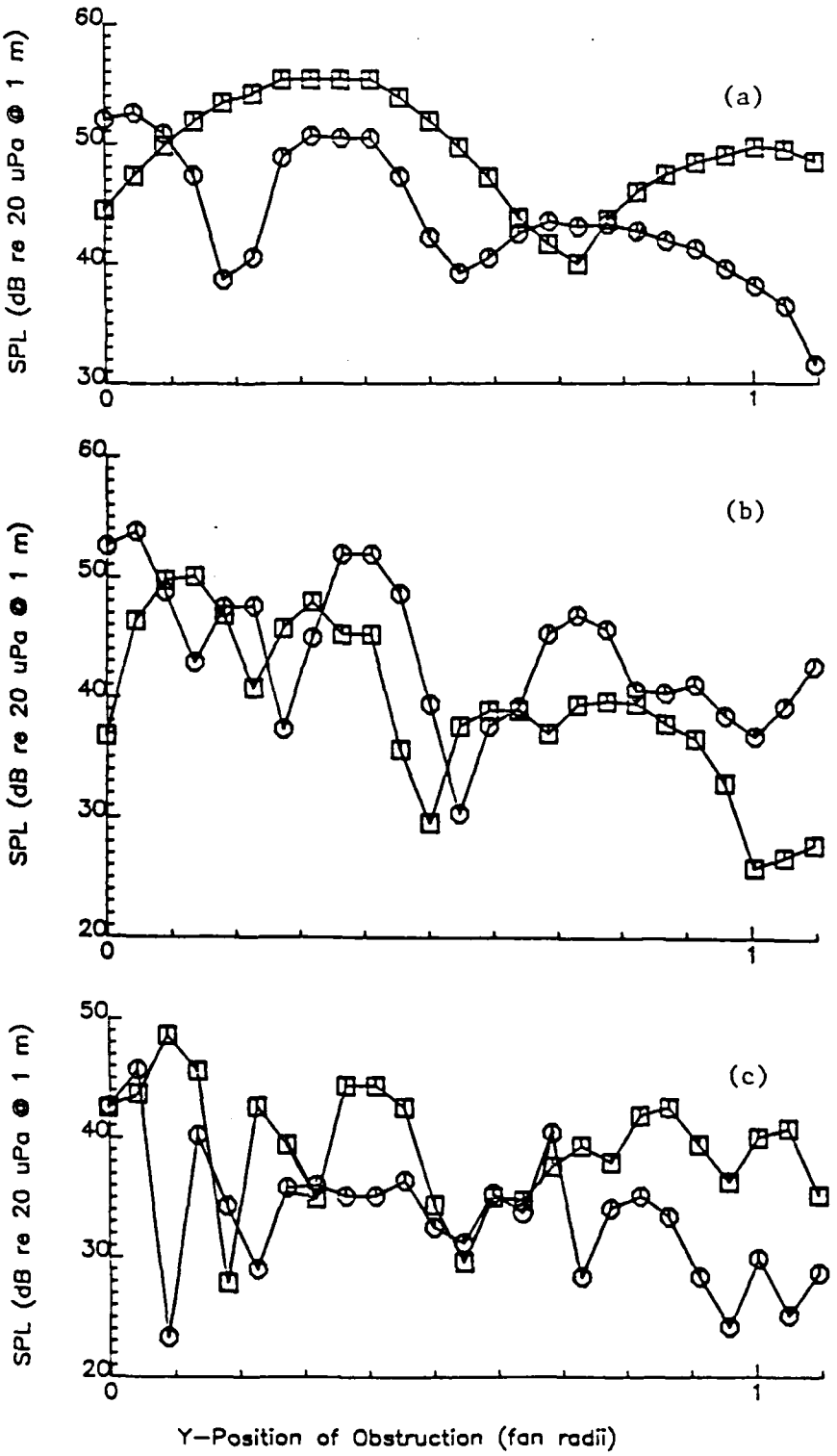

Figure 3.2.6 . SPL of Blade Passage Tones of the Muffin XL vs. Radial Location of a Cylindrical Obstruction. (z = 0.0 Fan Radii, 4 Hz Bandwidth.)

(a) □ -- BPF x 1, ○ -- BPF x 2.
(b) □ -- BPF x 3, ○ -- BPF x 4.
(c) □ -- BPF x 5, ○ -- BPF x 6.

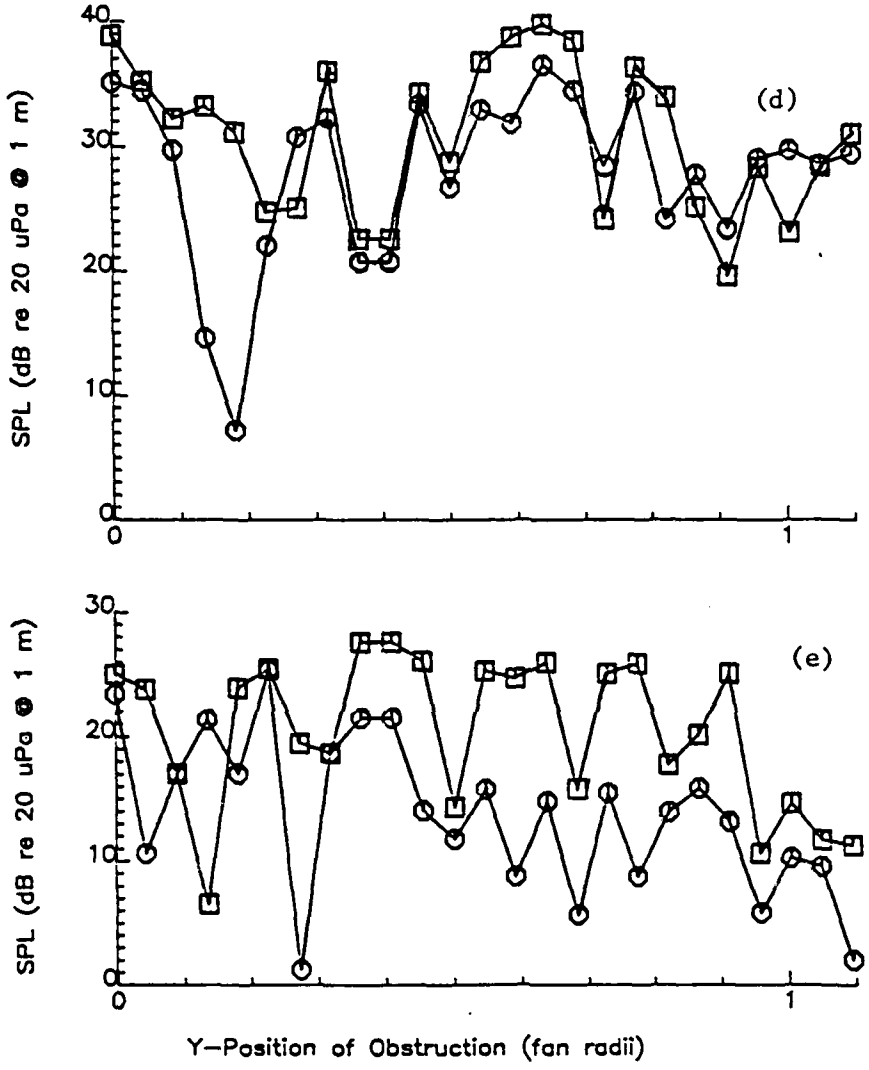

Figure 3.2.6 . Continued.

(d) □-- BPF x 7, ○-- BPF x 8.
(e) □-- BPF x 9, ○-- BPF x 10.

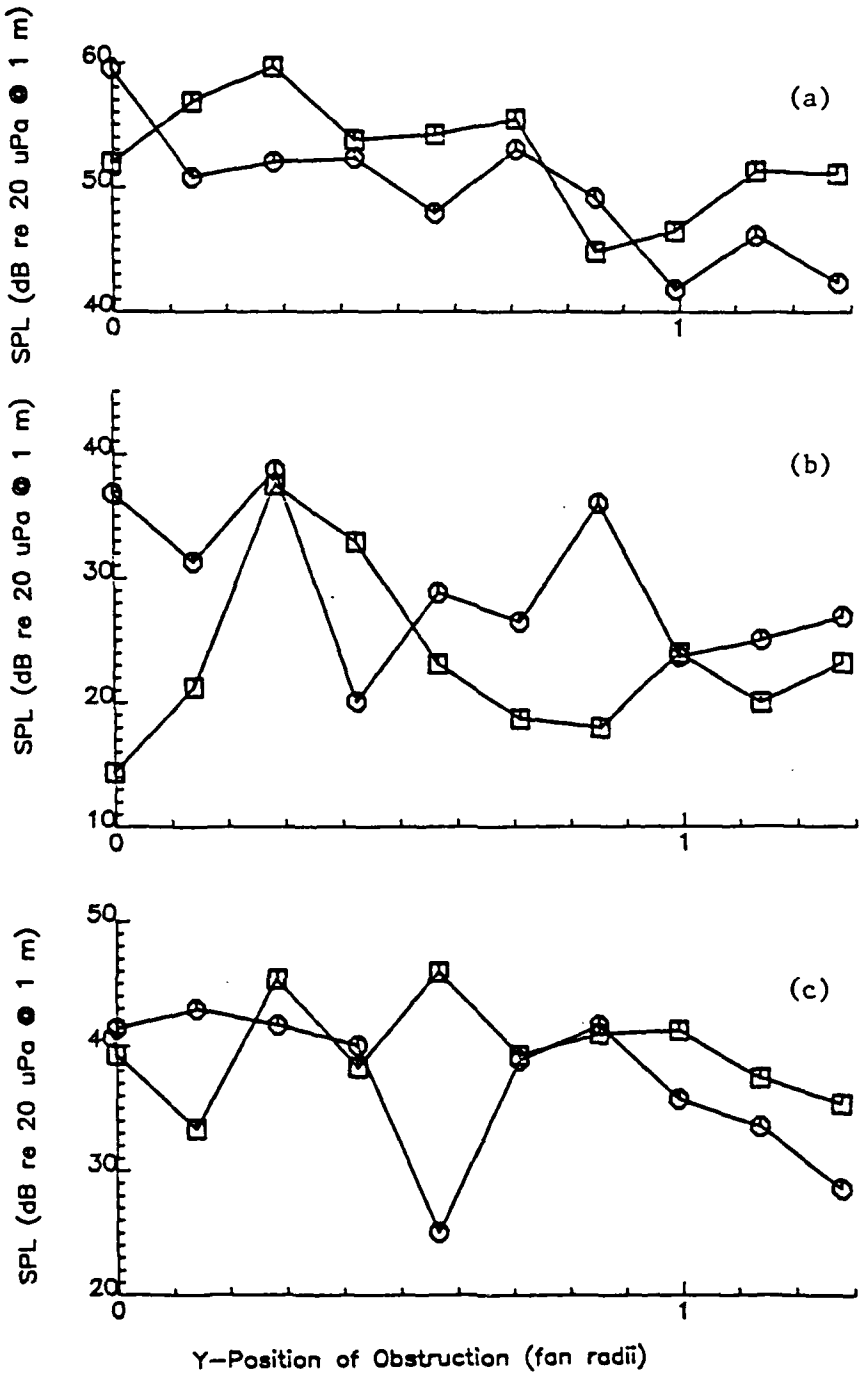

Figure 3.2.7 . SPL of Blade Passage Tones of the Patriot vs. Radial Location of a Cylindrical Obstructions. (z = 0.0 Fan Radii, 8 Hz Bandwidth.)

(a) □-- BPF x 1, ○-- BPF x 2.
(b) □-- BPF x 3, ○-- BPF x 4.
(c) □-- BPF x 5, ○-- BPF x 6.

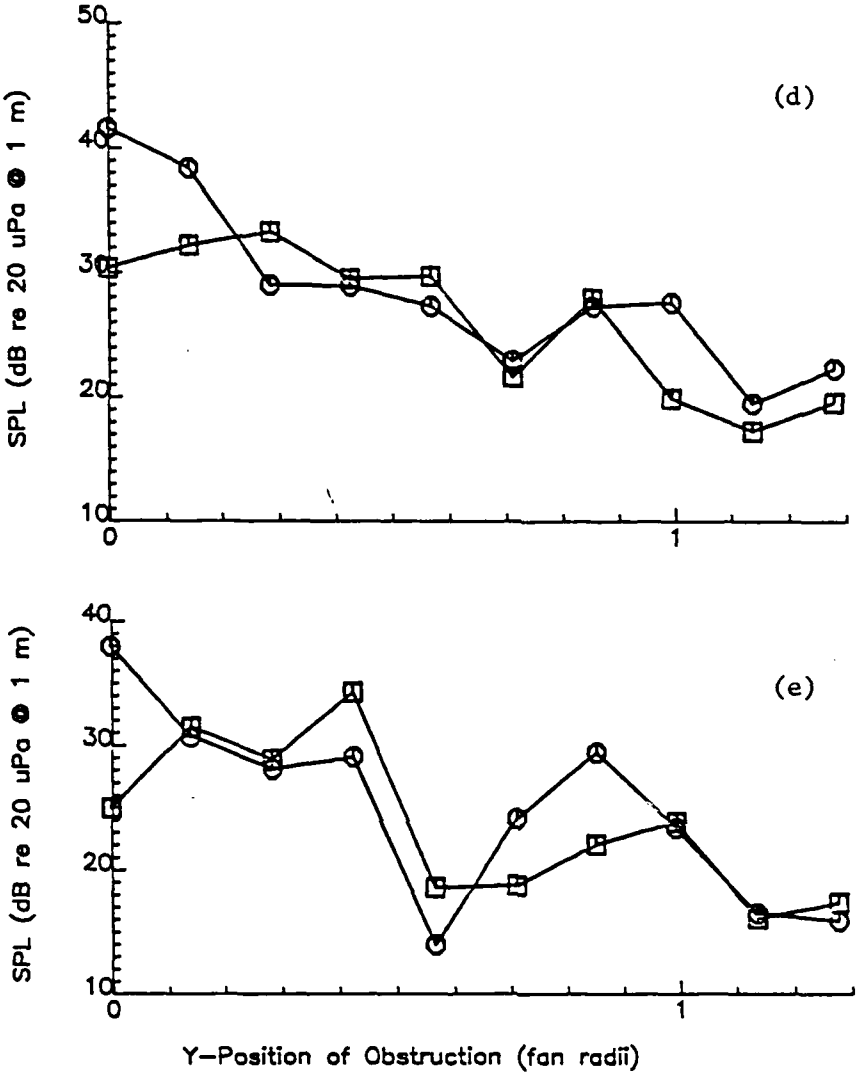

Figure 3.2.7 . Continued.

(d) □-- BPF x 7, ○-- BPF x 8.
(e) □-- BPF x 9, ○-- BPF x 10.

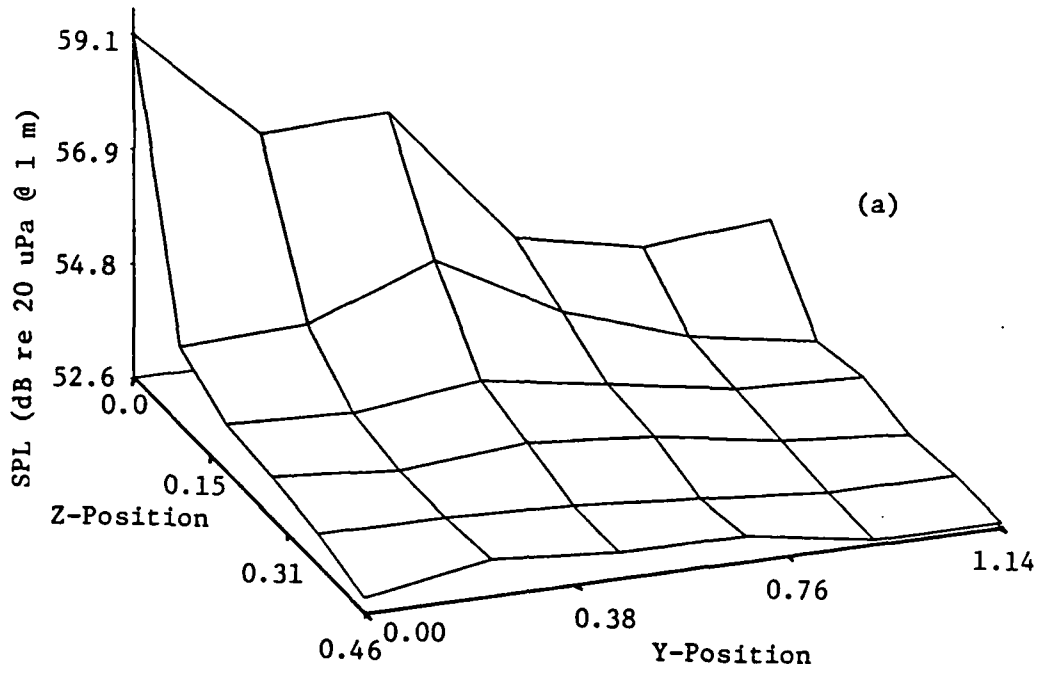

Figure 3.2.8 . SPL for the Muffin XL vs. Axial and Radial Locations of a Cylindrical Obstruction. (4 Hz Bandwidth.)

(a) OASPL (20 kHz Bandwidth).

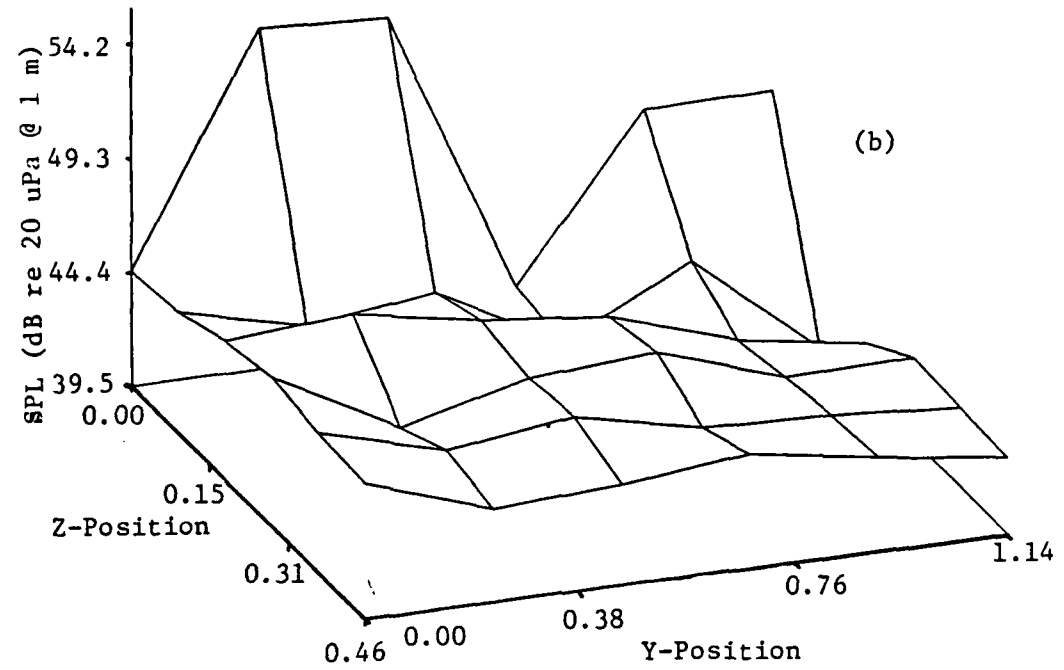

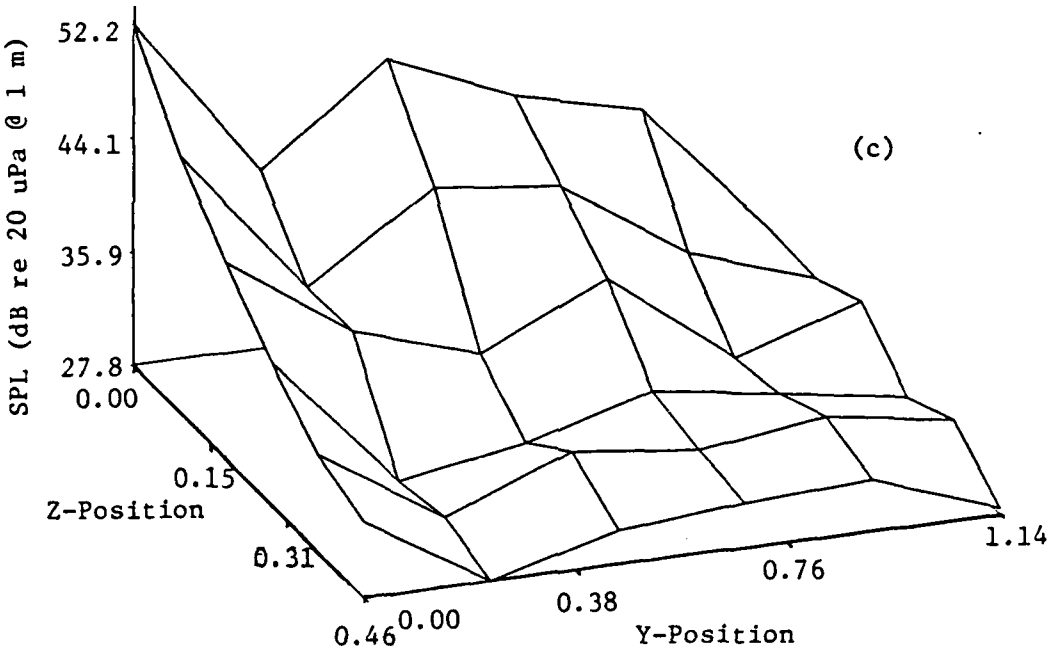

Figure 3.2.8 . Continued.

(b) BPF x 1.
(c) BPF x 2.

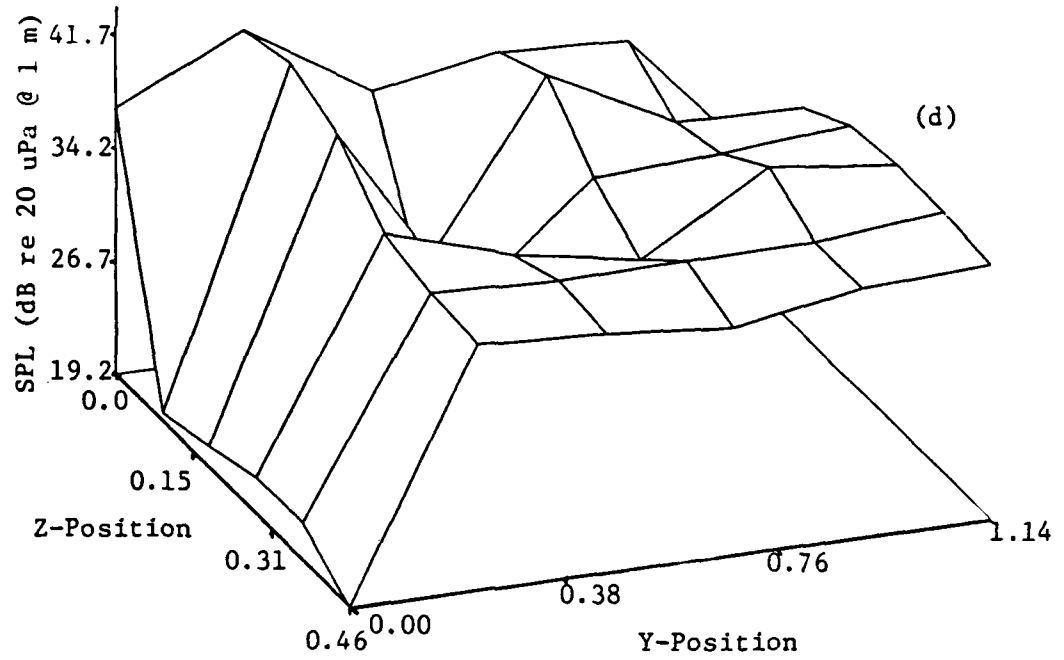

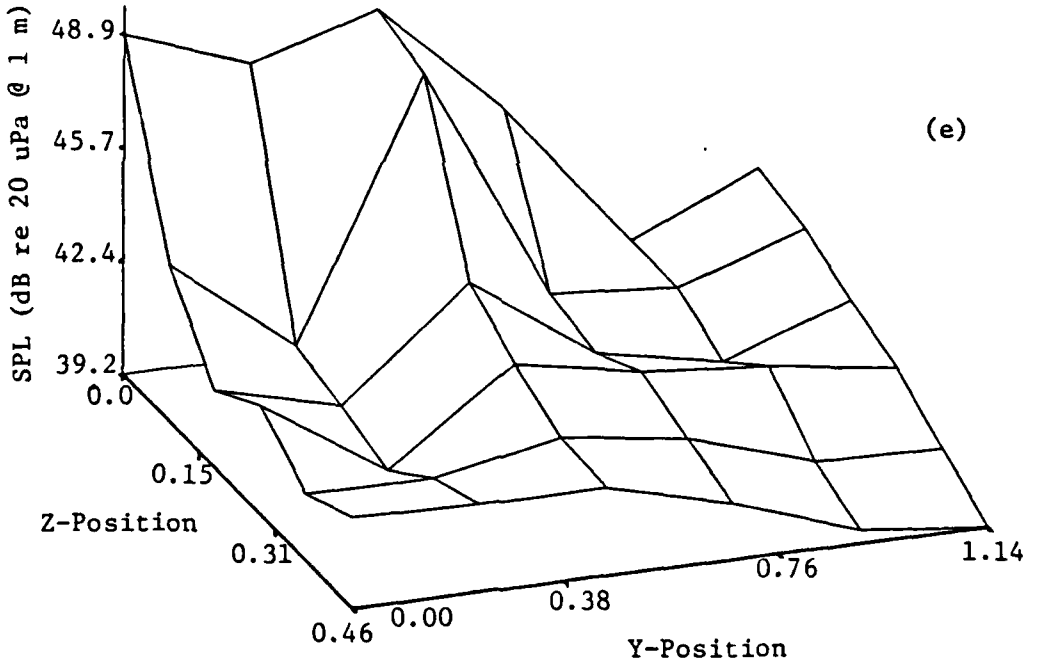

Figure 3.2.8 . Continued.

(d) BPF x 3.
(e) BPF x 4.

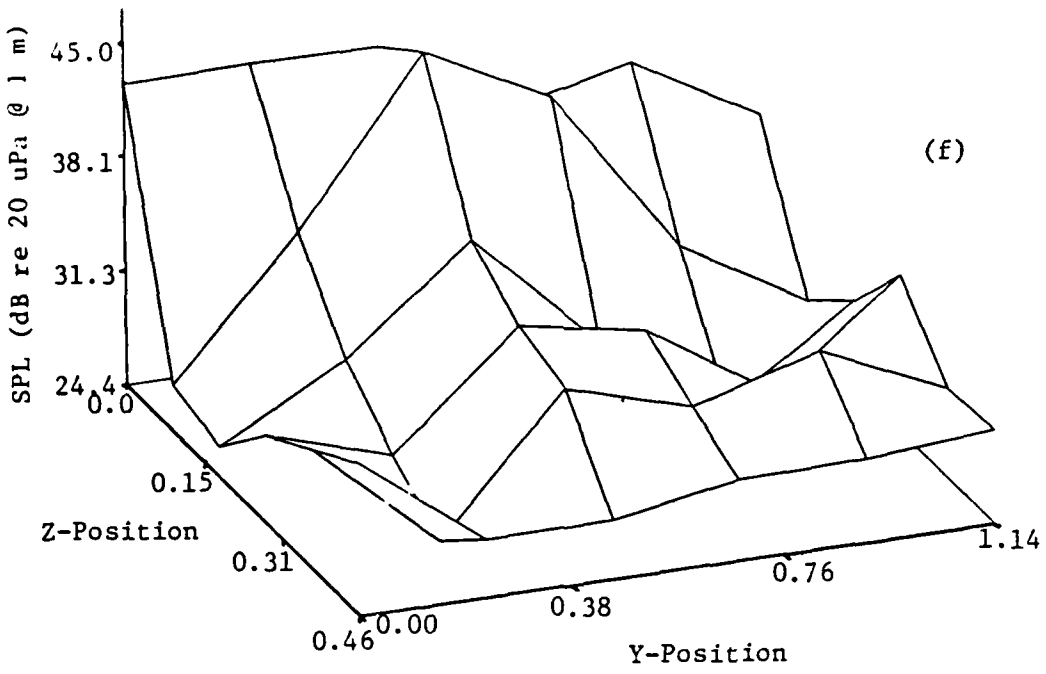

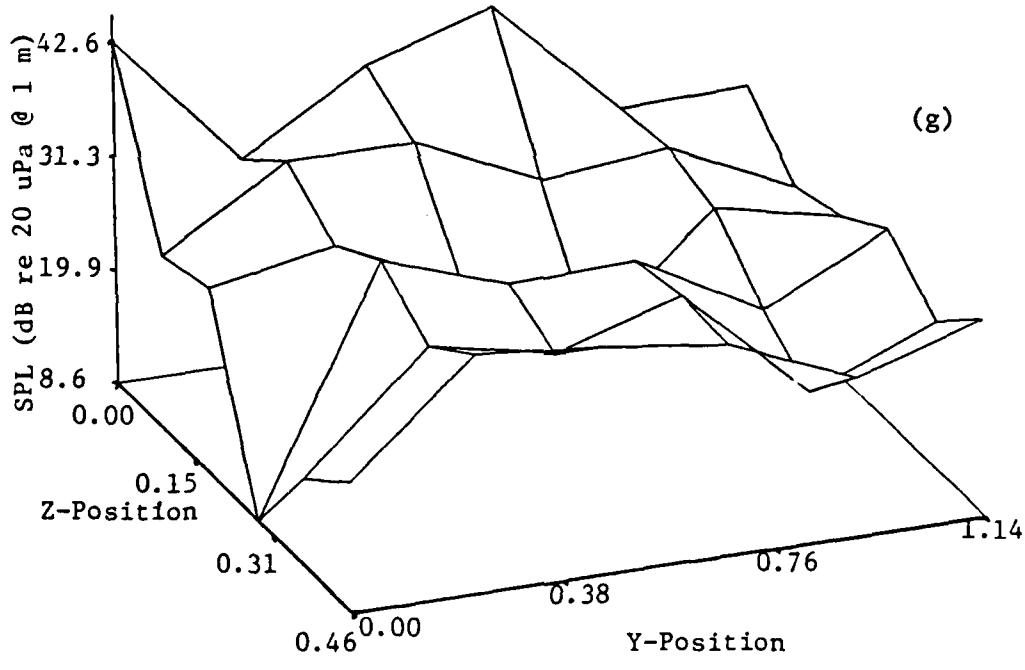

Figure 3.2.8 . Continued.

(f) BPF x 5.
(g) BPF x 6.

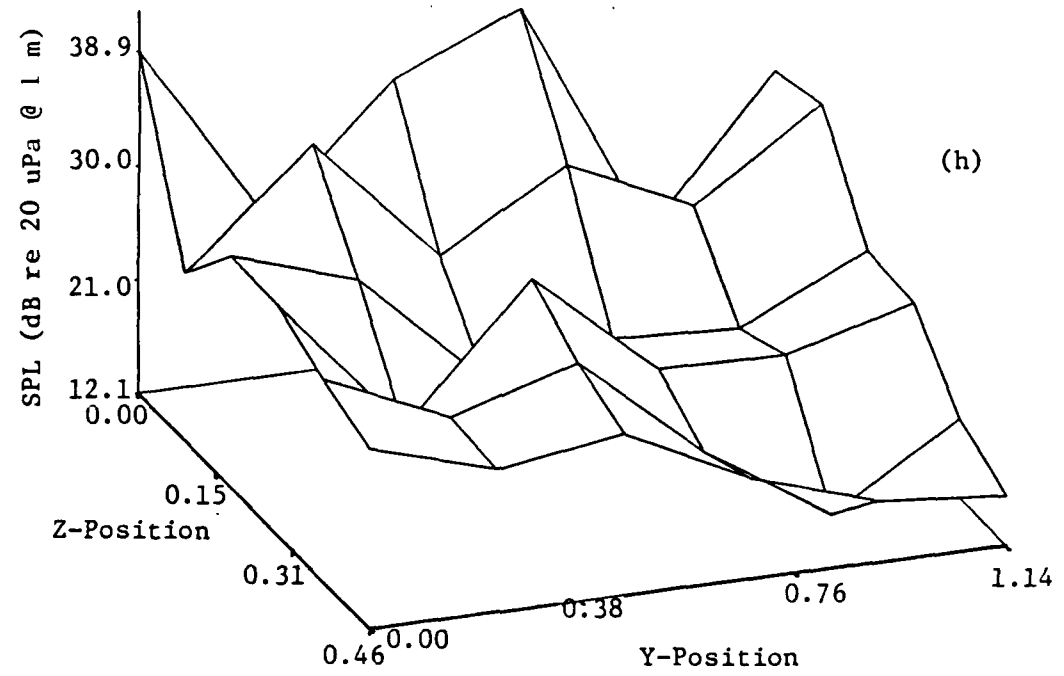

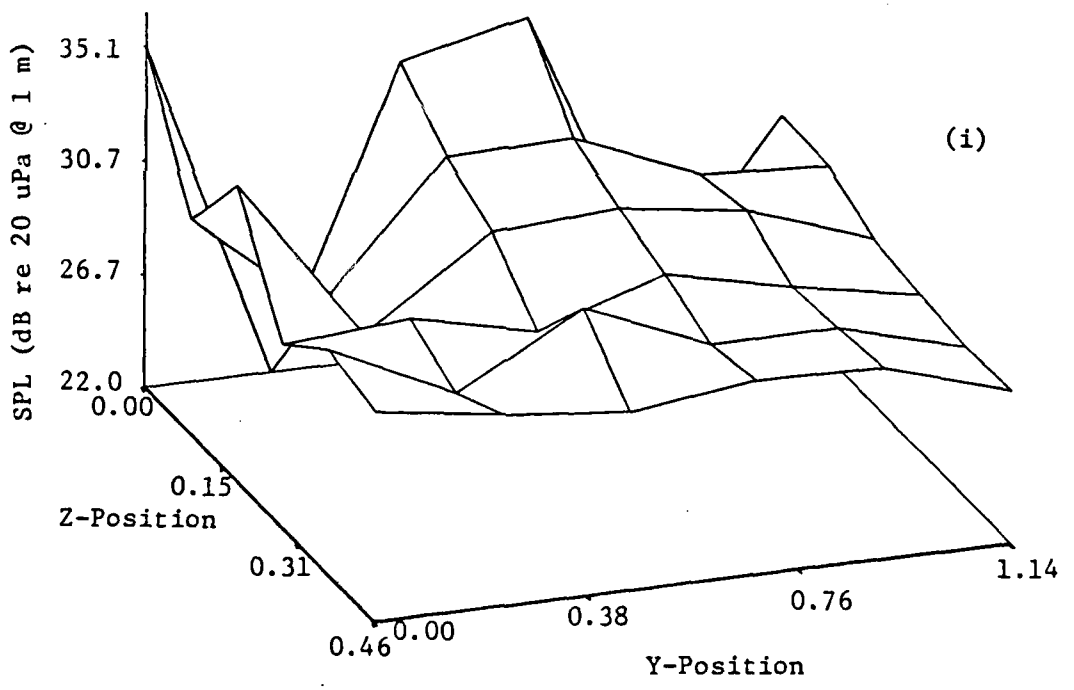

Figure 3.2.8 . Continued.

(h) BPF x 7.
(i) BPF x 8.

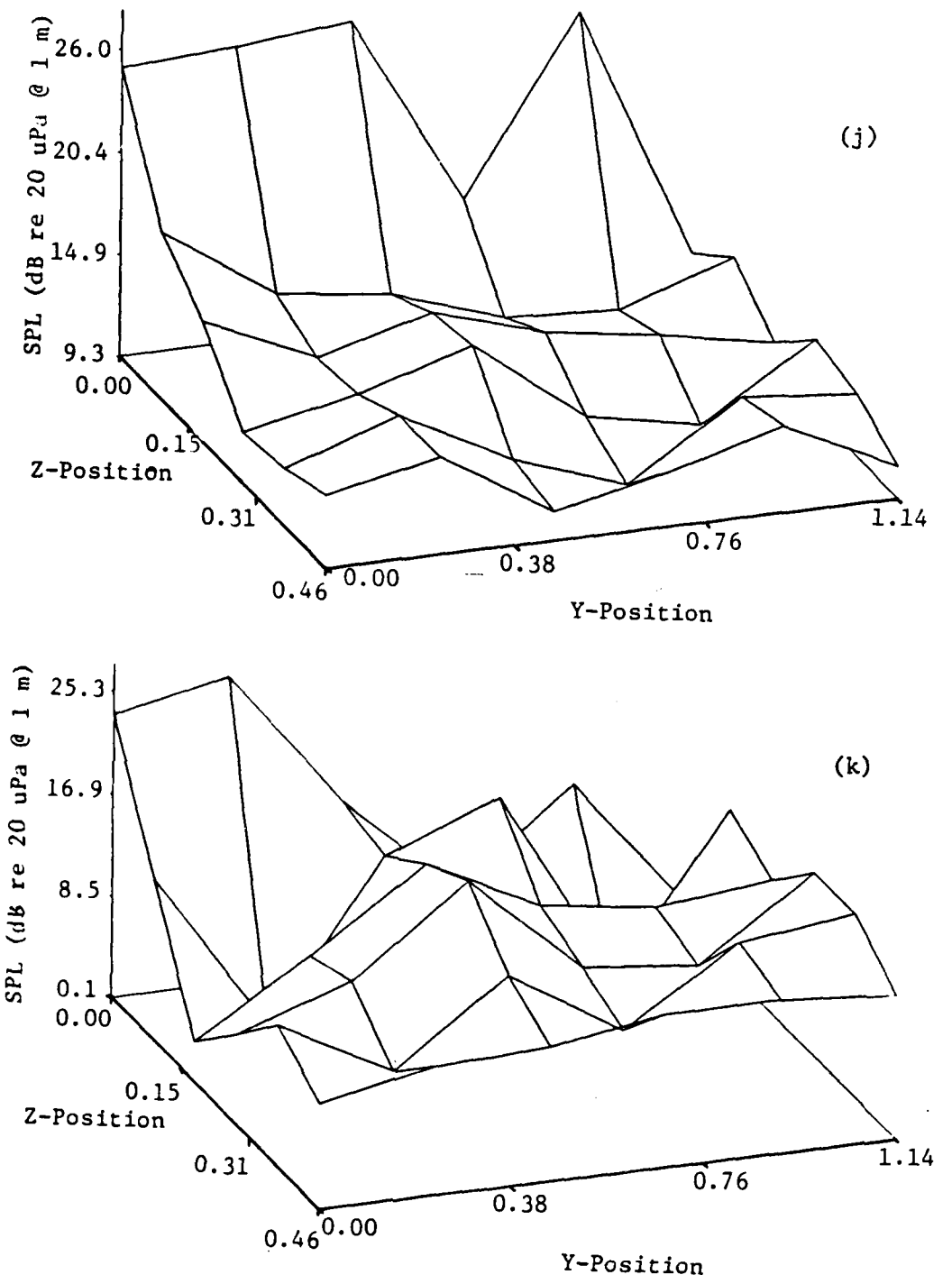

Figure 3.2.8 . Continued.

(j) BPF x 9.
(k) BPF x 10.

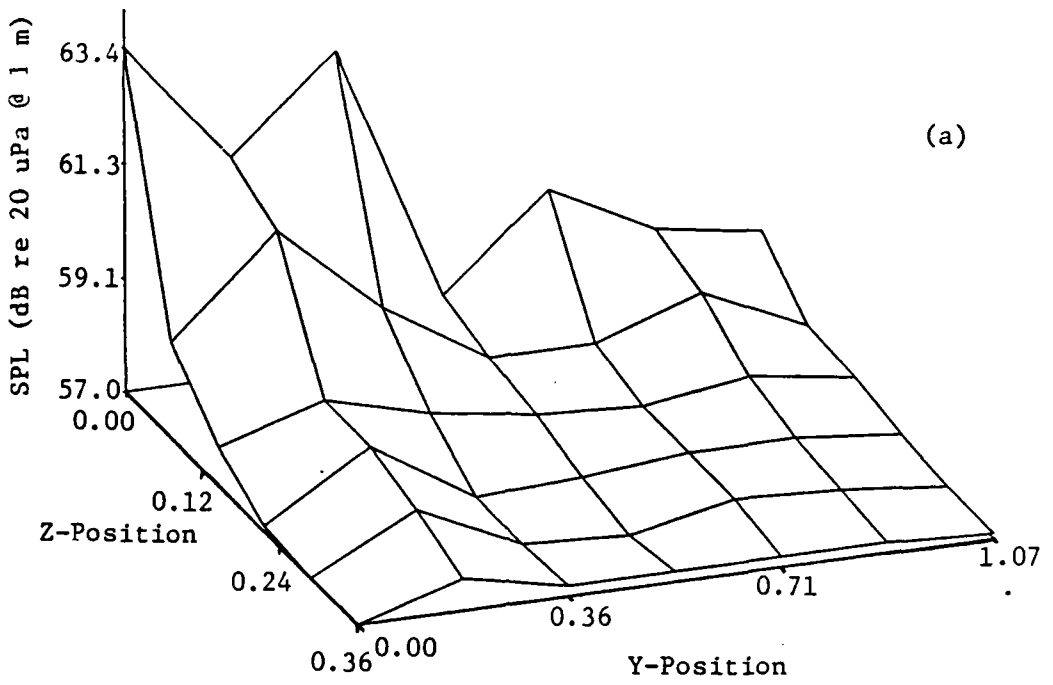

Figure 3.2.9 . SPL for the Patriot vs. Axial and Radial Locations of a Cylindrical Obstruction. (8 Hz Bandwidth.)

(a) OASPL (20 kHz Bandwidth).

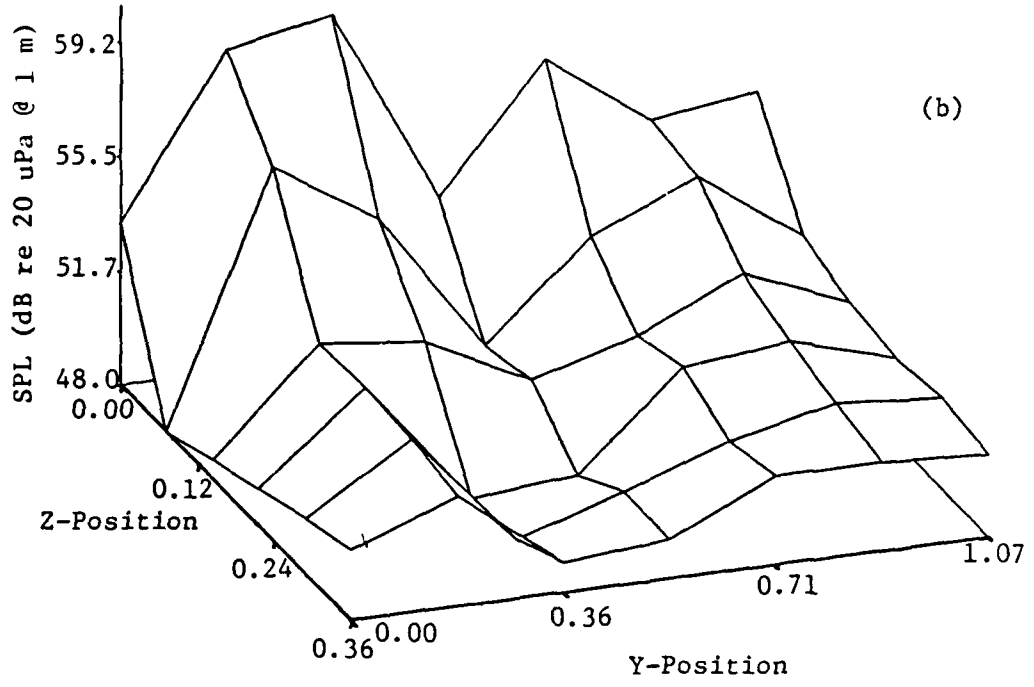

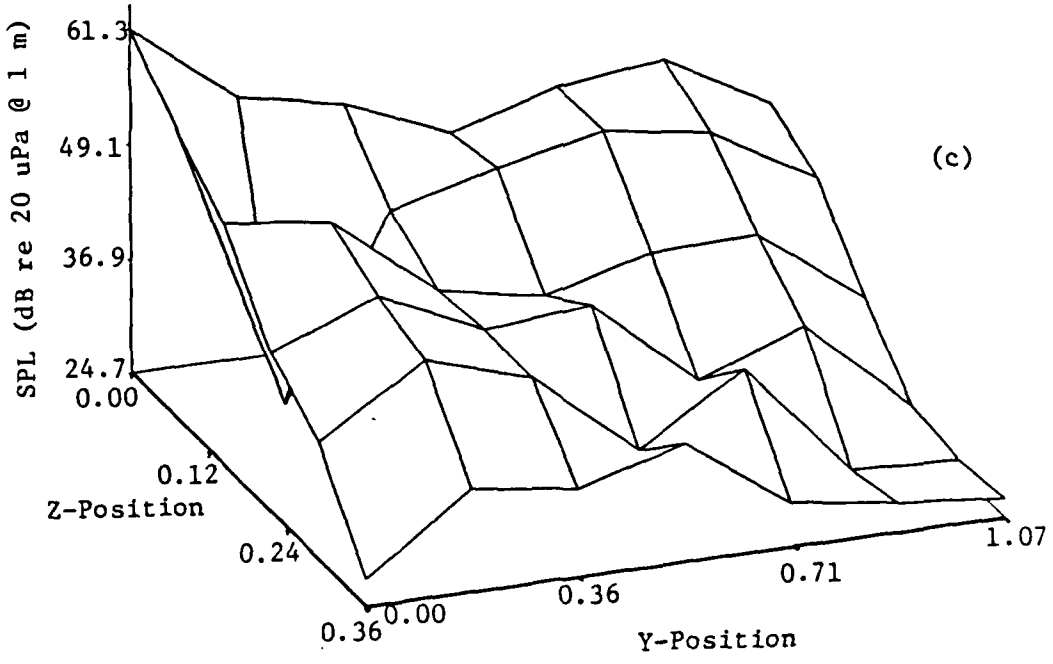

Figure 3.2.9 . Continued.

(b) BPF x 1.
(c) BPF x 2.

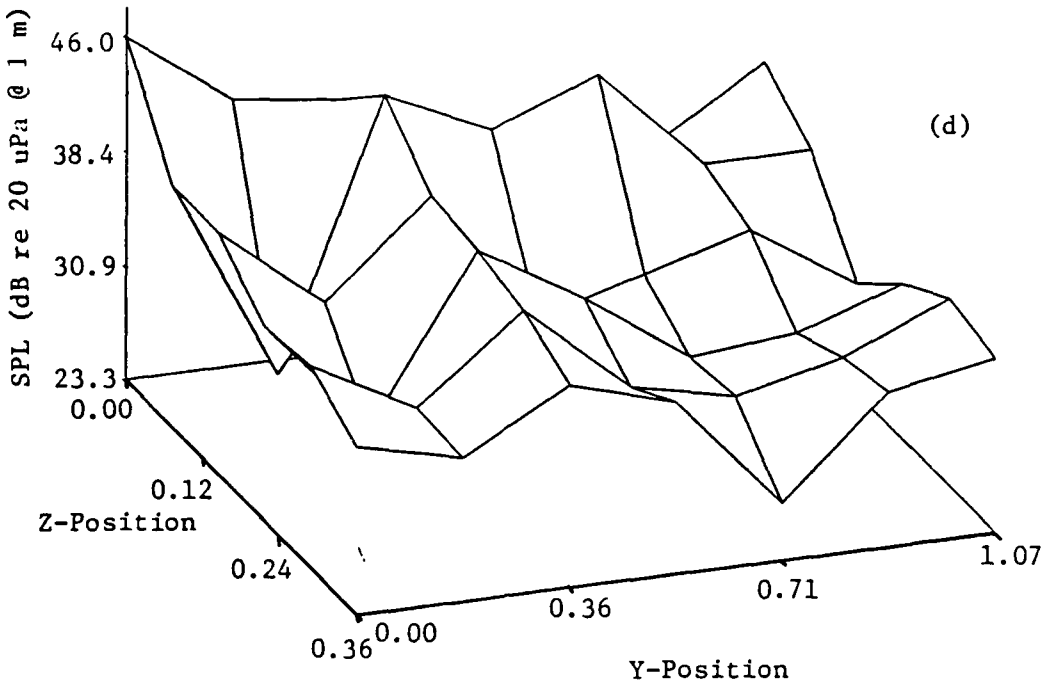

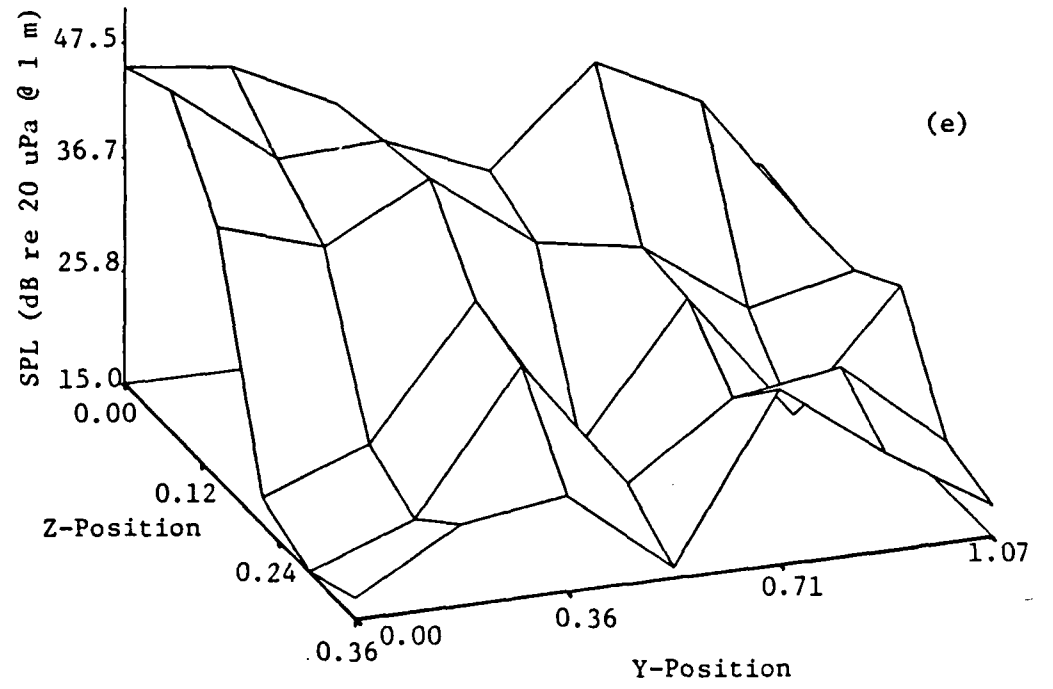

Figure 3.2.9 . Continued.

(d) BPF x 3.
(e) BPF x 4.

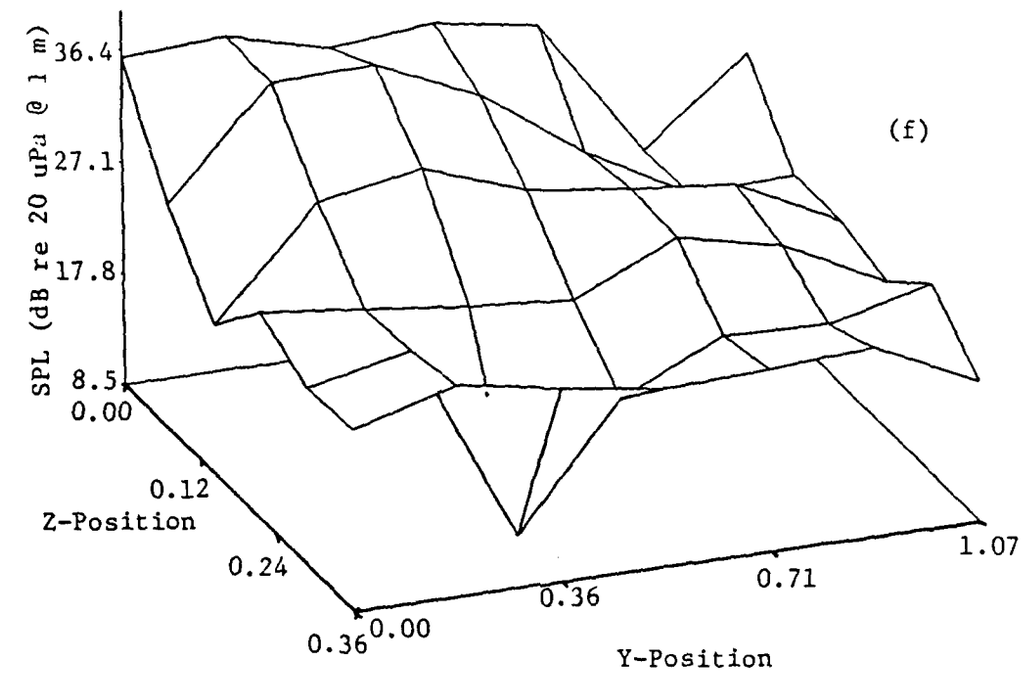

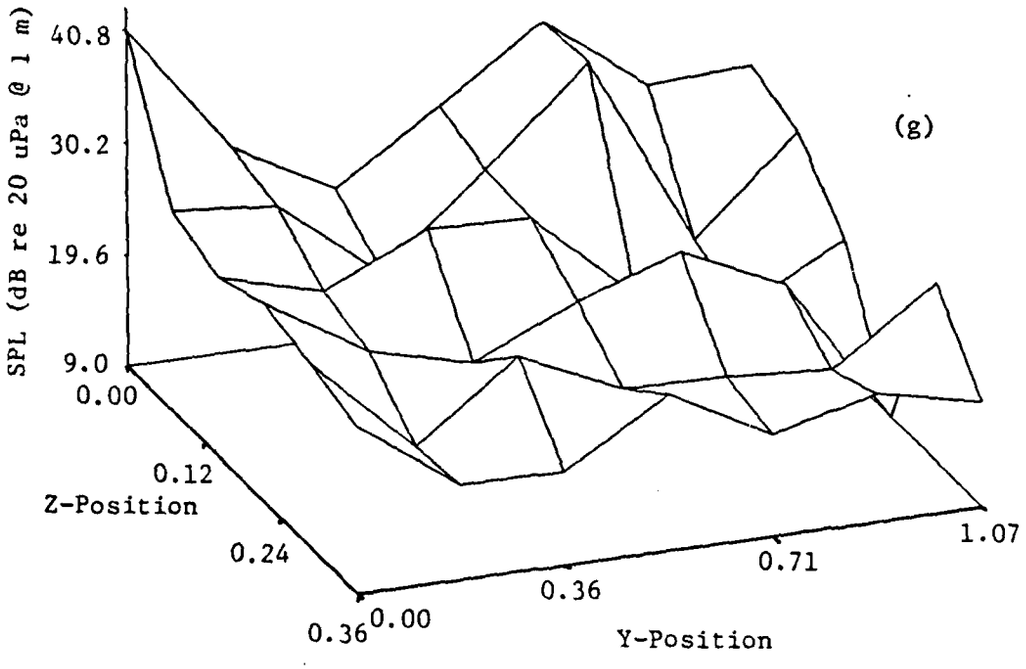

Figure 3.2.9 . Continued.

(f) BPF x 5.
(g) BPF x 6.

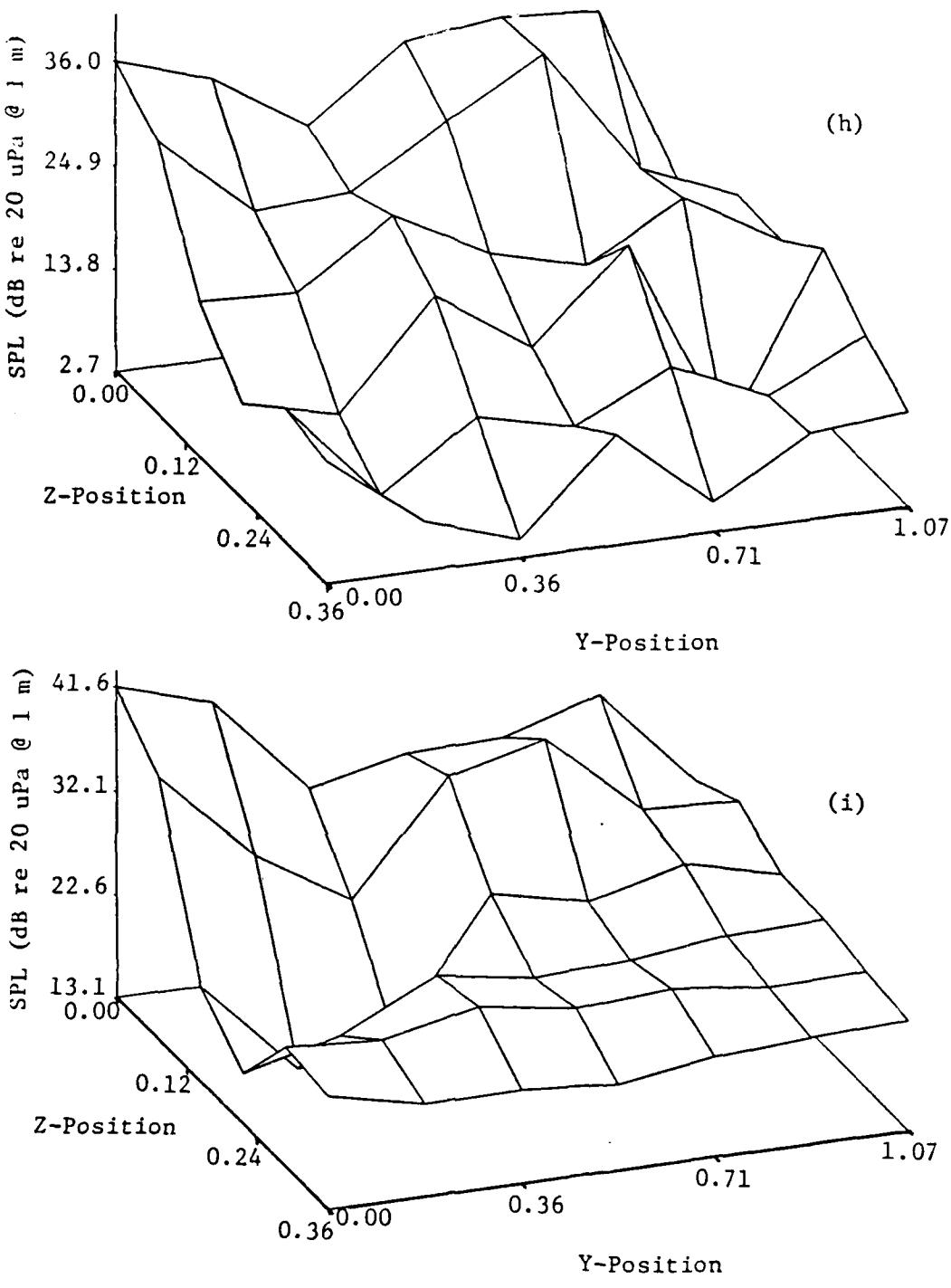

Figure 3.2.9 . Continued.

(h) BPF x 7.
(i) BPF x 8.

AD-A160 579 EFFECTS OF INFLOW CONDITIONS ON DISCRETE FREQUENCY NOISE GENERATED BY SMA..(U) PENNSYLVANIA STATE UNIV UNIVERSITY PARK APPLIED RESEARCH LAB.. 2/2

UNCLASSIFIED K B WASHBURN ET AL. SEP 85 F/G 13/1 NL

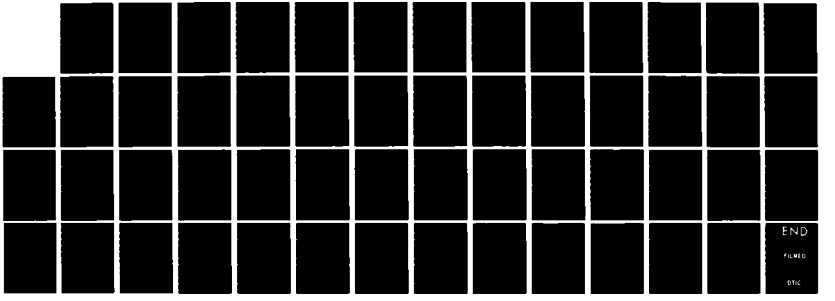

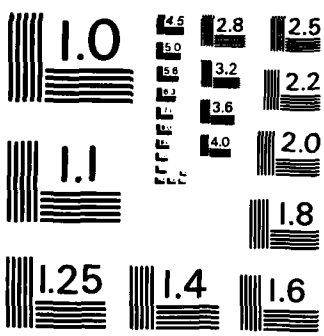

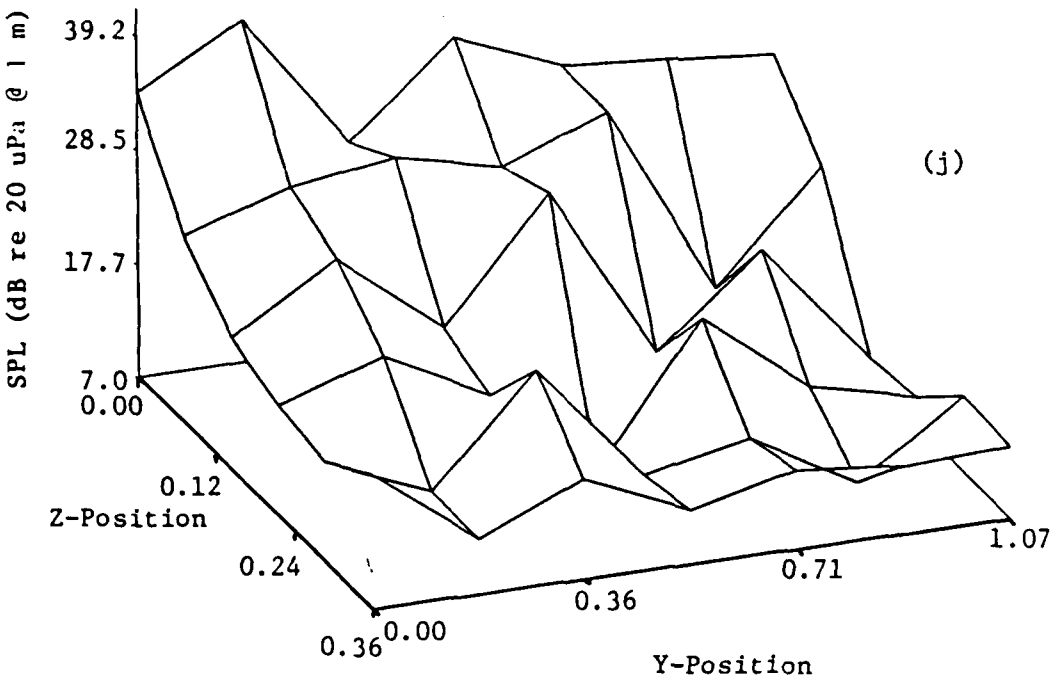

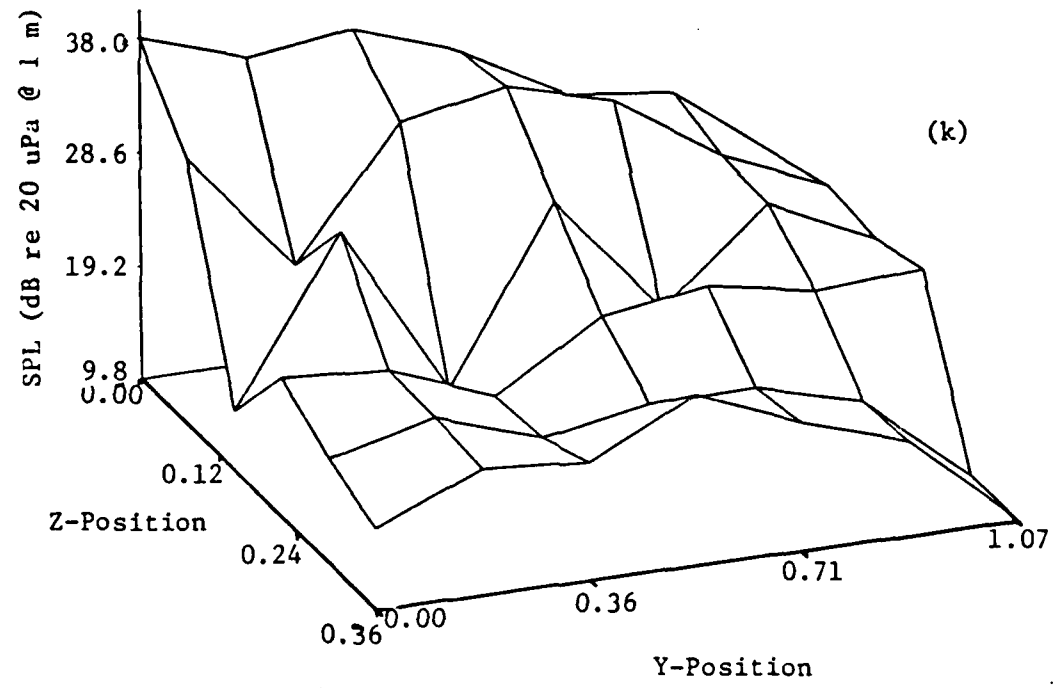

Figure 3.2.9 . Continued.

(j) BPF x 9.
(k) BPF x 10.

support the logical conclusion that increased separation distance (or, equivalently, decreased flow velocity encountered by the obstruction) is the most consistent means of reducing noise.

While the BPF x 1 tone is strong relative to the other tones for small axial separations, it decreases sharply toward its baseline value as separation increases for both fans. In contrast, the BPF x 2 tone decreases more gradually. This is expected, since the BPF x 2 tone is generated by rotor/wake interaction and the obstruction wake is sharply defined in the regions plotted. As noted before, the behavior of the higher harmonics is difficult to explain.

It is assumed that the trends for these tones depend on such details as flow velocity at the obstruction, wake profile, angle of attack between the blade leading edge and the wake, path length of the blade through the wake, and the span region of the blade affected by the wake. One interesting feature is the BPF x 3 tone for the Muffin XL. On the z-axis (y = 0.0 fan radii), the tone decreases sharply, while off the axis, it remains on a plateau in the 30 - 35 dB SPL range.

3.2.2. The Thin, Rectangular Obstruction

Because the trailing edge of a thin, rectangular obstruction is abrupt, flow separation is more complete; hence, its wake profile is sharper than that of the cylinder and the vleocity deficit is more pronounced. As a result, the fluctuations of unsteady lift on the blades are expected to be greater and the interaction tones stronger.

3.2.2.1. The Effect of Axial Location

Figure 3.2.10 shows the OASPL as a function of upstream location

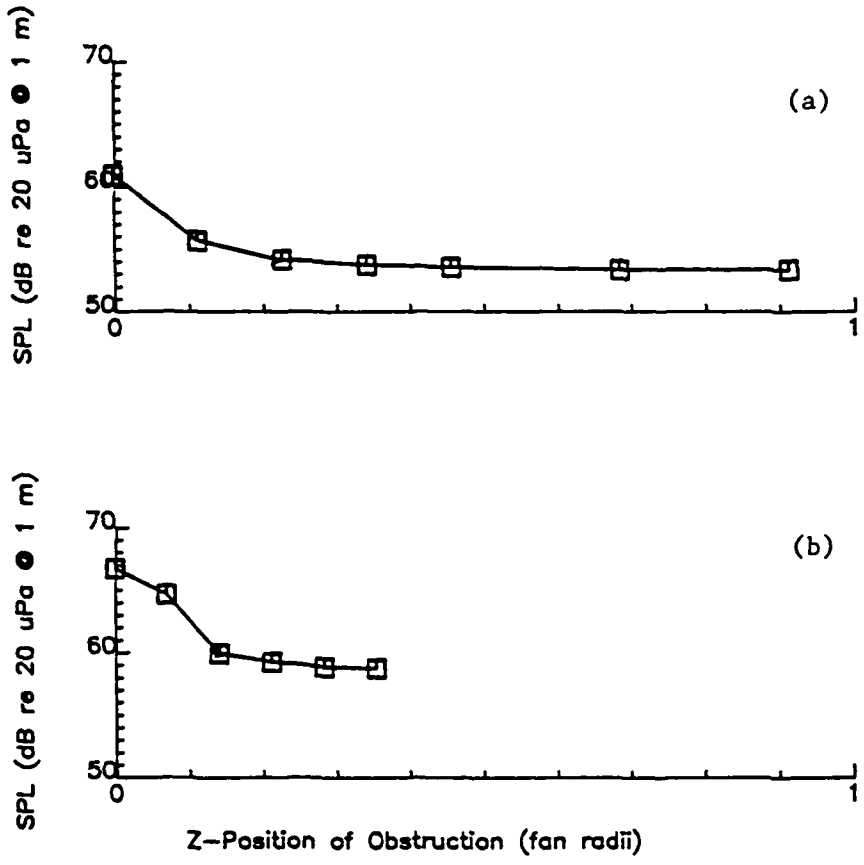

Figure 3.2.10 . OASPL vs. Axial Location of a Thin, Rectangular Obstruction. (y = 0.0 Fan Radii, 20 kHz Bandwidth.)

(a) Muffin XL.
(b) Patriot.

for the Mufffin XL and Patriot. Comparing these data with Figure 3.2.1, it is obvious that the noise levels are higher for the thin rectangle than for the cylinder at small separation distances. Also, the distance at which the curves reach asymptotic baseline noise levels is slightly larger: about 0.35 fan radii in contrast to 0.3 fan radii for the cylinder. This larger interaction distance and associated stronger noise generation provides evidence of a stronger wake behind the thin rectangle.

The plots for the discrete tones at BPF x 1 through BPF x 10 are shown in Figure 3.2.11 for the Muffin XL and in Figure 3.2.12 for the Patriot. The BPF x 1 tones are relatively unaffected by the obstruction; however, slight increases at small separation distances suggest that there is some contribution from unsteady loading. The interaction tones beginning with BPF x 2 are quite strong for small separations, and fall off smoothly to their baseline values. The higher harmonics (BPF x 5 and above) exhibit similar trends. This was not as clear for the cylindrical obstruction. Since the wake of the thin rectangle is more pronounced, it produces a stronger series of blade loading harmonics, which make greater contributions to the higher radiating blade passage harmonics.

3.2.2.2. The Effect of Radial Location

The OASPL's for the Muffin XL and Patriot are shown in Figure 3.2.13 as a function of radial location of the thin, rectangular obstruction. The axial separation is 0.0 fan radii, so the wake is very pronounced. The trends of the curves are similar to those shown for the cylindrical obstruction in Figure 3.2.5. Again the levels are higher due to stronger rotor/wake interaction.

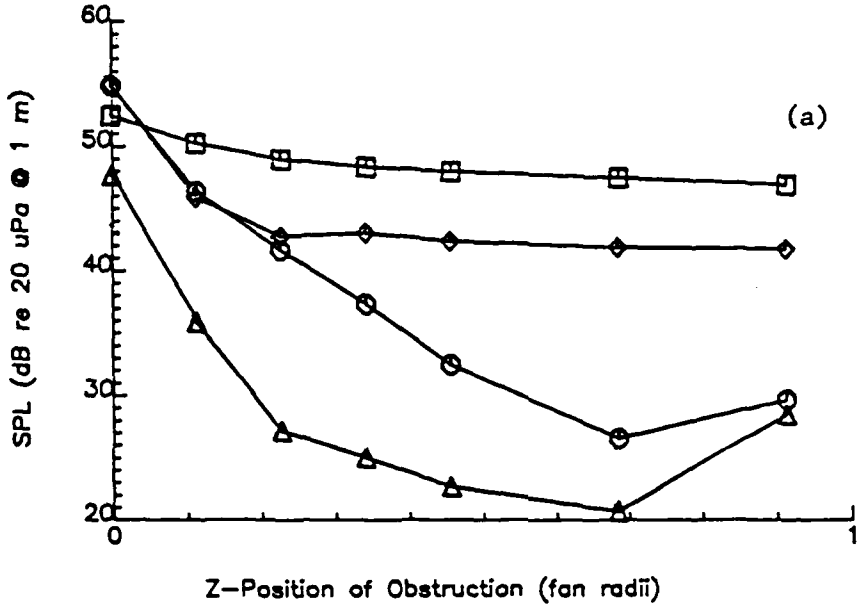

Figure 3.2.11 . SPL of Blade Passage Tones of the Muffin XL vs. Axial Location of a Thin, Rectangular Obstruction. (y = 0.0 Fan Radii, 4 Hz Bandwidth.)

(a) □-- BPF x 1, ○-- BPF x 2, Δ -- BPF x 3, ◇-- BPf x 4.

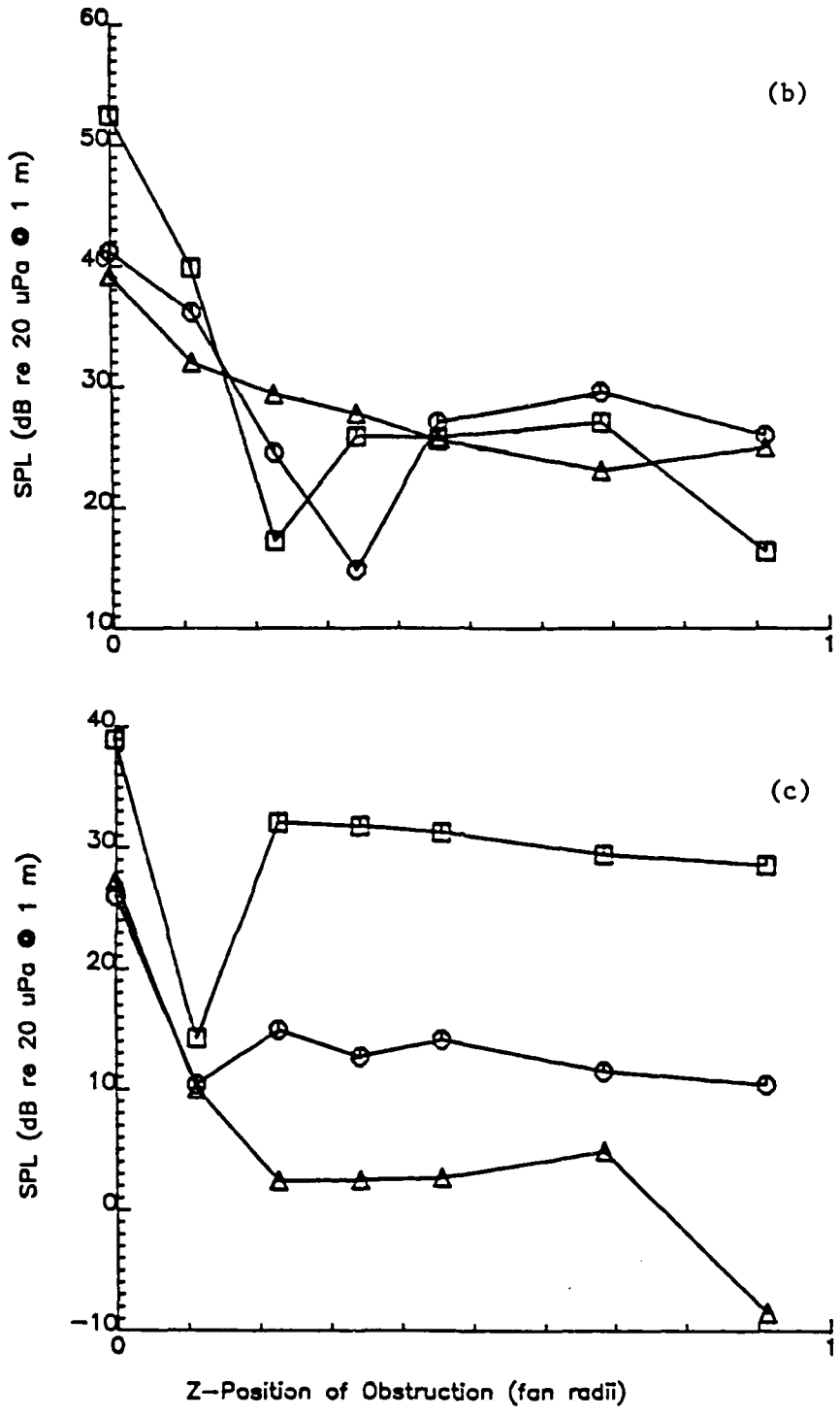

Figure 3.2.11 . Continued.

(b) □-- BPF x 5, ○-- BPF x 6, Δ -- BPF x 7.
(c) □-- BPF x 8, ○-- BPF x 9, Δ -- BPF x 10.

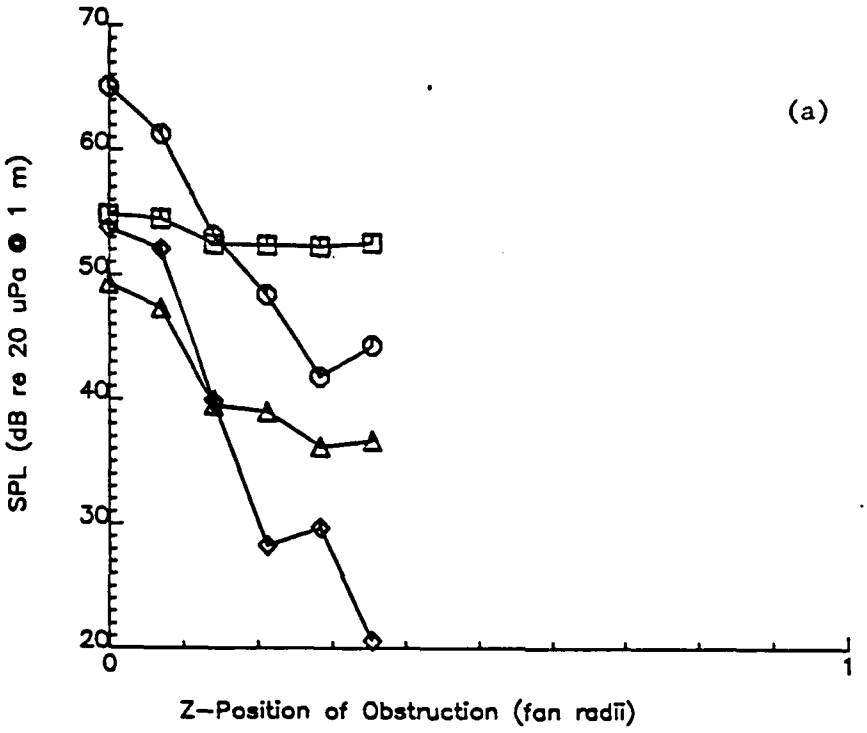

Figure 3.2.12 . SPL of Blade Passage Tones of the Patriot vs. Axial Location of a Thin, Rectangular Obstruction. (y = 0.0 Fan Radii, 8 Hz Bandwidth.)

(a) □-- BPF x 1, ○-- BPF x 2, Δ -- BPF x 3, ◇-- BPF x 4.

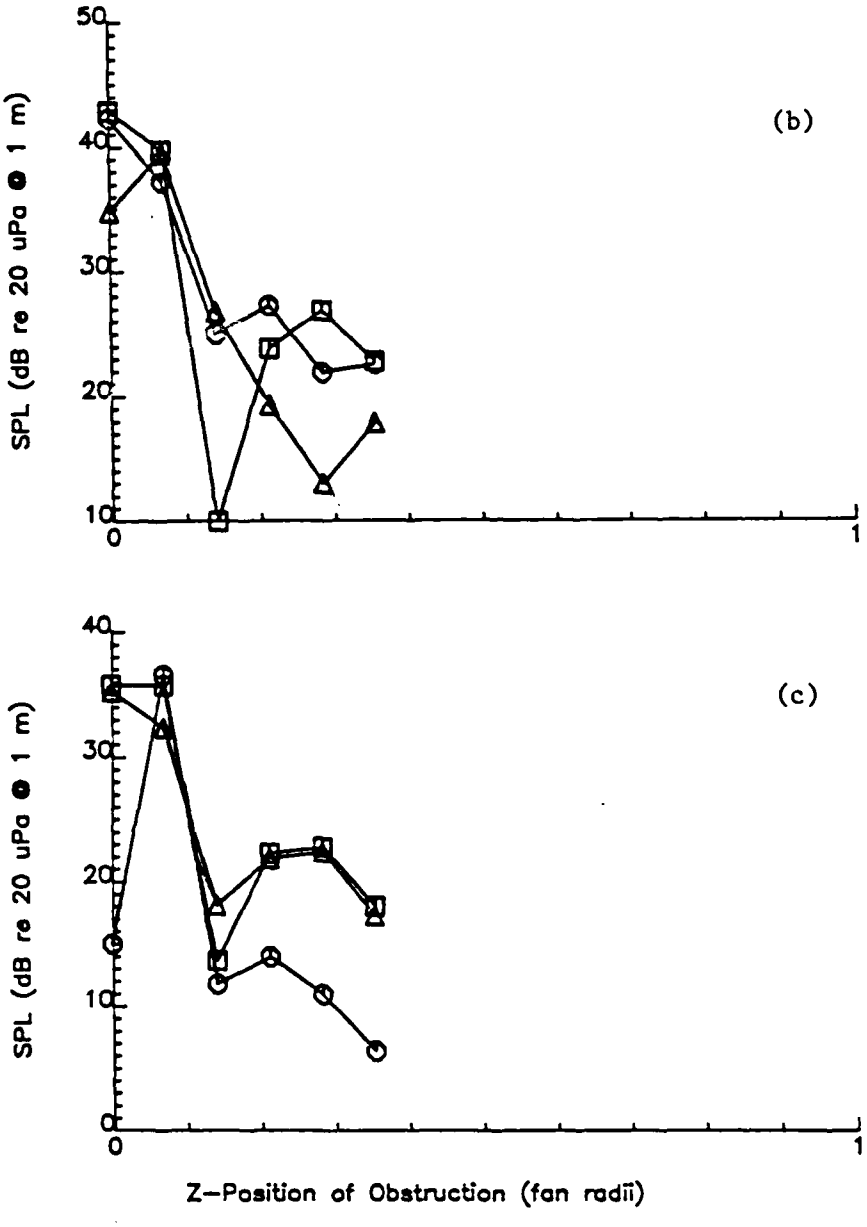

Figure 3.2.12 . Continued.

(b) □-- BPF x 5, ○-- BPF x 6, Δ -- BPF x 7.
(c) □-- BPF x 8, ○-- BPF x 9, Δ -- BPF x 10.

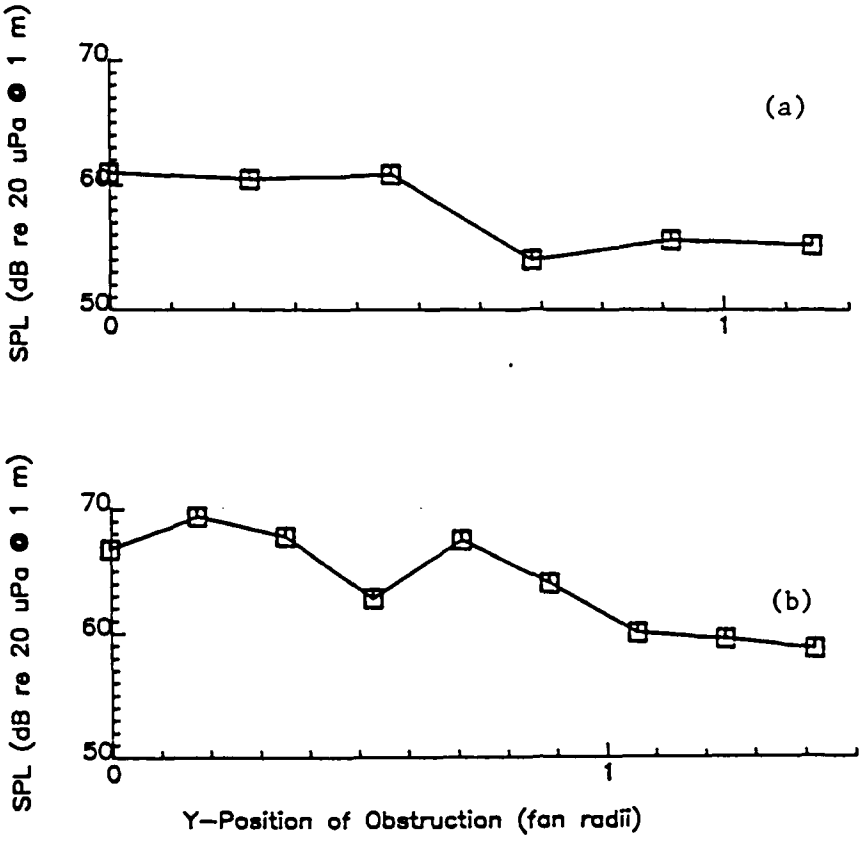

Figure 3.2.13 . OASPL vs. Radial Location of a Thin, Rectangular Obstruction. (z = 0.0 Fan Radii, 20 kHz Bandwidth.)

(a) Muffin XL.
(b) Patriot.

The plots for the blade passage tones are shown for the Muffin XL in Figure 3.2.14 and for the Patriot in Figure 3.2.15. There is a region near 0.7 fan radius on the Muffin XL where most of the tones (and the OASPL) decrease markedly. This region coincides with the mid-span of the blades. The data for the Patriot are scattered more, but they follow the trends of the cylindrical obstruction more closely.

3.2.3. The Thick, Rectangular Obstruction

The thick, rectangular obstruction, as described in Section (2.3.1.1.), had a width of one fan radius, and as such it obstructed a large percentage of the fan inlet. Its presence does not simply create a wake which the fan ingests, but represents a true blockage which greatly alters the overall aerodynamics of the fan. For very small axial separation distances, the fan was choked and approached a flow condition near stall. The noise generation was modified accordingly. Because the flow patterns were so complicated, interpretation of the noise data is less certain than for the smaller-width obstructions.

3.2.3.1. The Effect of Axial Location

Beginning from an axial location of 0.0 fan radii, the fans operated near stall. Because the volume flow and steady thrust were reduced, the rotor speed increased a few rpm. As the obstruction was pulled away slightly, some flow, particularly near the inlet shroud, was restored, and stall noise decreased. This can be seen in Figure 3.2.16, which shows OASPL for the Muffin XL and the Patriot. A further increase in separation distance restored a large percentage of the baseline volume flow, and the effect of the wake generated by the obstruction begins to show in increased noise generation. The noise

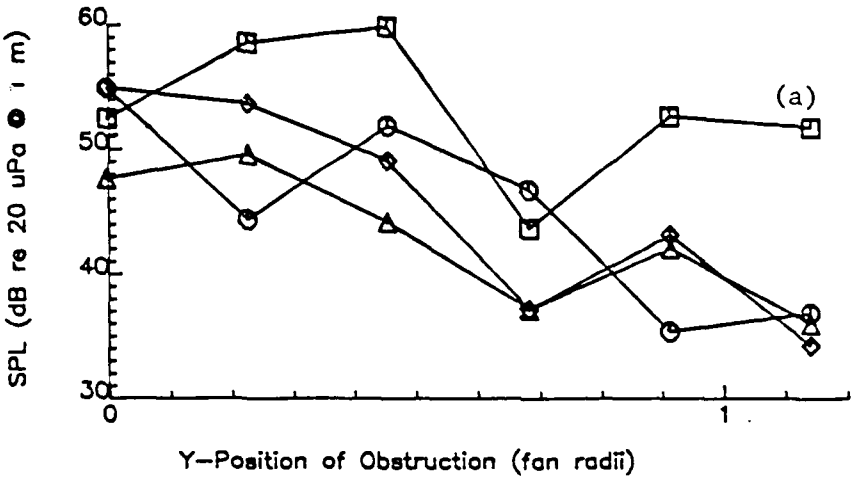

Figure 3.2.14 . SPL of Blade Passage Tones of the Muffin XL vs. Radial Location of a Thin, Rectangular Obstruction. (z = 0.0 Fan Radii, 4 Hz Bandwidth.)

(a) □-- BPF x 1, ○-- BPF x 2, Δ -- BPF x 3, ◇-- BPF x 4.

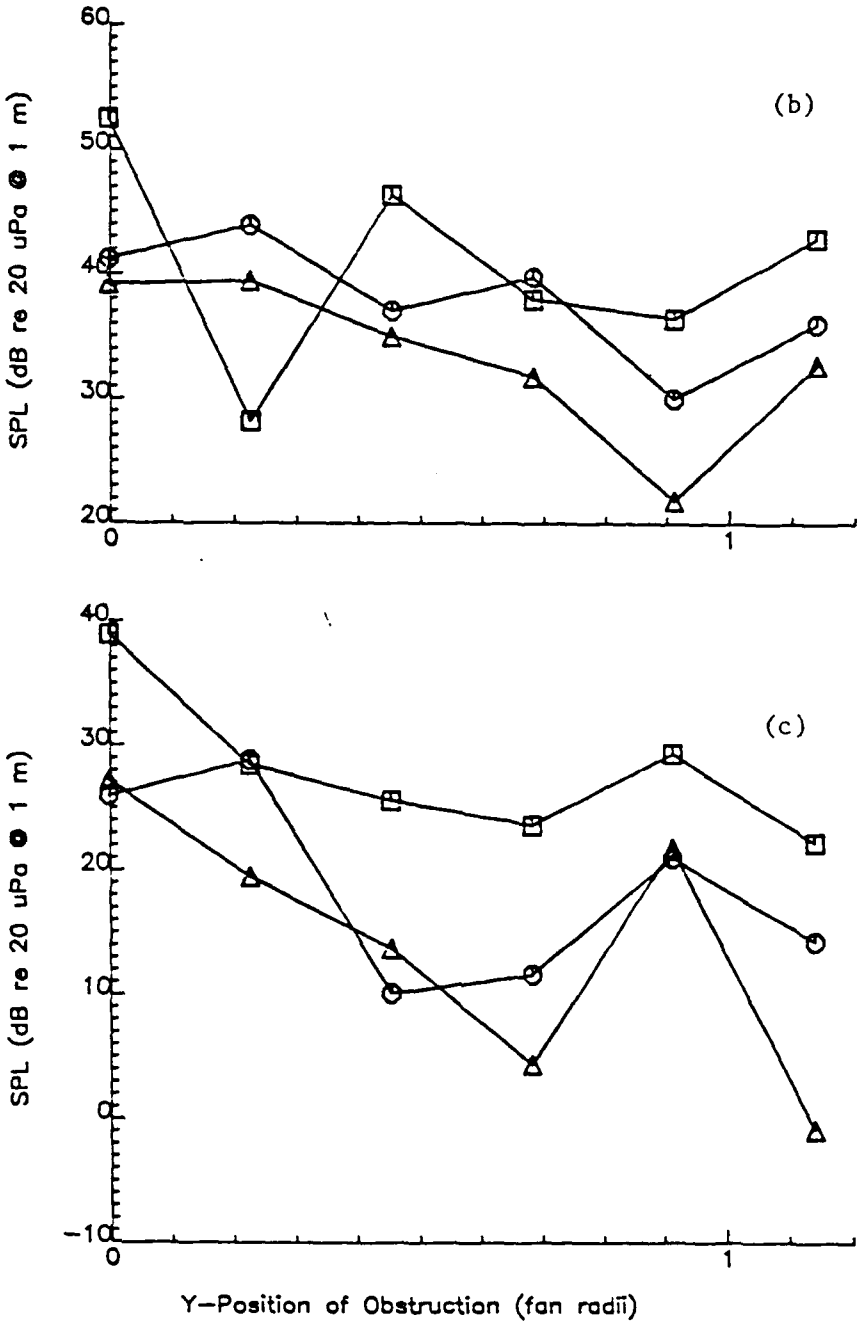

Figure 3.2.14 . Continued.

(b) □ -- BPF x 5, ○ -- BPF x 6, Δ -- BPF x 7.
(c) □ -- BPF x 8, ○ -- BPF x 9, Δ -- BPF x 10.

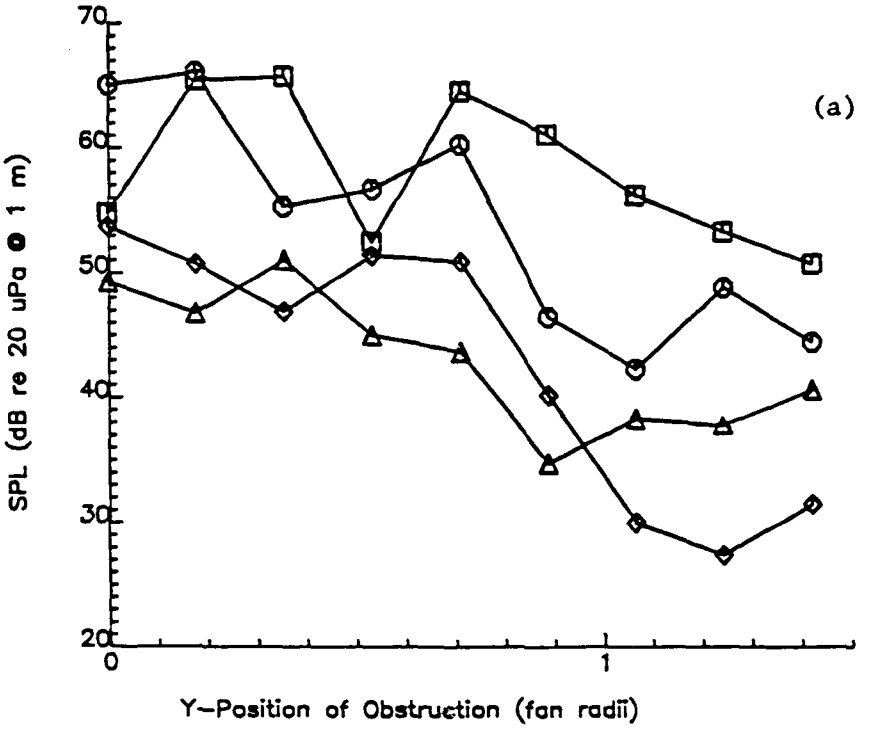

Figure 3.2.15 . SPL of Blade Passage Tones of the Patriot vs. Radial Location of a Thin, Rectangular Obstruction. (z = 0.0 Fan Radii, 8 Hz Bandwidth.)

(a) □-- BPF x 1, ○-- BPF x 2, Δ -- BPF x 3, ◇-- BPF x 4.

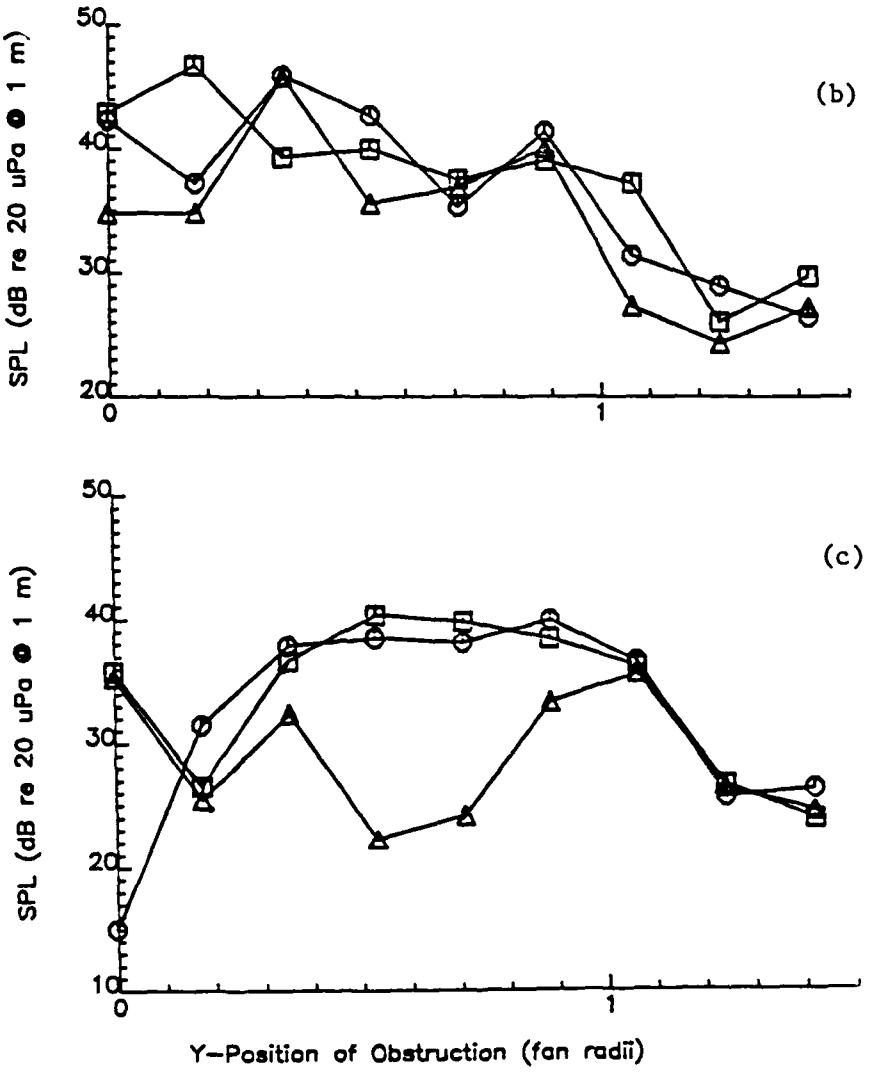

Figure 3.2.15 . Continued.

(b) □-- BPF x 5, ○-- BPF x 6, Δ -- BPF x 7.
(c) □-- BPF x 8, ○-- BPF x 9, Δ -- BPF x 10.

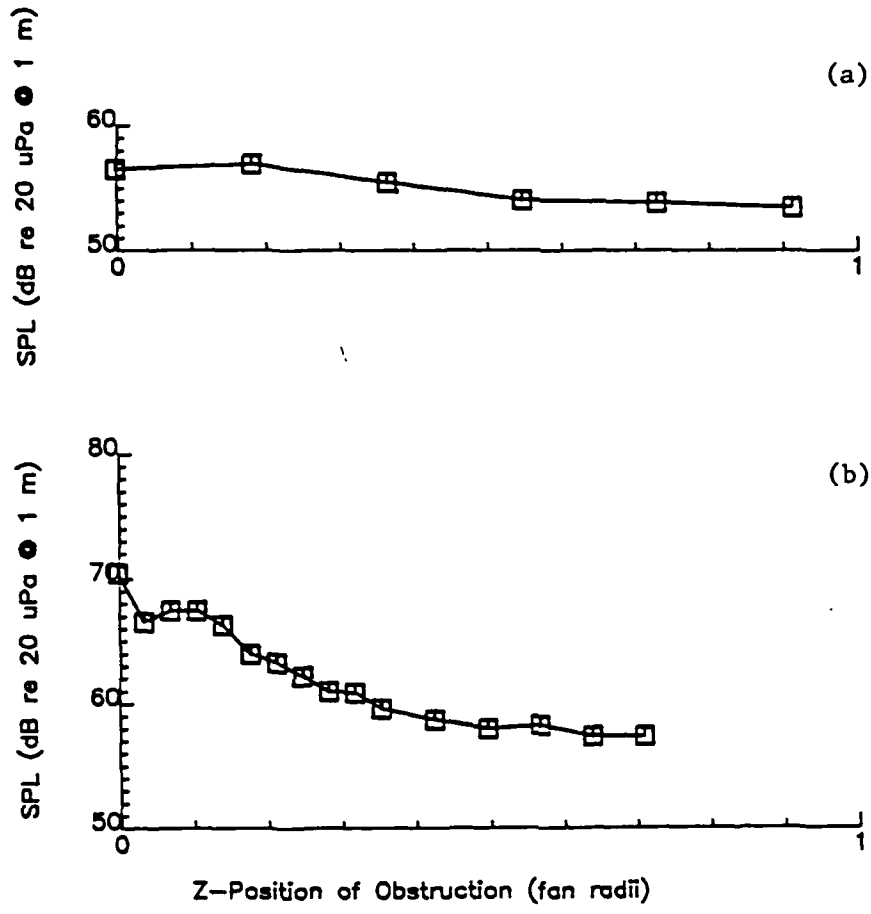

Figure 3.2.16 . OASPL vs. Axial Location of a Thick, Rectangular Obstruction. (y = 0.0 Fan Radii, 20 kHz Bandwidth.)

(a) Muffin XL.
(b) Patriot.

then decreases with increasing separation, but with a slope that is smaller than those observed for the smaller obstructions.

The data for the discrete tones are shown in Figure 3.2.17 for the Muffin XL and in Figure 3.2.18 for the Patriot. In the Muffin XL data, the tones from BPF x 4 through BPF x 10 all have a "turn-on" point. For axial separations less than 0.1 fan radii, the levels are like those of the fan in stall. With increasing separation, interaction forces dominate and the tones increase in level until the distance is great enough that the wake begins to weaken. For the Patriot, the behavior is more complex, but a similar pattern develops.

It might be tempting to place a blockage that is near a fan inlet very close because the tones are reduced. This is not recommended for two reasons: First, in the region where the tones apppear reduced, many are above baseline. Secondly, the overall noise is still high in this case and is characterized by the "tearing" sound of stall.

3.2.3.2. The Effect of Radial Location

The radial position of the obstruction is measured with respect to its centerline. The OASPL's of the Muffin XL and the Patriot are plotted as a function of radial position in Figure 3.2.19. These data exhibit remarkable similarity. The overall noise is a minimum when the centerline of the obstruction is at the center of the hub and again when it meets the edge of the hub. This behavior is tied to the complex flow around the obstruction. The path length of the blade behind the obstruction, along with the number of times it passes behind the obstruction in one revolution, are also factors in the amount and type of noise generated.

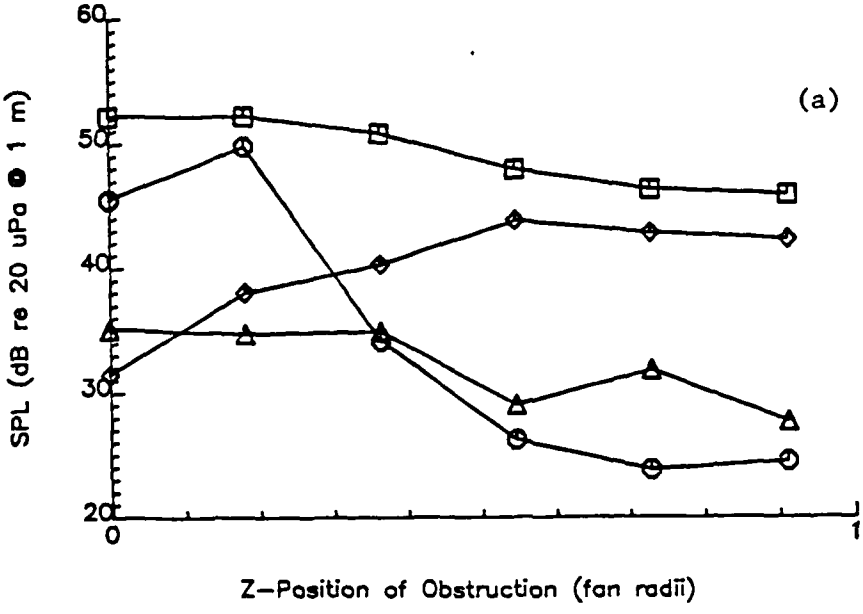

Figure 3.2.17 . SPL of Blade Passage Tones of the Muffin XL vs. Axial Location of a Thick, Rectangular Obstruction. (y = 0.0 Fan Radii, 4 Hz Bandwidth.)

(a) □ -- BPF x 1, ○ -- BPF x 2, Δ -- BPF x 3, ◇ -- BPF x 4.

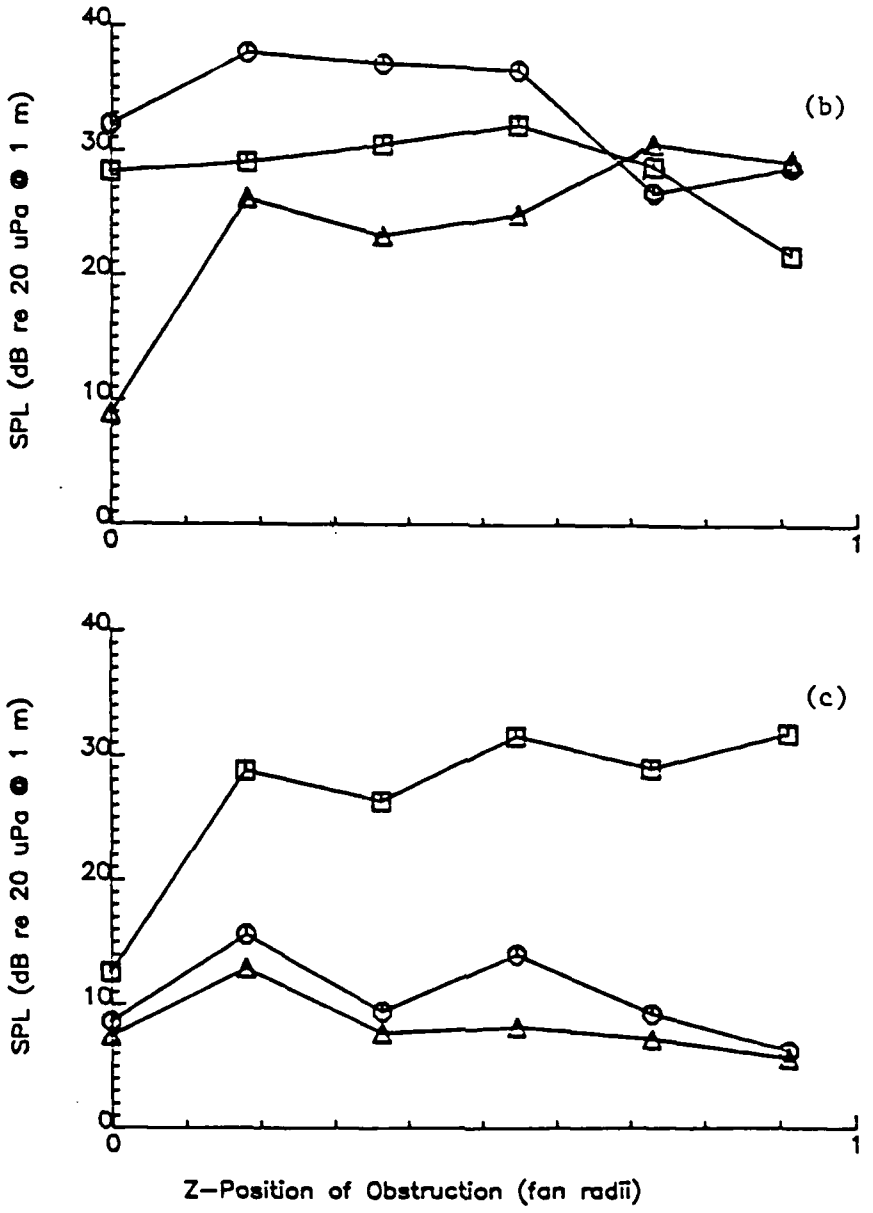

Figure 3.2.17 . Continued.

(b) □-- BPF x 5, ○-- BPF x 6, Δ -- BPF x 7.
(c) □-- BPF x 8, ○-- BPF x 9, Δ -- BPF x 10.

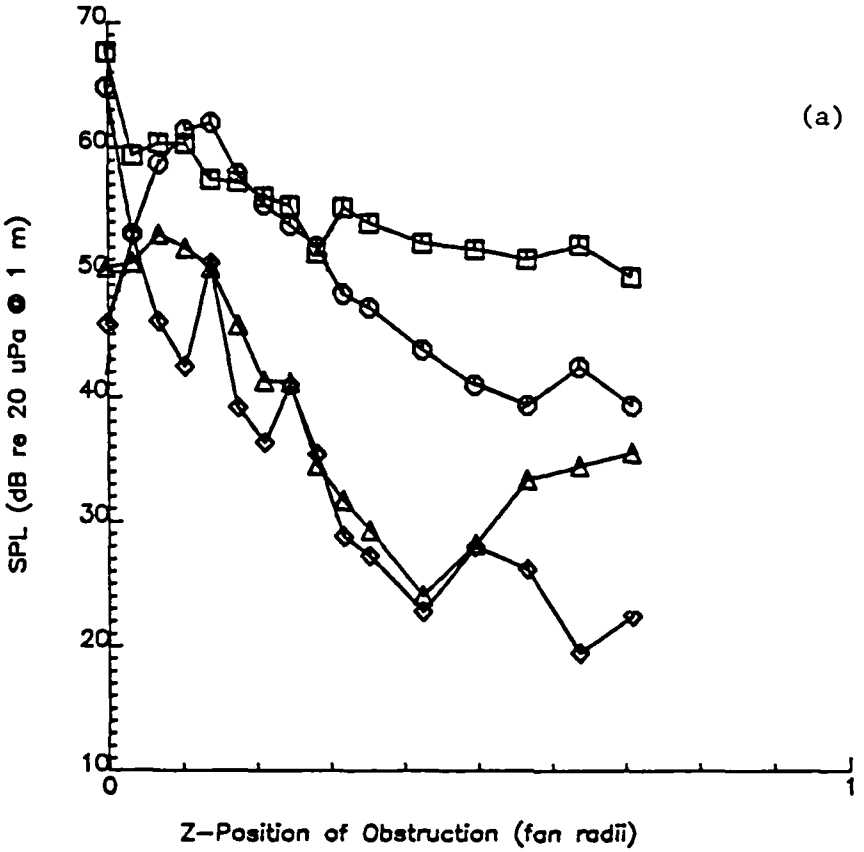

Figure 3.2.18 . SPL of Blade Passage Tones of the Patriot vs. Axial Location of a Thick, Rectangular Obstruction. (y = 0.0 Fan Radii, 8 Hz Bandwidth.)

(a) □-- BPF x 1, ○-- BPF x 2, Δ -- BPF x 3, ◇-- BPF x 4.

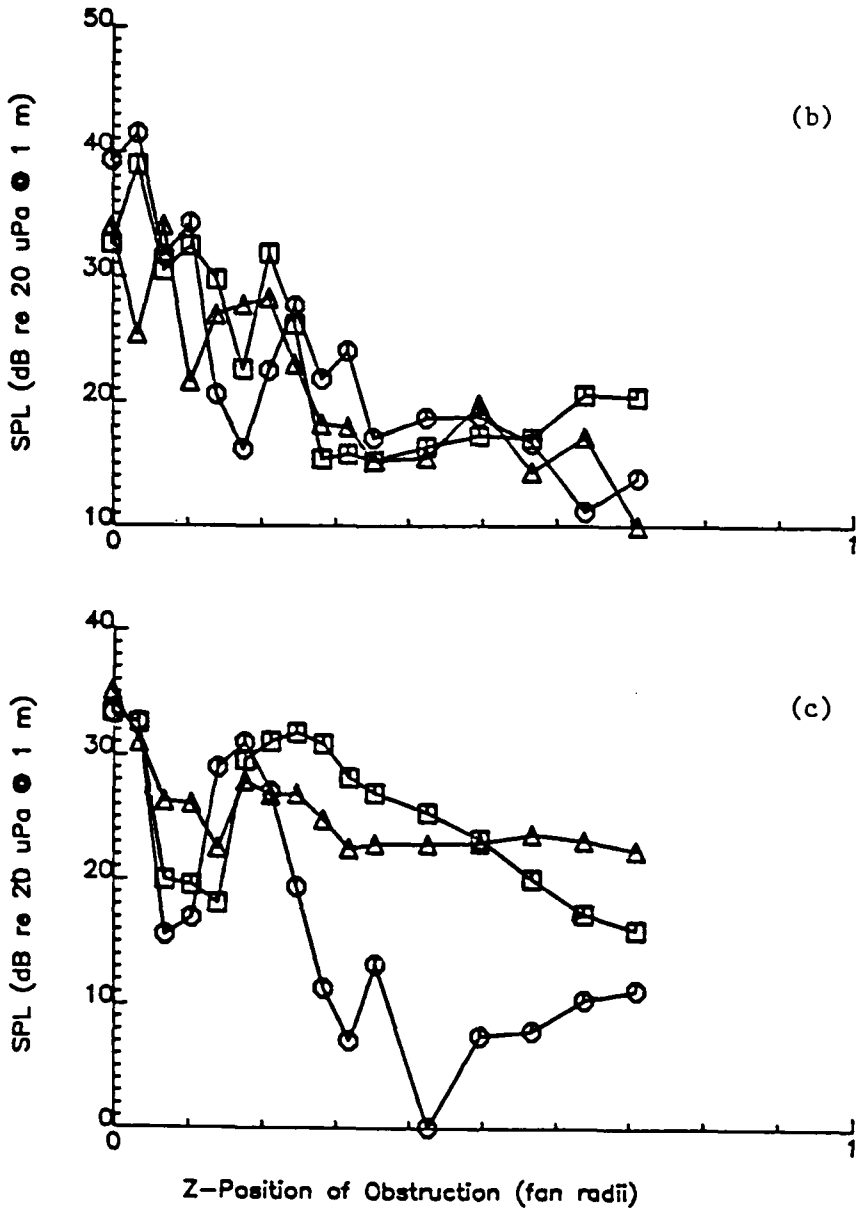

Figure 3.2.18 . Continued.

(b) □-- BPF x 5, ○-- BPF x 6, Δ -- BPF x 7.
(c) □-- BPF x 8, ○-- BPF x 9, Δ -- BPF x 10.

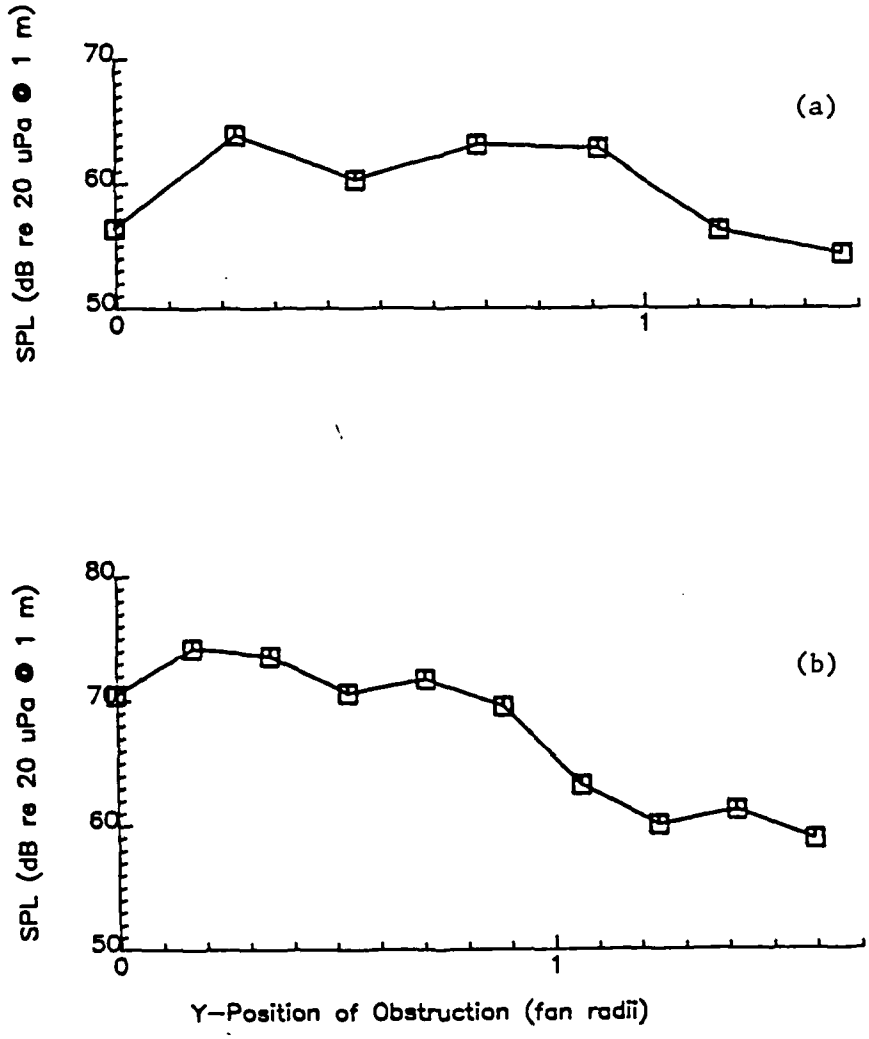

Figure 3.2.19 . OASPL vs. Radial Location of a Thick, Rectangular Obstruction. (z = 0.0 Fan Radii, 20 kHz Bandwidth.)

(a) Muffin XL.
(b) Patriot.

The BPF tones for each fan are plotted in Figures 3.2.20 and 3.2.21. Note that the interaction tones (BPF x 2 and above) are at maximum levels in regions where the overall noise is minimum. This suggests a tradeoff between the sources of discrete tone and broadband noise energy in terms of the available flow energy, dependent on the local structure of the flow. The BPF x 1 tones have the same curve shapes as the corresponding OASPL's. Since broadband noise tends to be a function of total flow and the BPF x 1 tone is a function of steady loading, this result might be expected. Of course, the OASPL contains the BPF x 1 tone within its bandwidth. When the tone is well above the background, it is a major contributor to the OASPL.

3.2.4. The Card Gate Model

The card gate model was purposely constructed so that its dimensions were larger than the diameter of either fan. It was centered on the z-axis with the electronics cards set vertically. The model was moved only axially.

Figure 3.2.22 shows the OASPL for the Muffin XL and the Patriot. The unique feature of these curves is the shallow slope of each, compared to those of the simpler obstructions. This is due to the cumulative effect of having many wakes entering the fan. Each individual wake behaves like that of a simple obstruction, but the sum of them increases the unsteady blade loading over larger separation distances.

The discrete tone plots are shown in Figure 3.2.23 for the Muffin XL and Figure 3.2.24 for the Patriot. As is the case for the thick rectangular obstruction, the BPF x 1 tone curves are similar to

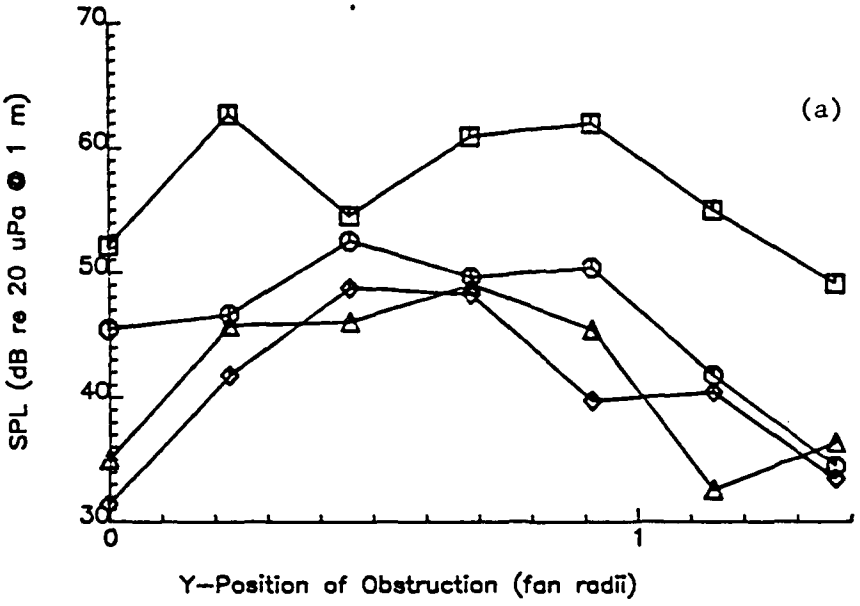

Figure 3.2.20 . SPL of Blade Passage Tones of the Muffin XL vs. Radial Location of a Thick, Rectangular Obstruction. (z = 0.0 Fan Radii, 4 Hz Bandwidth.)

(a) □-- BPF x 1, ○-- BPF x 2, Δ -- BPF x 3, ◇-- BPF x 4.

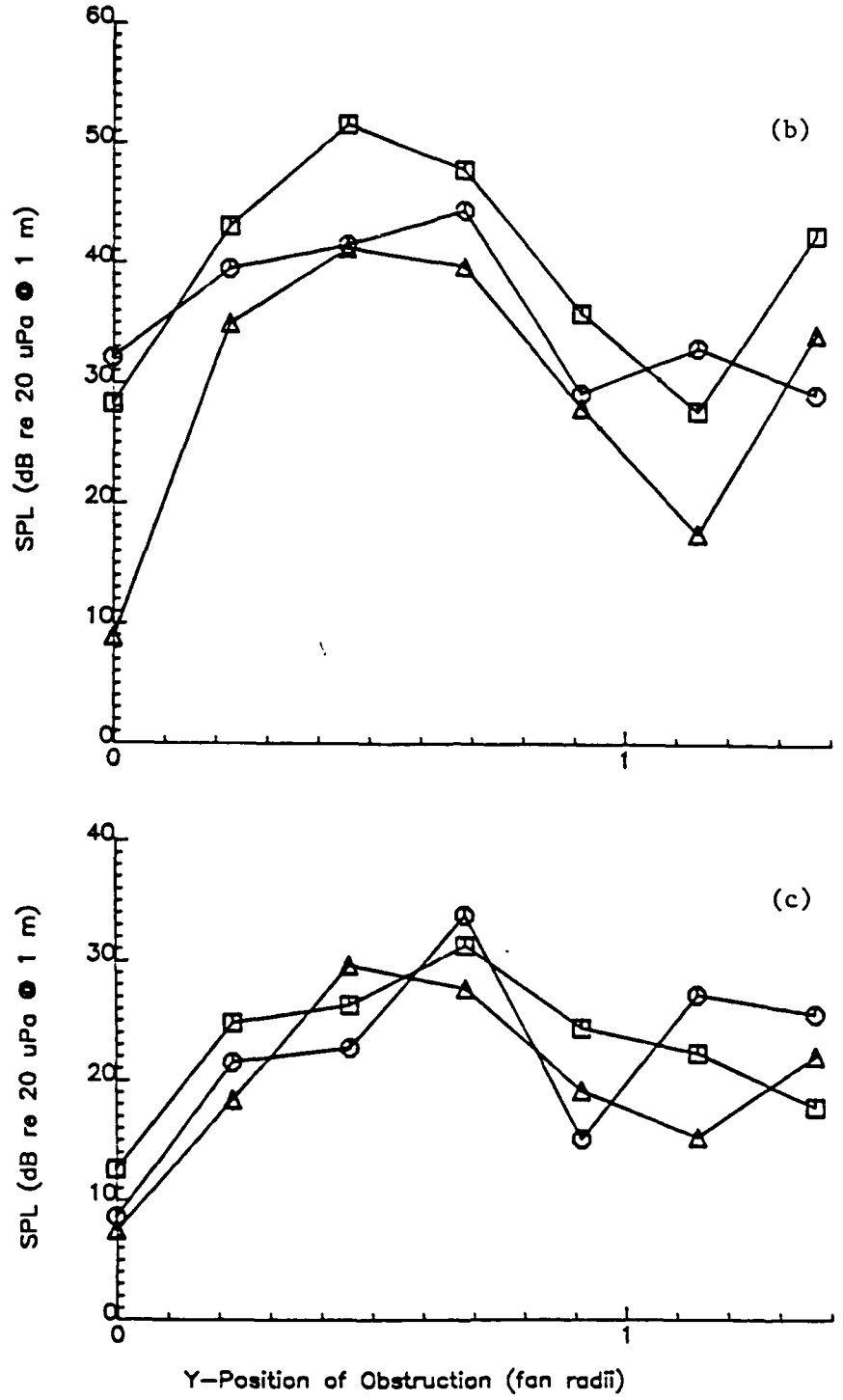

Figure 3.2.20 . Continued.

(b) □-- BPF x 5, ○-- BPF x 6, Δ -- BPF x 7.
(c) □-- BPF x 8, ○-- BPF x 9, Δ -- BPF x 10.

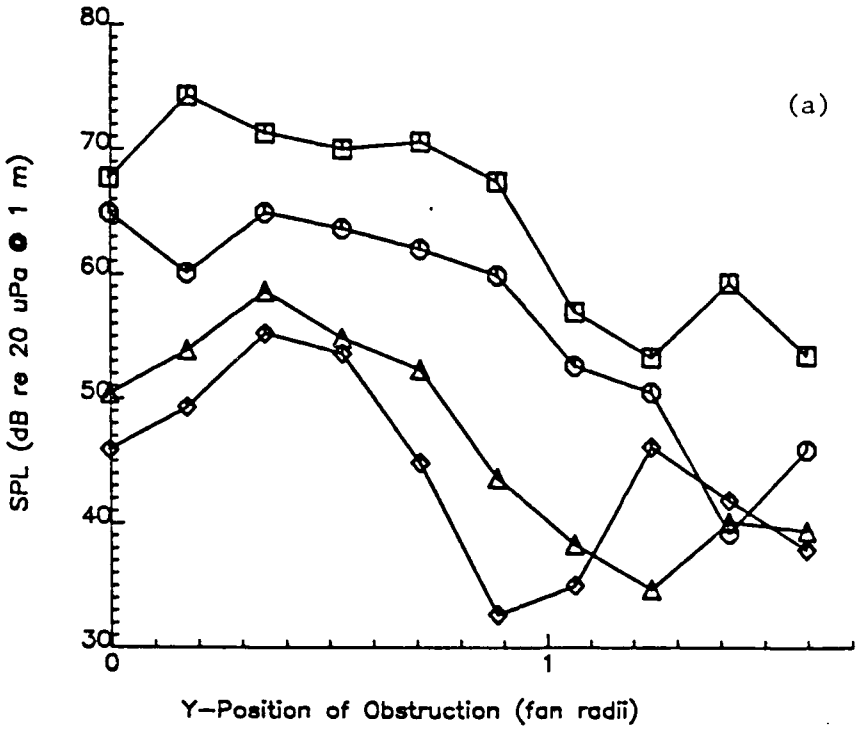

Figure 3.2.21 . SPL of Blade Passage Tones of the Patriot vs. Radial Location of a Thick, Rectangular Obstruction. (z = 0.0 Fan Radii, 8 Hz Bandwidth.)

(a) □ -- BPF x 1, ○ -- BPF x 2, Δ -- BPF x 3, ◇ -- BPF x 4.

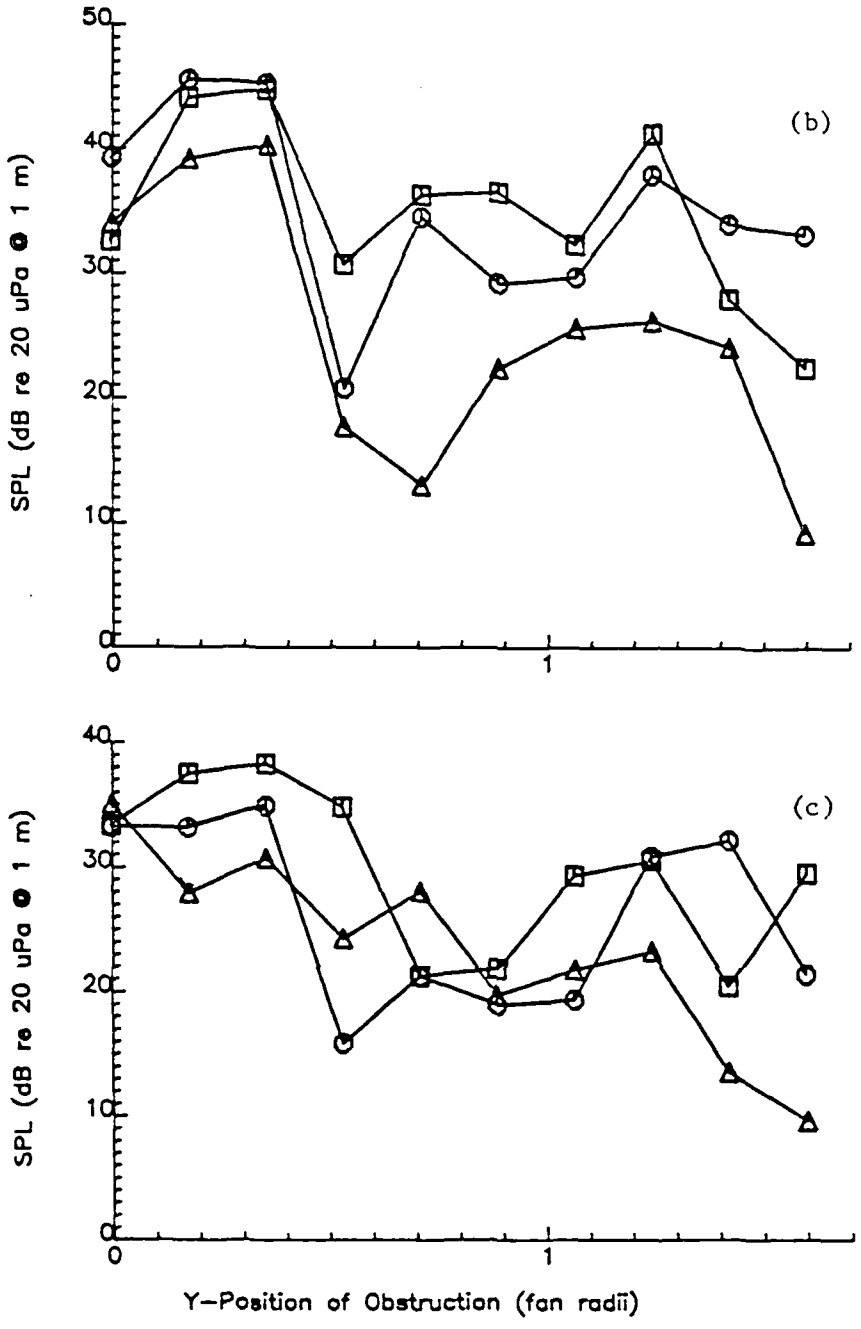

Figure 3.2.21 . Continued.

(b) □-- BPF x 5, ○-- BPF x 6, Δ -- BPF x 7.
(c) □-- BPF x 8, ○-- BPF x 9, Δ -- BPF x 10.

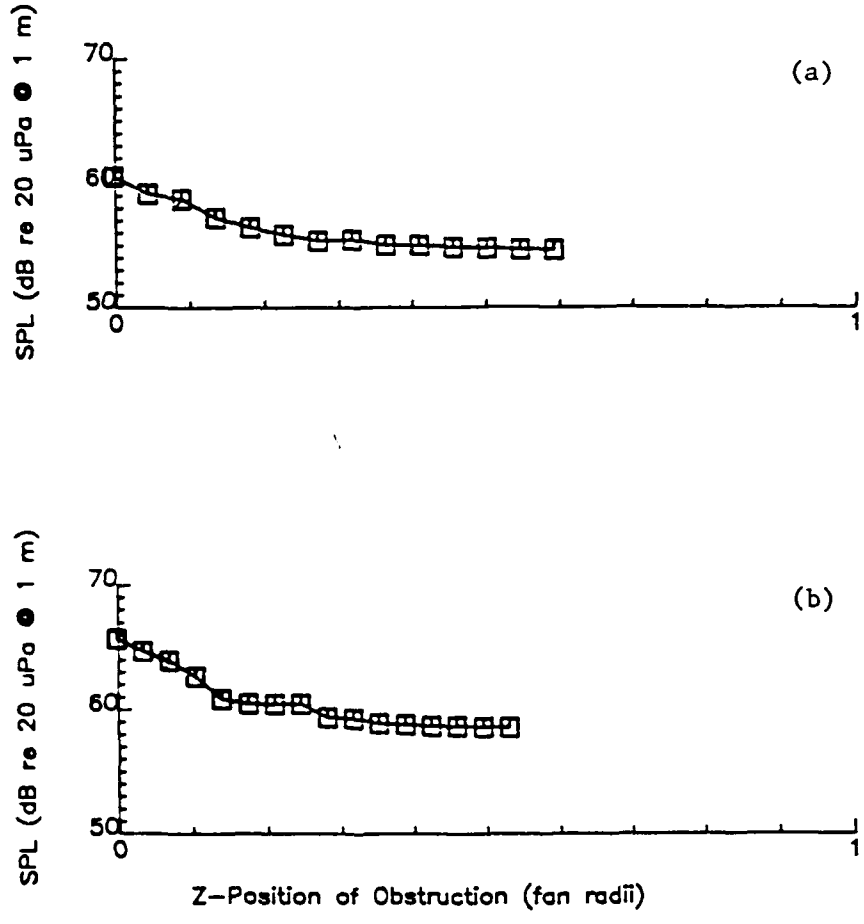

Figure 3.2.22 . OASPL vs. Axial Location of a Card Gate Model Obstruction (Measured From the Cards' Trailing Edges). (v = 0.0 Fan Radii, 20 kHz Bandwidth.)

(a) Muffin XL.
(b) Patriot.

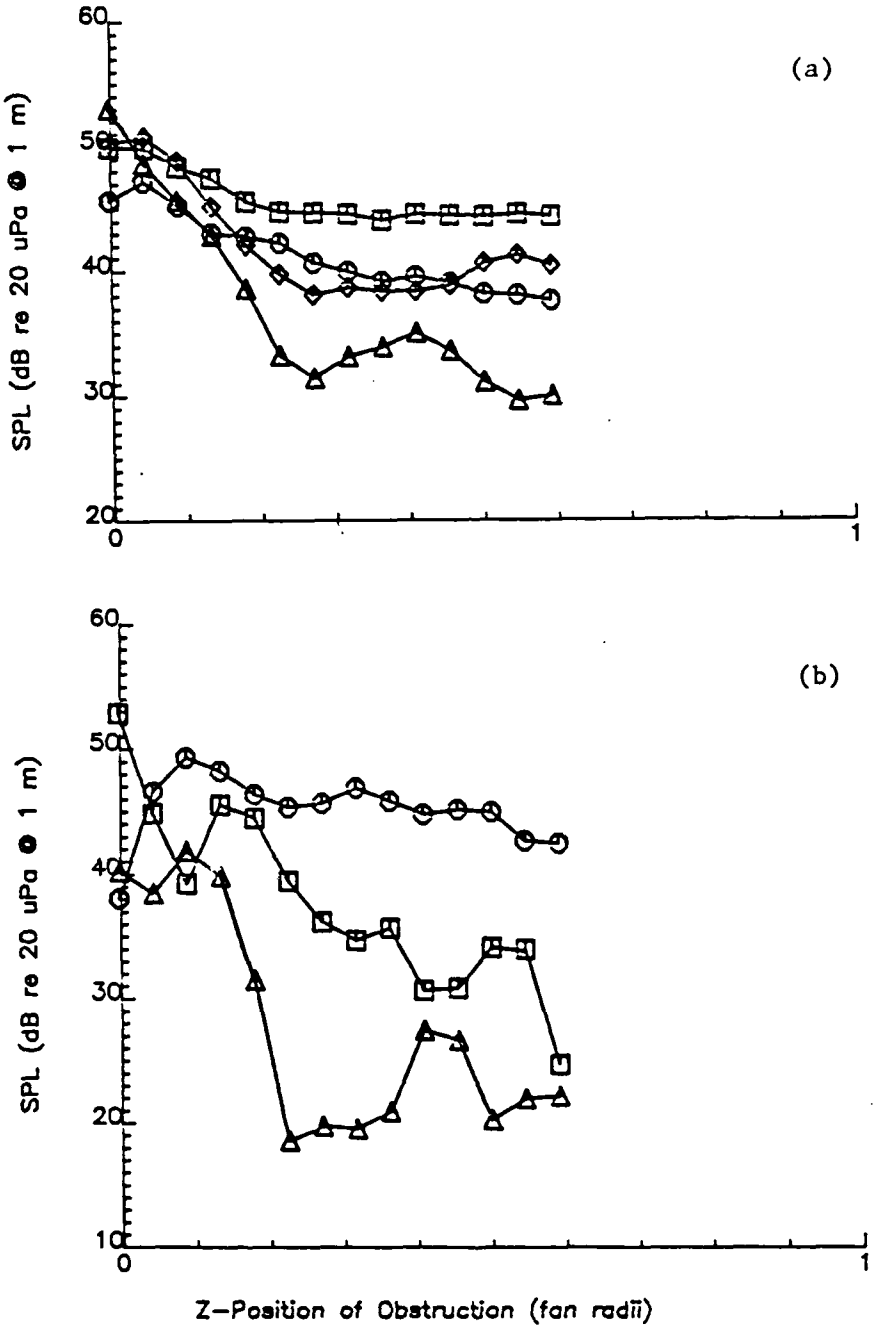

Figure 3.2.23 . SPL of Blade Passage Tones of the Muffin XL vs. Axial Location of a Card Gate Model Obstruction. (y = 0.0 Fan Radii, 4 Hz Bandwidth.)

(a) □-- BPF x 1, ○-- BPF x 2, Δ -- BPF x 3, ◇-- BPF x 4.
(b) □-- BPF x 5, ○-- BPF x 6, Δ -- BPF x 7.

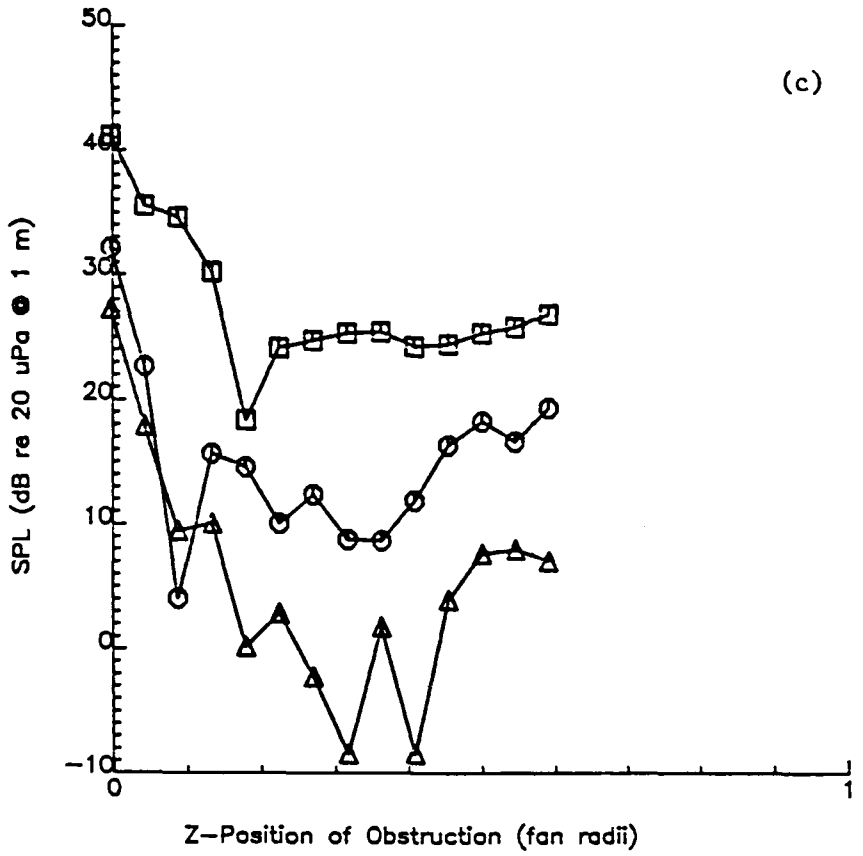

Figure 3.2.23 . Continued.

(c) □-- BPF x 8, ○-- BPF x 9, Δ -- BPF x 10.

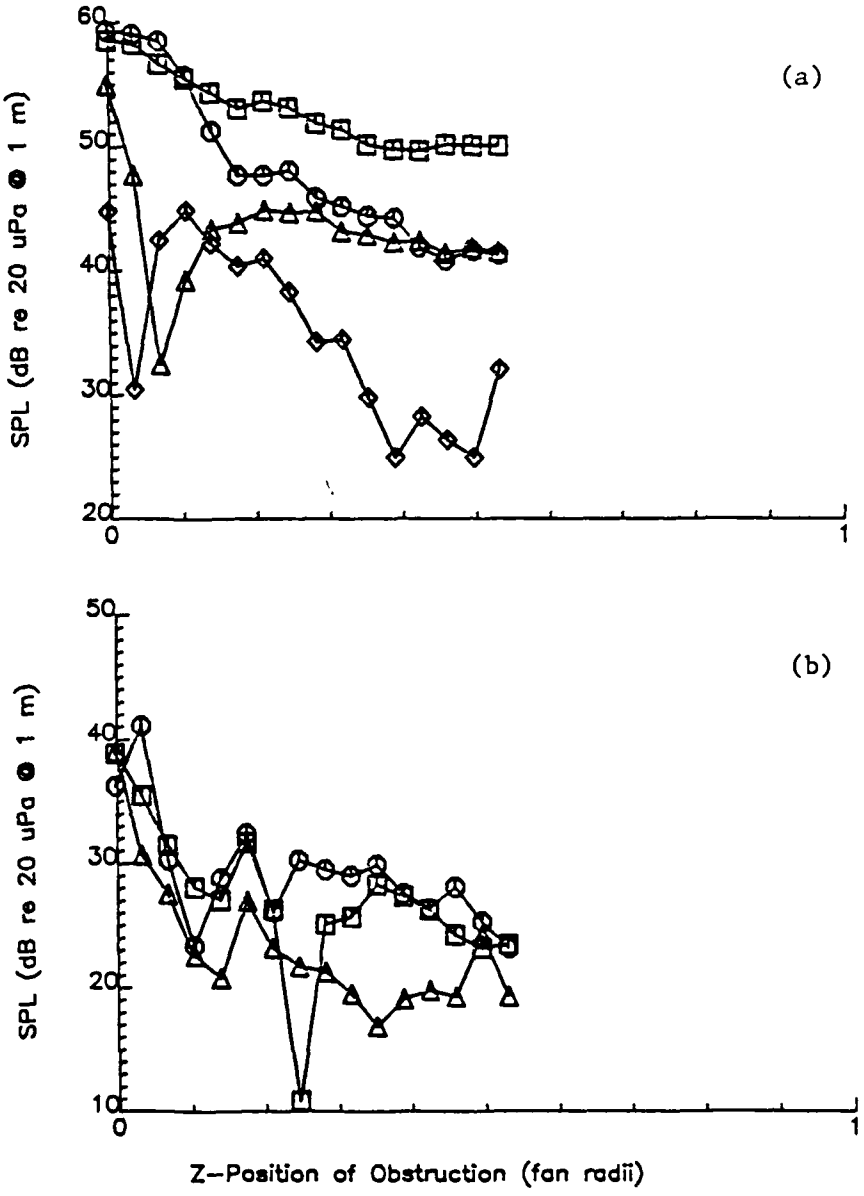

Figure 3.2.24 . SPL of Blade Passage Tones of the Patriot vs. Axial Location of a Card Gate Model Obstruction. (y = 0.0 Fan Radii, 8 Hz Bandwidth.)

(a) □-- BPF x 1, ○-- BPF x 2, Δ -- BPF x 3, ◇-- BPF x 4.

(b) □-- BPF x 5, ○-- BPF x 6, Δ -- BPF x 7.

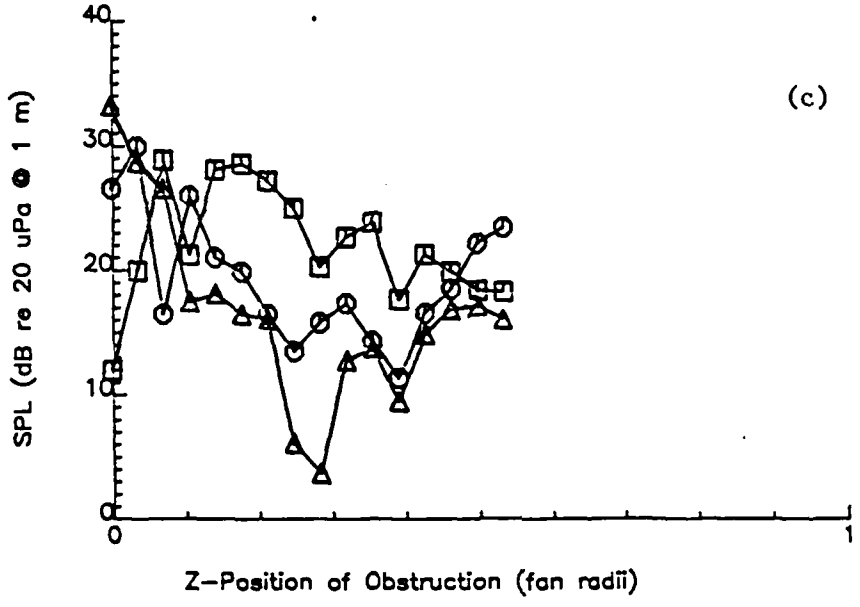

Figure 3.2.24 . Continued.

(c) □-- BPF x 8, ○-- BPF x 9, Δ -- BPF x 10.

the OASPL curves. Most of the higher harmonics of the Muffin XL have large levels for the smallest separation distances which decrease rapidly with increasing separation. They do not reach their baseline values within the maximum separation distance shown by these data. Apparently the complex wake structure persists even at the largest distances considered. The trends for the interaction tones of the Patriot are more complicated and are not easily explained except to point out that with its larger flow velocity, the wake structure is even more complex than that generated by the Muffin XL flow.

3.3. Phase II: Inlet Configurations

In this phase the Muffin XL was studied in detail. Selected tests were also conducted on the Patriot, in support of the conclusions drawn for the XL. The data presented are for the Muffin XL only.

3.3.1. Inlet Baffles

A study of overall noise generated by a blade as a function of local blade radius revealed that most of the noise is generated by the region of the blade within the 10% radius from the tip (Gray, 1983). Thus, the immediate inflow environment surrounding the shroud is critical in noise generation. When it was discovered that this environment was a major contributor to certain blade passage harmonic tones (see Section (3.2.1.)) for the Muffin XL, various modifications to the inlet were considered. If possible, a circular bellmouth is installed, as Fitzgerald (1982) did. However, space constraints (and flow conditions) within a typical device being cooled by these fans will not permit such large structures. Usually, the fan will be mounted just outside the cabinet (see Figure 2.3.1), with the cabinet

wall acting like a baffle. There is no reason why such a baffle, if devoid of discontinuities near the inlet, could not function as an inlet bellmouth. By investigating a baffle-type inlet, two purposes are served: First, it may act like a smooth bellmouth inlet acoustically, and second, it more closely resembles the immediate flow environment of the fan when actually installed in a cabinet.

The baffle for the Muffin XL is described in Section (2.3.2.1.). The acoustic results are plotted in Figure 3.3.1, and are denoted as the "Unmodified Inlet Baffle." The results are surprising. The BPF x 4 tone, whose presence was one of the motivating factors in using a baffle, is reduced nearly 20 dB. The tones at BPF x 5 through BPF x 9 are reduced more than 15 dB. This is a noteworthy improvement, but there is a tradeoff. The first interaction tone, at BPF x 2, is increased more than 13 dB. The BPF x 1 and BPF x 3 tones are each up about 6 dB. This implies that the energy content of the higher harmonic unsteady blade loading spectrum has been shifted to the primary loading harmonic.

The most apparent cause of the increase in the BPF x 2 tone is the asymmetry of the baffle inlet as it was mated with the fan housing. The baffle was cut by hand from plywood, and even with the care exercised, the match was not perfect, exhibiting asymmetry and smaller edge discontinuities. While a better solution to this problem would have been to machine an inlet from sheet metal, this was not feasible for this experiment. Instead, the inlet was lined with moldable wax as shown in Figure 3.3.2 , and smoothed by hand. The results for this condition are plotted in Figure 3.3.1 and denoted as the "Fully-lined Inlet Baffle." A 5 dB reduction for the BPF x 2 tone, along with

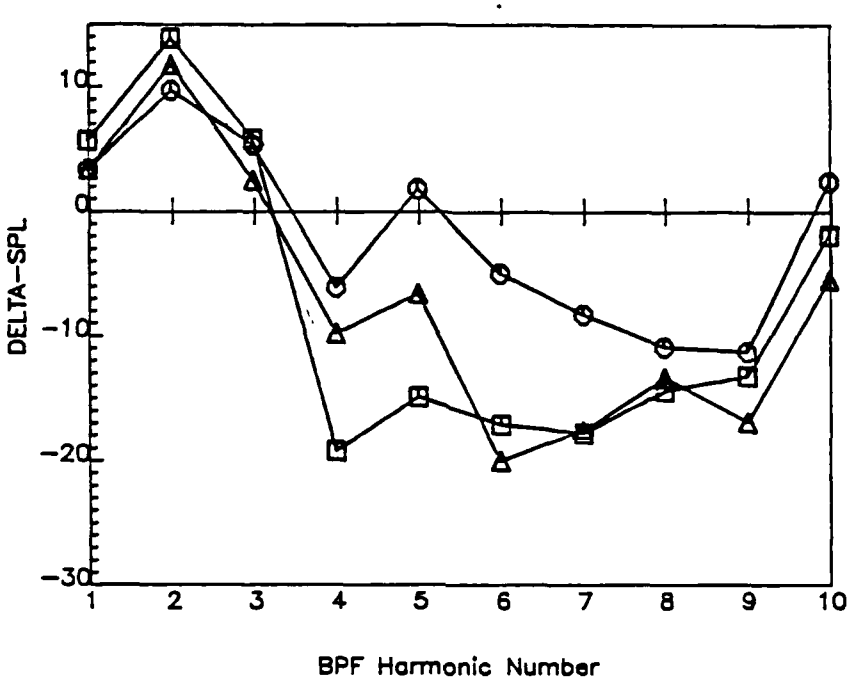

Figure 3.3.1 . Difference, in dB, of SPL's of Blade Passage Tones of the Muffin XL From the Baseline (Unobstructed) Levels for Various Inlet Baffle Configurations vs. Multiple of the BPF. (Synchronized Spectra, 4 Hz Bandwidth.) □-- Unmodified Inlet Baffle, ○-- Fully-Lined Inlet Baffle, Δ -- Partially-Lined Inlet Baffle.

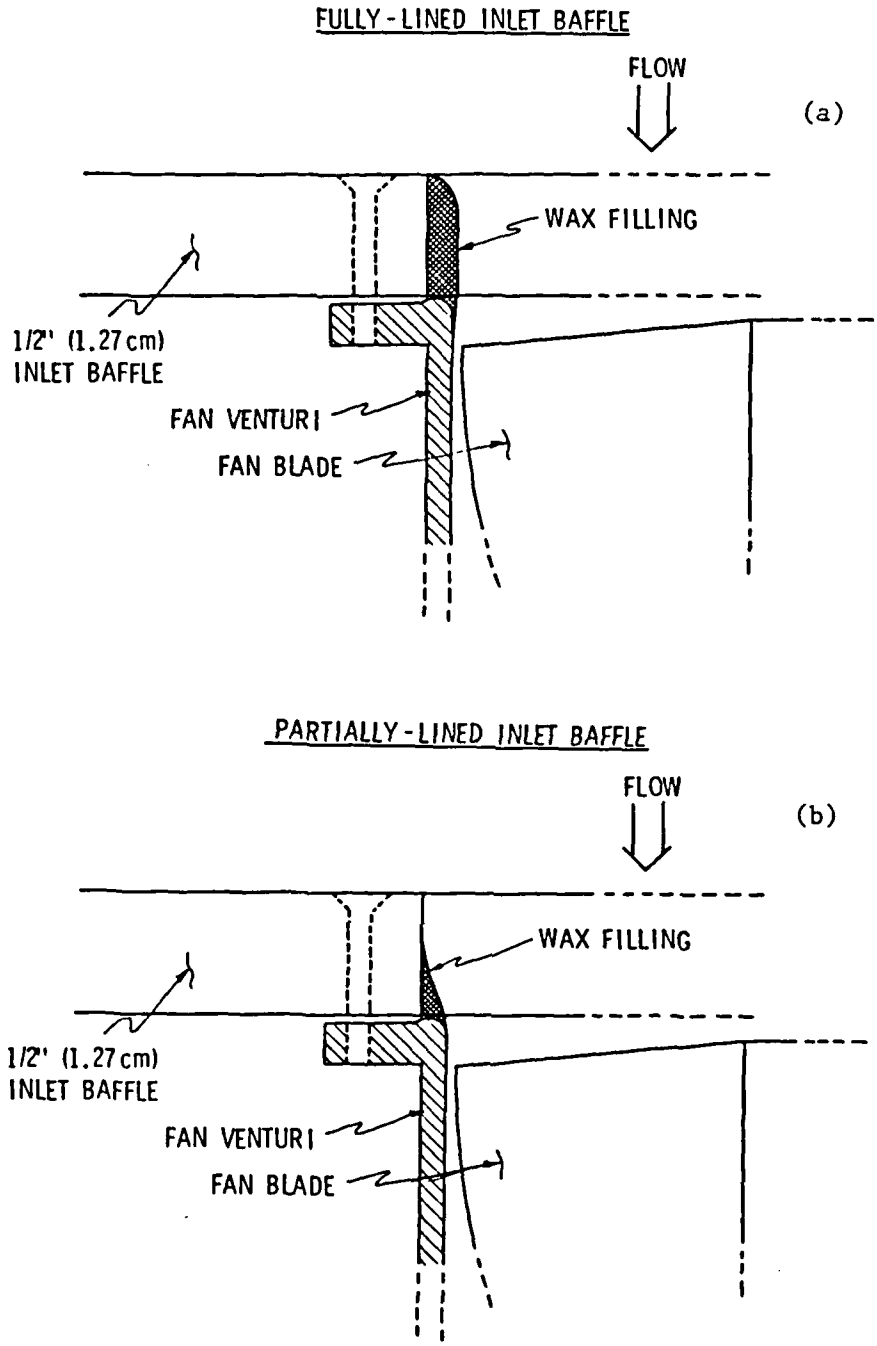

Figure 3.3.2 . Schematic Diagram of the Cross-Section of the Muffin XL Inlet Baffle Modifications.

(a) Fully-Lined Inlet with Wax Filling From Fan Shroud to Baffle Edge.
(b) Partially-Lined Inlet with Wax Filling Tapering From Fan Shroud to Center of Baffle Inlet.

smaller reductions for the BPF x 1 and BPF x 3 tones, is mitigated by slight increases in the higher harmonics. The BPF x 5 tone is increased above the baseline value by about 2 dB.

Further examination of the wax filling in the baffle inlet revealed additional symmetries. They were not as severe as the unmodified baffle, but they were significant. To reduce this, most of the wax filling was removed from the inlet. Just enough was left to mate the baffle to the fan inlet smoothly, as is shown in Figure 3.3.2. The results, shown in Figure 3.3.1, are those denoted "Partially-lined Inlet Baffle." The first three blade passage tones are still above their baseline levels, but the BPF x 3 tone has its lowest value of the three configurations. The BPF x 2 tone is increased from the fully-lined baffle, but its level is below the unmodified baffle level. The higher harmonics are reduced again, as desired. The BPF x 4 tone is not quite as low as for the unmodified baffle, but it nevertheless falls 10 dB below baseline.

The results indicate that large reductions can be achieved in blade passage harmonic levels by using an inlet baffle. It is critical, however, that the inlet be smooth and symmetric about the fan rotation axis. In practice, this could be very effectively achieved through the use of an accurately manufactured insert ring placed where the fan is bolted to the cabinet wall.

3.3.2. Finger Guards

Finger guards are required for safety in any fan installation. Therefore, their effect on discrete tone generation must be assessed. The finger guards shown in Figure 2.3.4 were tested on the Muffin XL.

Two configurations were investigated: guards mounted on the otherwise unmodified fan, and guards mounted on the inlet baffle. The results of the tests on two types of guards are shown in Figure 3.3.3. The levels are relative to the baseline levels for the noted tones.

The best configuration, as expected, is the circular screen mounted on the partially-lined inlet baffle. The square screen, with its bulky frame and low profile, increases the levels of most of the tones, even when baffled. When mounted directly on the fan, it increases the BPF x 4 tone by nearly 10 dB. All configurations increased the level of the BPF x 10 tone. Possibly the small wakes shed from the wires increase the higher unsteady loading harmonics which generate higher frequency tones. The BPF x 6 tone was a problem for both screens when mounted directly on the fan. It is noted that the circular guard mounted directly to the fan induced slightly lower tones at BPF x 3, 4, 5, 7, and 9. It is possible that the supports for the guard, which bolt onto the fan housing corners, are breaking up the local flow in a way that reduces, rather than increases, the unsteady blade loading harmonics responsible for the tones. This suggests that other guard configurations may be appropriate. Perhaps stiff wire mesh screens would be effective in reducing the coherence of local flow inhomogenities. This would require further investigation.

Circular-geometry guards with very small diameter wires, combined with an inlet baffle, are a useful means of reducing tonal noise when guards are necessary. Further improvements will be gained if the guard supports are moved as far (radially) from the inlet as possible, the support feet are integrated smoothly into the inlet baffle, and the guards are placed upstream of the inlet as far as possible.

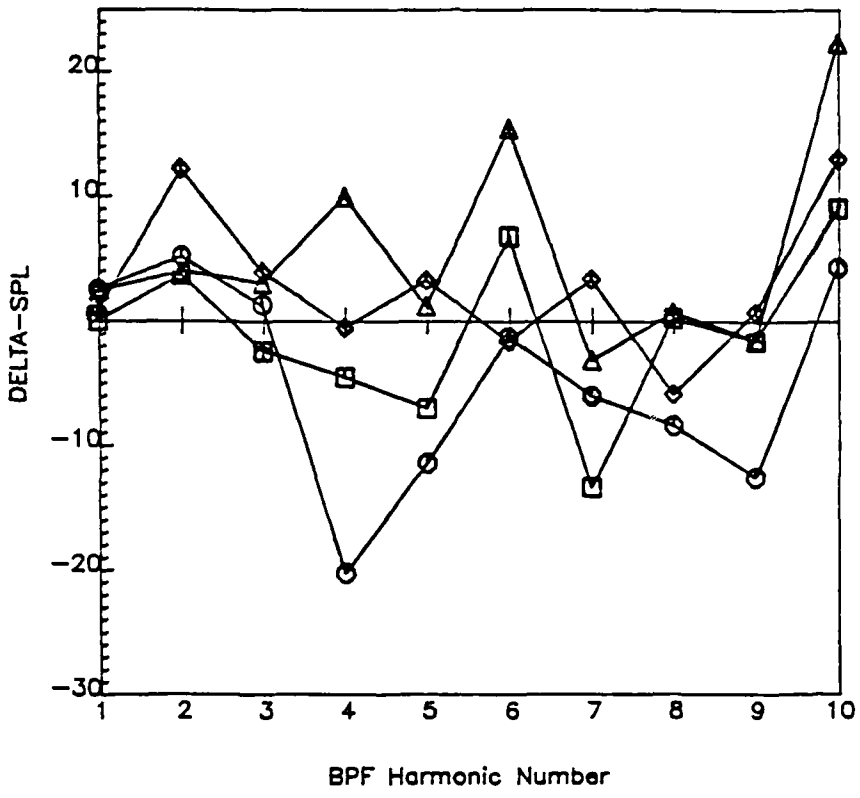

Figure 3.3.3 . Difference, in dB, of SPL's of Blade Passage Tones of the Muffin XL From the Baseline (Unobstructed) Levels for Various Inlet Finger-Guards vs. Multiple of the BPF. (Synchronized Spectra, 4 Hz Bandwidth.) □ -- Circular Wire Guards Only, ○ -- Circular Wire Guard on Partially-Lined Inlet Baffle, Δ -- Square Wire Guard Only, ◇ -- Square Wire Guard on Partially-Lined Inlet Baffle.

3.3.3. Honeycomb Flow Straightener

The success of workers in turbofan acoustics with the use of Inlet Flow Control Devices led to a hope that honeycomb mesh upstream might alleviate the unsteady blade loading and reduce the generation of discrete tones. As Figure 3.3.4 shows, the trials met with mixed success.

The tones from BPF x 2 through BPF x 9 are reduced significantly when the honeycomb is mounted flush against the inlet. Then, beginning with BPF x 10 , a whole series of tones appear up to about 8 kHz. This change is shown clearly in Figure 3.3.5. These are narrowband, unsynchronized spectra for the Muffin XL baseline and with honeycomb. The tones with the highest levels are harmonics of the blade passage frequency. It is more informative to think of them as integer multiples of the BPF x 2 tone, the first unsteady-lift tone. An explanation is as follows. The Reynolds number (based on cell diameter) for flow through a cell of the honeycomb mounted on the Muffin XL is about 140. This is far below the critical Reynolds number of 2300 required for pipe flow to transition from laminar to turbulent (Schlichting, 1979, p.39). Thus, the flow exiting the honeycomb consists of many laminar jets whose wakes interact strongly with the blades to produce high-frequency unsteady lift. Lumley and MacMahon (1967) describe the downstream flow of an untransitioned honeycomb as more turbulent than for transitioned flow. The reduction in the low-order harmonics is primarily due to the "baffle" effect of sealing the honeycomb to the fan housing.

The only way to reduce the discrete character of the individual cell wakes is to mix them, and this can only be done over distance,

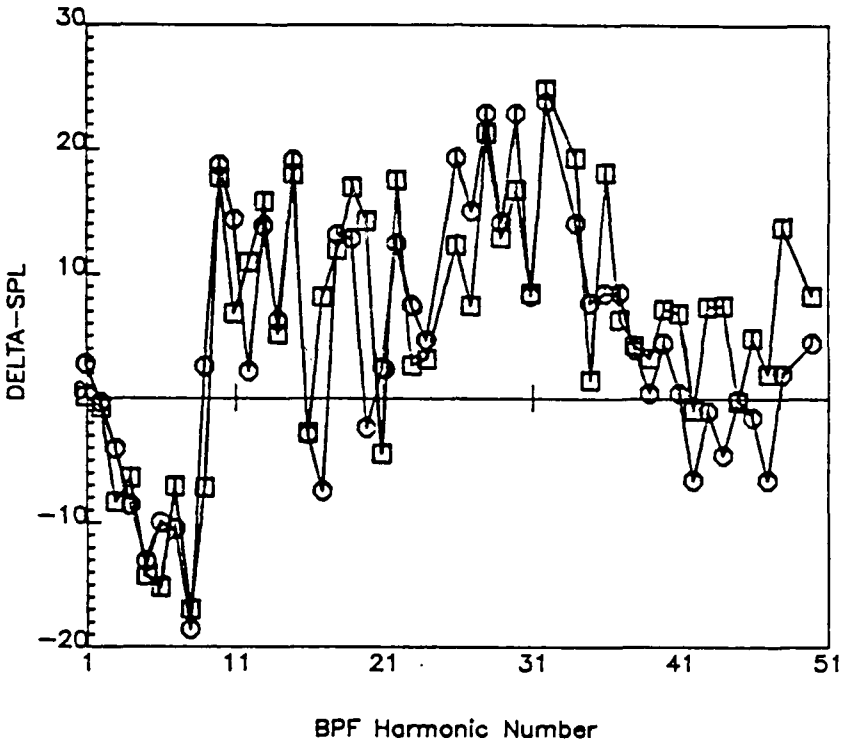

Figure 3.3.4 . Difference, in dB, of SPL's of Blade Passage Tones of the Muffin XL From the Baseline (Unobstructed) Levels for Honeycomb Inlets vs. Multiple of the BPF. (Synchronized Spectra, 20 Hz Bandwidth.)
□ -- Honeycomb Mounted Flush to Fan Inlet Shroud,
○ -- Honeycomb Mounted with 0.32 cm (1/8 in.) Gap From Shroud.

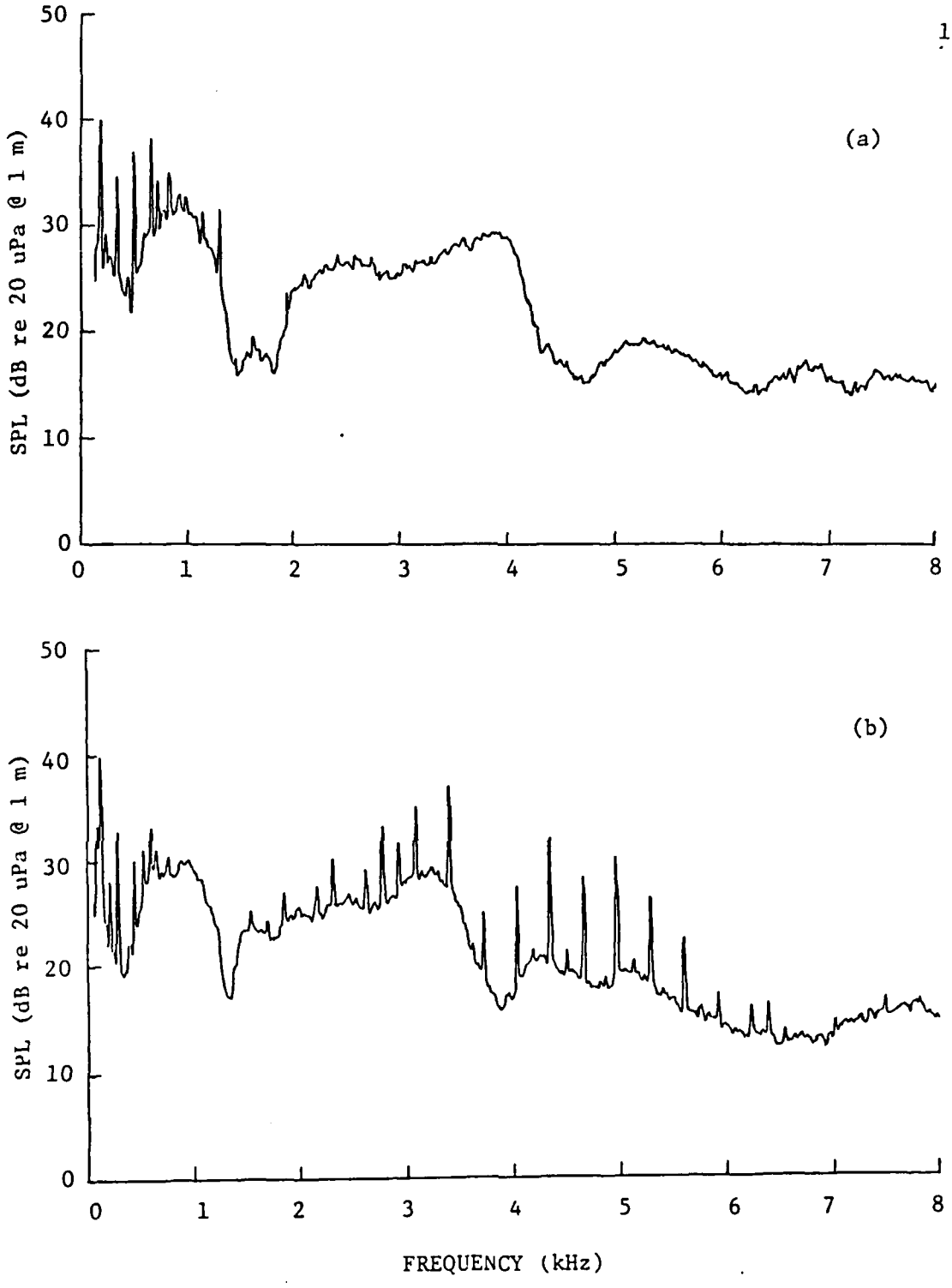

Figure 3.3.5 . Narrowband Spectra of Noise Generated by the Muffin XL. (Unsynchronized Spectra, 10 Hz Bandwidth.)

(a) Unobstructed Inlet.
(b) Flush-Mounted Honeycomb Inlet.

i.e. larger Reynolds numbers. This is the key to the success of the large IFCD's (Woodward, et al., 1977; Ho, et al., 1979), and was also demonstrated by Le S. Filleul (1966) in testing fan noise with an upstream honeycomb matrix. As with the inlet bellmouth, however, many electronic devices are too cramped to afford proper mixing distances. A second test was performed with the honeycomb separated from the fan by 0.32 cm (0.125 in.). It was (as before) sealed to the fan housing. The results are plotted in Figure 3.3.4; no significant changes are apparent. The only way a honeycomb will provide the desired noise reduction is to provide for operation at Reynolds numbers above 2300. Based on the available space in typical applications, this seems impractical.

4. CONCLUSIONS

4.1. Fan Aerodynamic Effects

Discrete frequency noise is generated by two mechanisms. The first is the propeller-like rotating pressure pattern associated with each blade under steady lift. Since the pattern is not a simple sinusoid, it contains Fourier components at multiples of the blade passage frequency. Steady loading contributes mainly to the tone at the BPF; higher harmonics fall away quickly. The second mechanism is the unsteady blade loading caused by fluctuating lift experienced by the blade as it passes through periodic inflow velocity distortions. This mechanism is the dominant contributor to the BPF x 2 tone and higher harmonic

Steady loading noise reduction is achieved only by reducing the thrust required of each blade. This can be accomplished by increasing the number of blades (Wright, 1971), increasing the blade solidity, and optimizing the fan aerodynamics for the largest, lowest tip-speed fan possible for a given pumping requirement (Metzger and Hanson, 1972). A designer might wish to use a variable-speed, DC-powered fan set to operate at a speed which minimizes noise for the given pumping requirement at normal operating temperatures. A thermistor feedback circuit could then be employed to control the fan speed, giving the user in a cooler environment an added measure of noise reduction. Employing the blade modificiations which Fitzgerald (1982) describes, particularly suction-side serrations, will re... the BPF tone.

Higher blade passage harmonics will be reduced by the removal of fluctuating forces from the blade (Wright, 1969). This is the first

priority in quieting fans, and is discussed further in the following section.

4.2. Survey Results Applied to Installation Design Recommendations

The survey results presented in Chapter 3 lead to many suggestions for installing axial flow fans in a manner that will minimize discrete frequency noise. Some of the suggestions are derived directly from specific data. Others are conclusions drawn from the sum total results or related trends.

Synchronized signal averaging is an effective means of enhancing the study of discrete frequency signals which are contaminated by broadband noise of equivalent levels. The process reduces background by as much as 40 dB while preserving phase-coherent data. If some harmonic of the fundamental repetition rate is of particular interest, the synchronization frequency should be that of the harmonic. This assures that the particular harmonic will be averaged over the number of ensembles desired by the user, allowing control over the amount of random error in the magnitude of that harmonic.

The obstruction location surveys did not reveal a particular low-noise region close to the fan inlet. However, they do serve as broad guidelines to obstruction positioning. It is critical that any obstruction be located at least 0.3 fan radii (about one blade chord) upstream of the inlet. Otherwise, the combination of potential flow field interactions, boundary layer separation and ingestion, and impulsive blade loading will create a blade loading spectrum which is large in magnitude and rich in harmonics. The result is a considerable increase in interaction tonal noise for all blade passage harmonics.

In terms of radial position, obstructions should not be placed near the edge of the hub or near the shroud/blade tip region. Transverse flow in these regions undergoes the greatest acceleration and contraction of the inlet flow. Local flow deficits are exaggerated in these regions, and mixing from nearby flow is minimized relative to that which would occur if the obstruction was located in the mid-span region. The shroud region is particularly important since the last 10% of the blade span generates the largest share of the noise. This is the area of the blade which interacts with inflow crossing the shroud.

The number of discrete harmonics and their magnitudes increase as the profile of the obstruction wake becomes more pronounced and acute. This was observed in the increase in noise generated by the thin, rectangular obstruction relative to the cylindrical obstruction. The implication is obvious: if it is necessary that an obstruction of small cross section be placed in the vicinity of the fan inlet, it must be smoothed aerodynamically to minimize noise.

Large cross-section obstructions, especially those placed asymmetrically with respect to the fan inlet, must be avoided. Not only do they induce severe fluctuating loads on the blades, they can change the operating point of the fan. Such obstructions distort inflow greatly, and they are apt to reduce cooling flow in critical areas. If such an obstruction requires cooling, it should be placed well away from the inlet and have an aerodynamically smooth housing.

Once fans are installed, a baffle with a smoothed shroud should be placed on the inlets. As demonstrated with the Muffin XL, the local shroud geometry must be smooth and axisymmetric. This symmetry is critical and must be maintained within approximately 0.5 fan radii from

the blade tip. This implies that fans operating in tandem should be separated by at least this distance. Mounting bolts, wiring, and other protrusions should be covered by the baffle/shroud combination. A full bellmouth inlet is unnecessary. A low profile inlet shroud is sufficient as long as it removes inlet asymmetries.

If it is necessary to use finger guards, they should be raised above the fan inlet. Circular geometries are preferred, and supporting members should be non-radial. The mounting feet should extend radially away from the inlet so that they are bolted at least 0.5 fan radii from the inlet. It would be best to have the feet hidden underneath the inlet baffle to prevent creation of wakes along the inlet shroud.

Honeycomb flow straighteners did not prove to be useful. Because the flow Reynolds numbers (relative to cell diameter) were too low at the inlet, cell flow never became fully turbulent, and individual, laminar jets formed that increased the high-harmonic content of the blade-loading spectrum. This has implications for the use of the fans to cool electronics. Since many electronic cards contain mostly chip-type devices of a low profile, the cards are placed quite close together. If the ends of the cards are within 0.5 fan radii of the fan inlet, it is possible that the flow from each gap may not undergo sufficient mixing. Each gap flow would then be a discrete load on the blades, increasing discrete tone noise. Sufficient separation between the cards and the fan must be maintained, and care should be taken to provide that flow between the cards is turbulent and well mixed as it exits the card gate.

The following design suggestions are the results of considering the survey results as a whole.

To facilitate transition from the rectangular geometry of the machine to the cylindrical geometry of the fan, the fan should be mounted at or near the center of the largest flat area available. The devices to be cooled can then be mounted to maximize flow. A smoothed inlet shroud cover should be installed to alleviate flow obstructions such as mounting bolts, finger guard mounts, and so forth. Because it can undergo only limited turbulent mixing, lateral flow along the machine surface to which the fan is mounted must never be interrupted, even at large distances. Corners where cabinet walls meet should be coved or have an internal cove molding to minimize stagnation points from which large eddies might emanate. Low-profile obstructions such as wiring that must be mounted against the wall containing the fan should have a smoothing cover mounted over them to minimize flow deficits.

Channels are created when surfaces are parallel (or nearly so) and flow is drawn through them. Because mass flow is conserved, the volume velocities at the "channel" inlet can be as high as at the fan inlet. Obstructions to these channel inlets, while they may be quite far from the fan inlet, can still have a dominant effect on discrete tone generation, since flow deficits created by the obstructions are not alleviated when they reach the fan. Any design must account for the local volume flow velocity in each region relative to that at the fan inlet.

Finally, the overall spacing of components must be uniform relative to the fan inlet, to avoid directions of favored flow. This is necessary to achieve proper cooling as well as reduction of tonal noise, but it is often overlooked. If the components are such that

this kind of balancing is impractical, devices should be installed to compensate for their presence, and to aid in the transition from rectangular to cylindrical geometry.

If the above suggestions are followed to the degree practical, but sufficient noise reduction cannot be achieved, then alternative methods of cooling should be investigated.

4.3. Suggestions for Further Research

As pointed out by Gray (1983), upstream obstructions are responsible for more discrete tone generation than downstream obstructions. With this in mind, only upstream conditions and noise radiated upstream were studied in these surveys. In most installations, the fans exhaust to the exterior of the machine being cooled. It is important to determine how much of the power in each discrete tone is radiating out of the machine and by what propagation path. Likewise, the acoustic effects of mounting the fan such that its exit is very close to a surface must be investigated. If the gap is small and the machine is large, a significant change in acoustic impedance results, relative to the free-field case simulated in these surveys.

An investigation of a wire mesh screen or screens as an inlet flow controller should be undertaken. It might reduce inlet turbulence intensities and would also serve as a finger guard. Its effect on fan performance would have to be monitored.

A series of detailed aerodynamic measurements of the fans, both in free flow and as installed, might be more useful than further acoustic tests. Upstream flow surveys with hot-film or five-hole

probes would verify inflow properties assumed for this study. Determination of the actual blade loading spectrum, and correlation with the acoustic spectrum, would pinpoint discrete tone generation mechanisms. Quantification of turbulence intensities and inlet flow deficits would enable designers to further qualify the necessary shaping of unavoidable obstructions.

Finally, an integrated inlet shroud and baffle should be developed and tested. This low profile device would cover local protrusions that create deficits which enter the fan near the blade tips and aid in the transition of locally inhomogeneous flow to homogeneous inlet flow. Figure 4.1 shows a cross section of this suggested inlet shroud baffle (Washburn, 1985).

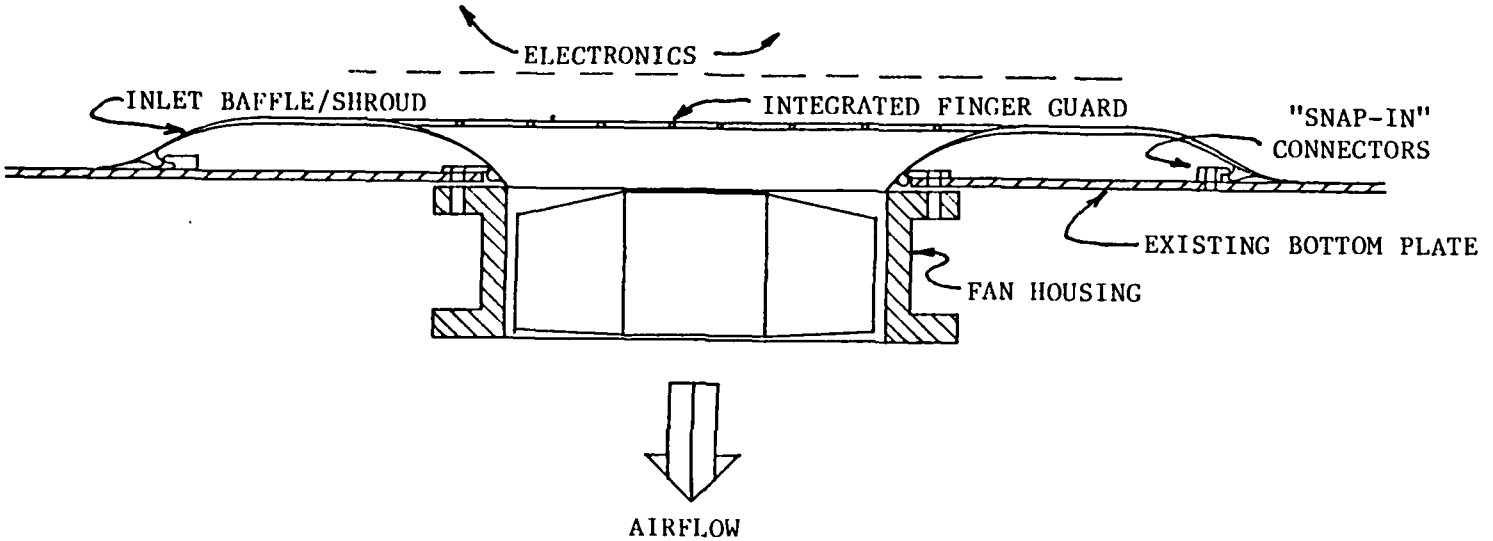

Figure 4.1 . Schematic Diagram of Integrated Fan Inlet Baffle, Shroud, and Fingerguard.

BIBLIOGRAPHY

Bekofske, K. L.; Sheer, R. E.; and Wang, J. C. F., "Fan Inlet Disturbances and their Effect on Static Acoustic Data," ASME Publication 77-GT-63 (1977).

Bendat, J. S. and Piersol, A. G., Engineering Applications of Correlation and Spectral Analysis, New York: John Wiley and Sons, Inc., 1980.

Chandrashekhara, N., "Experimental Studies of Discrete Tone Noise from an Axial Flow Fan," J. Sound and Vibration, 13, 43-49 (1970).

Ffowcs-Williams, J. E. and Hawkings, D. L., "Theory Relating to the Noise of Rotating Machinery," J. Sound and Vibration, 10, 10-21 (1969).

Filleul, N. Le S., "An Investigation of Axial Flow Fan Noise," J. Sound and Vibration, 3, 147-165 (1966).

Fitzgerald, J. M., "Discrete Frequency Noise and its Reduction in Small Axial-Flow Fans," The Pennsylvania State University, Applied Research Laboratory TM 82-76 (March, 1982).

Gray, L. M., "A Review of the Physics of Axial Fan Acoustics and Aerodynamics with a View Toward Noise Control," Proc. Noise-Con 83, 187-196 (1983).

Gutin, L., "On the Sound Field of a Rotating Airscrew," NACA TM 1195 (1948) (Translated from the German).

Hanson, D. B., "Spectrum of Rotor Noise Caused by Atmospheric Turbulence," J. Acoust. Soc. Amer., 56, 110-126, (1974).

Hanson, D. B., "Study of Noise and Inflow Distortion Sources in the NASA QF-1B Fan Using Measured Blade and Vane Pressures," NASA CR-2899, (September, 1977).

Ho, P. Y.; Smith, E. B.; and Kantola, R. A., "An Inflow Turbulence Reduction Structure for Scale Model Fan Testing," AIAA Publication 79-0655 (March, 1979).

Kantola, R. A. and Warren, R. E., "Reduction of Rotor-Turbulence Interaction Noise in Static Fan Noise Testing," AIAA Publication 79-0656 (March, 1979).

Kryter, K. D. and Pearsons, K. S., "Judged Noisiness of a Band of Random Noise Containing an Audible Pure Tone," J. Acous. Soc. Amer., 38, 106-112 (1965).

Lighthill, M. J., "On Sound Generated Aerodynamically: I. General Theory," Proc. Roy. Soc. (London) A-211, 564-587 (1952).

Longhouse, R. E., "Noise Mechanism Separation and Design Considerations for Low Tip-Speed, Axial-Flow Fans," J. Sound and Vibration, 48, 461-474 (1976).

Longhouse, R. E., "Vortex Shedding Noise of Low Tip-Speed, Axial-Flow Fans," J. Sound and Vibration, 53, 25-46 (1977).

Lumley, J. L. and McMahon, J. F., "Reducing Water Tunnel Turbulence by Means of a Honeycomb," J. Basic Engineering (Trans. ASME) 764-770 (December, 1967).

Magliozzi, B. and Metzger, F. B., "Fan Noise Control in Environmental Systems," Intersociety Conference on Environmental Systems (July, 1974).

Marboe, R. C. and Fizgerald, J. M., "The ARL/FED Anechoic Chamber," The Pennsylvania State University, Applied Research Laboratory TM 81-164 (August, 1981).

Mather, J. S. B.; Savidge, J.; and Fisher, M. J., "New Observations on Tone Generation in Fans," J. Sound and Vibration, 16, 407-418 (1971).

Mellin, R. C., "Selection of Minimum Noise Fans for a Given Pumping Requirement," Noise Control Engineering 4 (1), 35-45 (1975).

Metzger, F. B. and Hanson, D. B., "Low Pressure Ratio Fan Noise Experiment and Theory," ASME Publication 72-GT-40 (January, 1973).

Metzger, F. B. and Magliozzi, B., "New Directions in Aircraft Propulsor Noise Research," Soc. Auto. Eng., Business Aircraft Meeting Publication 75-0515 (April, 1975).

Morfey, C. L., "Rotating Blades and Aerodynamic Sound," J. Sound and Vibration, 28, 587-617 (1973).

Mugridge, B. D., and Morfey, C. L., "Sources of Noise in Axial Flow Fans," J. Acoust. Soc. Amer., 51, 1411-1426 (1972).

Pegg, R. J.; Magliozzi, B.; and Farassat, F., "Some Measured and Calculated Effects of Forward Velocity on Propeller Noise," ASME Publication 77-GT-70 (March, 1977).

Peracchio, A. A., "Assessment of Inflow Control Structure Effectiveness and Design System Development," AIAA Publication 81-2048 (October, 1981).

Prandtl, L., "Remarks on Aircraft Noise," Zietschrift fur Technische Physik, 2, 244-245 (In German).

Robbins, B., "Water Tunnel Measurements Behind a Honeycomb," J. Hydronautics, 12 (3), 122-128 (1978).

Robbins, B., and Lakshminarayana, B., "Effect of Inlet Turbulence on Compressor Noise," J. Aircraft, 11 (5), 273-281 (1974).

Schlichting, H., Boundary Layer Theory, New York: McGraw-Hill Book Co., Inc., 1979.

Sharland, I. J., "Sources of Noise in Axial Flow Fans," J. Sound and Vibration, 1, 302-322 (1964).

Shaw, L. M.; Woodward, R. P.; Glaser, F. W.; and Dastoli, B. J., "Inlet Turbulence and Fan Noise Measured in an Anechoic Wind Tunnel and Statically with an Inlet Flow Control Device," NASA TM-73723 (October, 1977).

Tyler, J. M. and Sofrin, T. G., "Axial Flow Compressor Noise Studies," Soc. Auto. Eng. Transactions, 70, 309-322 (1962).

Washburn, K. B., "An Integrated Inlet Shroud/Finger Guard for Small, Axial Flow Fans," Applied Research Laboratory Invention Disclosure #561 (April, 1985).

Woodward, R. P.; Wazyniak, J. A.; Shaw, L. M.; and MacKinnon, M. J., "Effectiveness of an Inlet Flow Turbulence Control Device to Simulate Flight Fan Noise in an Anechoic Chamber," NASA TM-73855 (December, 1977).

Wright, S. E., "Discrete Radiation from Rotating Periodic Sources," J. Sound and Vibration, 17, 437-498 (1971).

Wright, S. E., "Sound Radiation from a Lifting Rotor Generated by Asymmetric Disk Loading," J. Sound and Vibration, 9, 223-240 (1969).

END

FILMED

12-85

DTIC